Bias Dependence of Radiation Response and Reliability of AlGaN/GaN HEMTs

By

Rong Jiang

Dissertation

Submitted to the Faculty of the

Graduate School of Vanderbilt University

in partial fulfillment of the requirements

for the degree of

DOCTOR OF PHILOSOPHY

in

Electrical Engineering

May 11, 2018

Nashville, Tennessee

Approved:

Daniel M. Fleetwood, Ph.D.

Enxia Zhang, Ph.D.

Robert A. Reed, Ph.D.

Ronald D. Schrimpf, Ph.D.

Sokrates T. Pantelides, Ph.D.

ACKNOWLEDGEMENTS

The journey of my PhD study will end soon. Through this journey, the acquired knowledge and improved self-perception in this process will be the invaluable treasure of my life. I would like to take this great opportunity to express my gratitude to those who helped me in my PhD research and life. Without your contributions, this dissertation would not be possible.

First of all, I would like to foremost offer truly heartfelt thanks to my advisor Prof. Daniel M. Fleetwood for his invaluable guidance and support. His great overview of my research area and his professional advice towards my scientific research makes the PhD research become enjoyable to me. His profound knowledge and religious research attitude inspire me not only in the research but also in my life. It would be impossible to achieve my PhD degree without his help. I am lucky to have him as my advisor. I also would like to thank Dr. Ronald D. Schrimpf for sharing his broad knowledge and deeply understanding in semiconductor and semiconductor device physics in the class and through the countless discussions when I encounter difficulties in research during or after the group meeting. I thank Dr. Sokrates T. Pantelides and his group for their great contribution in the physical analysis. I thank Dr. Robert A. Reed for serving on my oral and reading committee.

Secondly, I would like to especially thank Dr. Enxia Zhang. Ever since I first start my PhD research, Dr. Enxia Zhang stands out in teaching me how to use the experimental equipment and how to package the devices. She gave me a lot of hands-on help in experiments even out of working hours. Her great ideas in experiments setup are also important in help me finish this work. I would

also thank Dr. Xiao Shen. He performed the density function theory (DFT) calculation for the defects in this work and explained the defects and physical mechanism clearly and precisely. He helped me understanding the mechanism and without his help I cannot finish the paper. I thank Dr. Jingtian Fang for his Monte Carlo simulation and TCAD simulations for explaining the result. I thank Mike McCurdy for his help in proton irradiation testing. I thank Dr. Anthony B. Hmelo and Dr. Bo Choi from Vanderbilt Institute of Nanoscale Science and Engineering (VINSE) for their experiment support.

I would also like to thank the sponsors of my project. I thank the DTRA, AFOSR and AFRL for financially supporting this work through grant No. 1-11-1-0023 and the Hi-REV program. I thank our collaborators at the University of California, Santa Barbara, for providing us the AlGaN/GaN HEMTs used in this work.

Then I would like to thank other students in RER group. I especially thank Dr. Jin Chen. She helped me a lot in learning to use the noise system in the lab. I thank Guoxing Duan for his helping me in learning wire bonding and doing the stress measurements. I thank Kai Ni and Huiqi Gong for the illuminating discussion. I am also grateful to my other friends in Vanderbilt University. I thank my classmate Bingshu Wang for his help in Python coding.

At last, I would like to thank my family for their unconditional love and support. It is their support and encourage that make me keep moving forward in my life journey.

TABLE OF CONTENTS

PAGE

ACKNOWLEDGEMENTS .... **ii**

LIST OF FIGURES .... **vi**

LIST OF TABLES .... **xii**

ABSTRACT **1**

Chapter

I. introduction **2**

1.1 GaN and AlGaN Material Properties 2

1.2 AlGaN/GaN HEMTs 4

1.2.1 GaN-based HEMTs architecture 4

1.2.2 Substrates 5

1.2.3 Growth processing 7

1.2.4 Passivation layer 7

1.3 Reliability issues 8

1.3.1 Degradation mechanisms 8

1.3.2 Radiation effects with high field stress 11

1.3.3 Techniques for characterization trapping phenomena 11

1.4 Overview 13

II. Background **16**

2.1 Hot carrier degradation in GaN HEMTs 16

2.2 OFF state dc degradation 19

2.3 Radiation effects in AlGaN/GaN HEMTs 22

2.3.1 Total ionizing dose effects 22

2.3.2 Displacement damage 24

2.4 Defects that cause degradation 27

2.4.1 Ga and N vacancies and interstitials 27

2.4.2 Oxygen related defects 31

2.4.3 Other defects 33

III. Experimental Setup **34**

3.1 Device information 34

3.2 DC Measurement 35

3.3 Low frequency 1/f noise 36

3.3.1 Introduction of 1/f noise testing 36

3.3.2 1/f noise measurement setup 40

3.4 Proton and X-ray irradiation setup 40
IV. Degradation and annealing effects caused by oxygen in AlGaN/GaN HEMTs **42**
4.1 Experimental details 42
4.2 Experimental results 43
4.3 Discussion 46
4.4 Conclusion 50
V. TID effects in passivated and unpassivated HEMTs **51**
5.1 Experimental details 51
5.2 Experimental results and analysis 52
5.2.1 TID and annealing responses of unpassivated HEMTs 52
5.2.2 TID and annealing responses of passivated HEMTs 53
5.2.3 Irradiation and annealing responses of unpassivated HEMTs with hot-carrier injection 54
5.3 Discussion 55
5.4 Conclusion 57
VI. Bias dependence of high field stress induced degradation in HEMTs **58**
6.1 Experimental details 59
6.2 Experimental Results 60
6.2.1 Gate bias dependence of high field stress induced degradation HEMTs at room temperature 60
6.2.2. Gate bias dependence of high field stress induced degradation at high temperature 65
6.2.3. Step drain bias stress induced degradation in AlGaN/GaN HEMTs 67
6.2.4 Low frequency noise 70
6.3 Discussion 73
6.4 Conclusion 78
VII. Worst-case bias for proton and 10-kev x-ray irradiation of AlGaN/GaN HEMTs **79**
7.1 Experimental details 79
7.2 Experimental results 81
7.2.1 Proton irradiation: GND bias 81
7.2.2 Proton irradiation and stress: OFF bias 83
7.2.3 Proton irradiation and on/semi-on state stress 85
7.2.4 Biased X-ray irradiation 87
7.3 Discussion 89
7.4 Conclusion 92
VIII. Summary and conclusions **94**
REFERENCES **97**

LIST OF FIGURES

Figure **Page**

Fig. 1.1. Schematic drawing of the crystal structure of wurtzite Ga-face and N-face GaN (after [12]). 4

Fig. 1.2. Basic HEMT structure. (after [7]).. 5

Fig. 1.3. Schematic diagrams of (a) I_D–V_D curve and (b) I_D-V_G curve. The red dot shows the typical bias point we us for reliability testing. 9

Fig.1.4 Schematic cross section of an AlGaN/GaN HEMT, identifying critical areas which can be subjected to degradation (after [39]). 9

Fig. 2.1. (a) Top: EL image (intensity in false colors) of a device biased at V_{DS} = 20 V, V_{GS} = 0 V. (b) Bottom: EL image taken in the same electrical conditions after 5-h OFF-state test at V_{DS} = 27 V, V_{GS} = −8 V. (after [39]) 17

Fig. 2.2. Intensity of the EL signal emitted by one of the analyzed HEMTs, as a function of the drain and gate voltage levels. (after [74]).. 18

Fig. 2.3. Electron-energy distribution at x = 0.4 μm with different gate biases (after [75]). The inset is [36, Fig. 6].. 18

Fig. 2.4. TEM images showing the variation of defect sizes at the center and near the edge along the gate finger; (a) and (b) are images from the same finger, but in different positions. (c) and (d) are images from the same positions as (a) and (b), but on a finger from a different device (after [48]). 19

Fig. 2.5. (left) Arrhenius plot of the time constant of the process responsible for the negative V_{th} shift during stress. The activation energy of 0.37 eV is reported. (right) Schematic representation of the process responsible for the negative Vth shift. The surface donors are not indicated for simplicity. (after [83]) 21

Fig. 2.6. Schematic energy band diagram for MOS structure under positive bias, indicating major physical processes underlying radiation response. After [91]. 23

Fig. 2.7. Drain current vs. gate voltage for the CGH40006P as a function of total ionizing dose using 10 keV X-rays up to a dose of 1 Mrad(SiO_2). Note a negative shift in threshold voltage. This plot shows the worst-case threshold voltage shift of the two Cree devices tested for TID. The arrow indicates the direction in increasing radiation. (after [58]) 24

Fig.2.8. Simple model for radiation defects created in GaN by protons and other ionizing radiation. After [62]. 25

Fig.2.9 (a) SRIM simulation results of (a) energy loss and as a function of target depth, (b) Threshold voltages shift and transconductance reduction as a function of irradiation energies at a fluence of $5x10^{15}cm^{-2}$. (after [98]) 26

Fig. 2.10. Formation energy of (a) Ga-N divacancies and (b) N vacancies as a function of the position of the Fermi level in the band gap of $Al_{0.3}Ga_{0.7}N$. (after [64]). The slopes indicate different charge states. 28

Fig. 2.11. Comparison of defect levels calculated from first-principles and trap concentration dependence on ammonia flow as in Ref. 44........ 29

Fig. 2.12. Energy barriers as a function of O–N distance and defect configurations (I) and (II) of O –H (smaller light atom). (after [65]) 33

Fig. 3.1. Schematic diagrams of passivated AlGaN/GaN HEMT structures ([13][25][27]). 34

Fig. 3.2 Topview of DUT [111]........ 35

Fig. 3.3. DC characterstics (a) I_d-V_g (left) and I_g-V_g (right) curves and (b) I_d-V_d curves for AlGaN/GaN HEMTs. 36

Fig. 3.4. high-speed package (after [112].) 36

Fig. 3.5. Example: excess voltage noise power spectral density S_{vd} as a function of frequency for AlGaN/GaN HEMTs at 300 K, V_{gs} - V_{th} = 0.8 V, V_d = 0.05 V. 37

Fig. 3.6. Experimental and calculated frequency exponent of noise power spectral density as a function of temperature from 85 K to 400 K.(after [61]) 39

Fig. 3.7 Low frequency 1/*f* noise measurement system. (after[123])........ 40

Fig.4.1 Threshold voltage shift and (b) normalized peak transconductance for V_{ds} = 0.5 V, 2 V, and 5 V as a function of stress and annealing time for NH_3-rich unpassivated devices. All measurements and stressing were performed at room temperature under room ambient conditions, with V_{ds} = 15 V and V_{gs} = -2 V. The post-stress annealing was performed with all pins grounded. Devices were not exposed to light during stressing, annealing, or measurement. 44

Fig. 4.2. Normalized peak transconductance at V_{ds} = 0.5 V as a function of stress and annealing time in

(a) NH_3-rich passivated devices and (b) Ga-rich unpassivated devices. 46

Fig. 4.3. Normalized peak transconductance at V_{ds} = 0.5V as a function of stress time in NH_3-rich unpassivated devices before and after baking in air at 400K for 1 h. The red dots and blue triangles show results for devices measured 1 hour after baking and 48 hours after baking, respectively. 46

Fig. 4.4. Formation energy of O_N in AlGaN as a function of the AlGaN Fermi level. The blue arrow shows the position of the +1/0 transition level. The dotted line shows the position of the CBM of GaN. The three straight lines with different colors represent three different charge states of O_N. 47

Fig. 5.1. Changes in (a) threshold voltage and (b) normalized peak transconductance as a function of total ionizing dose and annealing time for Ga/AlGaN HEMTs that vary in device processing and passivation.. 52

Fig.5.2. I_g-V_g curves for (a) ammonia-rich unpassivated HEMTs and (b) Ga-rich unpassivated devices at V_d = 0.5 V before and after X-ray irradiation.. 53

Fig. 5.3. (a) I_d-V_g curves AlGaN/GaN HEMTs at V_d = 0.5 V before and after X-ray irradiation with all pins grounded. (b) The threshold voltage as a function of total ionizing dose and time...................... 53

Fig. 5.4. (a) Threshold voltage shift and (b) changes in peak transconductance as a function of time under X-ray irradiation and/or voltage-stress at 15 V drain bias and -2 V gate bias............................ 55

Fig. 6.1. (a) Schematic diagram of HEMT structures grown on GaN-on-SiC substrates – not to scale. (After [23].) (b) Top view of DUT. The devices have two sources. For stressing and device testing in the OFF and Semi-ON states, both sources are connected. For ON state stressing and testing, only one of the two sources is connected to limit heating effects.. 59

Fig. 6.2. V_{th} shifts versus stress time and gate bias in AlGaN/GaN HEMTs with (a) PAMBE GaN substrates and (b) MOCVD GaN substrates. Red data points show the ON bias condition, blue points show the Semi-ON bias condition, and black points show OFF bias conditions. The applied drain voltage is 20 V in all cases, and all stresses and measurements were performed at room temperature............ 62

Fig. 6.3. Normalized peak transconductance degradation as a function of stress time under different gate bias in AlGaN/GaN HEMTs with (a) PAMBE GaN substrate and (b) MOCVD GaN substrate . The red data points show ON bias condition, blue points show Semi-ON bias condition and black points show OFF bias conditions 62

Fig 6. 4. (a) Measured V_{th} shifts and (b) peak transconductance degradation after 10 h stress as a function of gate bias. 63

Fig. 6. 5. (a) Threshold voltage and (b) normalized peak transconductance degradation as a function of stress time under V_{ds}=20V, V_{gs}-V_{th}=5.5V in AlGaN/GaN HEMTs with MOCVD GaN substrate for half device with single source and whole device with double source. 64

Fig 6. 6 (a) Threshold voltage shift and (b) normalized peak transconductance degradation as a function of stress time and room-temperature annealing time for AlGaN/GaN HEMTs with PAMBE and MOCVD grown substrates stressed under represenrative ON state, Semi-ON state and OFF state. Annealing was performed at room temperature with all pins grounded. 64

Fig. 6. 7. the normalized transconductance as function of V_{gs}-V_{th} (over drive gate bias) for MOCVD GaN substrate devices before and after 10 hours stress with V_{gs}-V_{th}=-3.6V, V_{ds} =10V......................... 65

Fig. 6.8. (a) Threshold voltage and (b) normalized peak transconductance degradation for ON (squares), OFF (triangles), and Semi-ON (circles) state stressed for Ga-rich PAMBE GaN substrate devices from UCSB that were stressed and measured at 300 K (solid symbols) and 400 K (open symbols). Similar trends in response were observed for devices on MOCVD substrates... 66

Fig. 6.9. Temperature dependence of (a) V_{th} shifts and (b) normalized peak transconductance degradation for Ga-rich PAMBE GaN substrate devices. 66

Fig. 6.10. I_d-V_g curves for AlGaN /GaN HEMTs at V_d = 0.5 V for Ga-rich PAMBE GaN substrate devices from UCSB before and after ON state bias stress. The gate bias is 1 V during the stressing process (ON state). The drain bias stress starts at 10 V, with a step of 5 V. For each condition, devices are stressed for ~ 10 h. 67

Fig. 6.11. (a) Threshold voltage and (b) normalized peak transconductance degradation under a series of drain biases for Ga-rich PAMBE GaN substrate devices from UCSB. The transconductance is normalized to the peak transconductance of a fresh device. 68

Fig. 6.12. I_d-V_g curves for AlGaN /GaN HEMTs at V_d = 0.5 V for Ga-rich PAMBE GaN substrate devices from UCSB before and after OFF state bias stress. The gate bias is -6 V during the whole process (OFF state). The drain bias starts from 10 V, with a step of 5 V. For each condition, devices are stressed for around 8 hours, which is sufficiently long for degradation to reach saturation at low biases............... 69

Fig. 6.13 (a) Threshold voltage shift and (b) normalized peak transconductance degradation under a series of drain biases for Ga-rich PAMBE GaN substrate devices. The transconductance is normalized to the peak transconductance of a fresh device. 69

Fig. 6.14 Example: excess voltage noise power spectral density S_{vd} as a function of frequency for AlGaN/GaN HEMTs at 300K, V_{gs}-V_{th} = 0.8 V, V_d = 0.05 V. 71

Fig. 6.15. Temperature-dependent noise measurements from 85 to 400 K, at f = 10 Hz for Ga-rich PAMBE devices fabricated at UCSB. The noise is measured under the same conditions as in Fig. 5. The temperature range corresponds to an activation energy scale ranging from 0.2 to 0.95 eV (top *x*-axis). The stress bias condition is (a) ON state and (b) OFF state. 72

Fig. 6.16 Experimental and calculated frequency exponent of noise power spectral density as a function of temperature from 85 K to 400 K. 72

Fig. 6.17. (a) Defect energy of substitutional O in AlGaN as a function of the distance from the ideal lattice site, showing the existence of a DX configuration. Black squares represent transition points between the charge states of O_N during the electron emission. The dashed line shows that the energy barrier to emit one electron from a negatively charged O DX center is 0.25 eV. (b) This diagram schematically illustrates the capture of one electron by the neutral charged oxygen O_N^0, which involves thermally excited tunneling (red arrow) of an electron from a GaN Fermi level to the empty level of O_N^0 defect in AlGaN. The activation energy of the capture is 0.35 eV. (After [71].) 77

Fig. 7.1. Schematic diagrams of HEMT structures regrown on GaN-on-SiC templates and FS GaN substrates[29]: (a) HEMT structures on GaN-on-SiC and (b) HEMT structures on FS GaN. 80

Fig. 7.2. I_d-V_g curves for AlGaN/GaN HEMTs at V_d = 1 V before and after proton irradiation with all pins grounded: (a) HEMT on GaN-on-SiC and (b) HEMT on FS GaN. DC characterization was performed with V_{ds} = 0.5 V. 82

Fig. 7. 3 (a) Peak transconductance and (b) threshold voltage as a function of proton fluence for the devices of Fig. 7.2. 82

Fig. 7. 4. Normalized peak transconductance of AlGaN/GaN HEMTs with (a) GaN on SiC substrate and (b) FS GaN substrate as function of proton fluence for OFF state (V_{ds} = 20 V, V_{gs} = -6 V) and GND irradiation and/or voltage stress. The solid line shows device response to pure high field stress. DC characterization was performed with V_{ds} = 0.5 V. The inset in (a) shows the changes in normalized transconductance as a function of V_g-V_{th} before and after 1h stress. 84

Fig. 7. 5. V_{th} shifts for the AlGaN/GaN HEMTs of Fig. 4.4 with (a) GaN on SiC substrates and (b) FS GaN substrates as function of proton fluence and/or stress time for OFF state bias (V_{ds} = 20 V, V_{gs} = -6 V) and GND bias. The solid line shows the device response to pure high field stress. 85

Fig. 7. 6. Normalized peak transconductance of AlGaN/GaN HEMTs with (a) GaN on SiC substrates and (b) FS GaN substrates as functions of proton fluence for ON state (V_{ds} = 20 V, V_{gs} = 1 V), Semi-ON state (V_{ds} = 20 V, V_{gs} = -2 V) and GND irradiation and/or voltage stress. The dark red and green lines (no symbols) show device response to pure high voltage stress. DC characterization was performed with V_{ds} = 0.5 V. 86

Fig. 7.7. V_{th} shift of the AlGaN/GaN HEMTs of Fig. 7.6 with (a) GaN on SiC substrates and (b) FS GaN substrates as function of proton fluence for ON state (V_{ds} = 20 V, V_{gs} = 1 V), Semi-ON state (V_{ds} = 20 V, V_{gs} = -2 V) and GND irradiation and/or voltage stress. The red and green lines (no symbols) show device response to pure high voltage stress. 87

Fig. 7.8. Normalized peak transconductance of AlGaN/GaN HEMTs with (a) GaN on SiC substrates and (b) FS GaN substrates as function of total ionizing dose and/or stress time for ON state (V_{ds} = 20 V, V_{gs} = 1 V) and OFF state (V_{ds} = 20 V, V_{gs} = -6 V) irradiation and/or stress. 89

Fig. 7.9. Vth shift of the AlGaN/GaN HEMTs of Fig. 4.8 with (a) GaN on SiC substrates and (b) FS GaN substrates as function of total ionizing dose and time for ON state (V_{ds} = 20 V, V_{gs} = 1 V) and OFF state (V_{ds} = 20 V, V_{gs} = -6 V) irradiation and/or stress. 89

Fig. 7.10. Temperature-dependent noise measurements from 85 K to 400 K, for unirradiated GaN on SiC devices from this work, and for unirradiated Qorvo devices from [61]. Here $V_g - V_{th}$ = 0.4 V, V_d = 0.03 V, and f = 10 Hz for the Qorvo devices, and $V_g - V_{th}$ = 0.5 V, V_d = 0.03 V and f = 10 Hz for the GaN on SiC devices fabricated by UCSB. 91

Fig. 7.11. Temperature-dependent noise measurements from 85 K to 400 K in (a) unirradiated devices and devices irradiated with worst-case ON bias for GaN on SiC devices fabricated by UCSB, and (b) Qorvo devices from [61] irradiated with worst-case semi-ON bias. Fluences are quoted in protons/cm^2. 92

LIST OF TABLES

Table **Page**

1-1: Comparison of material properties at room temperature (300K) (Si [10],GaAs[10], 4H-SiC [11], GaN[4][5][6],and AlN [4][5][6]) 3

1-2. Comparison of substrate properties [30]. Note that lattice mismatch and thermal mismatch are calculated by (Substrate-GaN/GaN). 6

2-1. Defects that responsible for electrical and radiation-induced degradation seen in previous work. The activation energy are calculated by DFT…...30

ABSTRACT

During the last three decades, GaN-based HEMTs are increasingly developed for their excellent application for high power, high frequency and radiation-tolerance. The improvements in GaN-based HEMTs fabrication result in a material with better quality and devices with better performance, which makes the defects generated during use a more obvious factor in device reliability. This results in a different degradation behavior after stress and some phenomena not observed before such as total ionizing dose effects. In this work, we tested AlGaN/GaN HEMTs with several different structures and growing processes. The bias dependence of reliability and radiation response of AlGaN/GaN HEMTs are studied. Density functional theory (DFT) calculations and low frequency 1/f noise measurements are used to help identify the possible defects responsible for the electrical stress induced degradation and radiation effects. We first compare the hot carrier degradation and annealing performance and total ionizing dose effects in devices with or without a passivation layer. Hydrogenated O_N defects are found to be important in hot carrier effects and total ionizing dose effects in AlGaN/GaN HEMTs. Then the bias dependence of high field stress and its combination effects with X-ray and proton irradiation are evaluated. Different worst bias case was found in devices with different growing processes. This is attributed to multiple defects that occur in different locations in the devices. These results emphasize the need to test devices under a wide range of conditions during characterization and qualification testing.

CHAPTER I

INTRODUCTION

The bias dependence of the radiation response and reliability of AlGaN/GaN HEMTs are investigated in this thesis. Gallium Nitride (GaN) is a III-V compound semiconductor with wide bandgap. GaN-based high electrical mobility transistors (HEMTs) have attracted a huge amount of attention over the last two decades for applications in high power and high efficiency radio-frequency systems. The lack of oxide layer also makes AlGaN/GaN HEMTs very robust in radiation environments [1][2][3], which makes them very promising in aerospace application. In this first chapter, a general overview of GaN-based devices is provided, including the material properties, device architectures, radiation effects and reliability issues.

1.1 GaN and AlGaN Material Properties

Gallium Nitride (GaN) and Aluminum Nitride (AlN) are both wide bandgap semiconductors, with band gaps as large as 3.4 eV and 6.2 eV, respectively. The breakdown field is 3.3 MV/cm for GaN and 12 MV/cm for AlN [4][5][6]. AlN can form thermal stable alloys with Ga. In particular, it is possible to tune the bandgap: from 6.2 eV (pure AlN) to 3.4 eV (pure GaN). The band gap of AlGaN can be well controlled by the component of Al. In AlGaN/GaN HEMTs, the component of Al is often around 0.25-0.3 [7][8], whose bandgap is around 4.1 to 4.3. The wide bandgap results in very low intrinsic carrier concentration even at high temperature. This allows high temperature

operation without excessive leakage. In addition, GaN has a high saturation electron velocity (~ 2.5×10^7 cm/s) [4]. Due to the band off-set at the AlGaN/GaN interface and the polarization, a quantum well and a layer of 2DEG (two dimensional electron gas) can spontaneously be formed at the AlGaN/GaN hetero-junction, allowing for high electron mobility. The room temperature mobility of the 2DEG is typically between 1200 and 2000 cm^2/Vs [9]. Due to the wide band gap and high electron mobility, AlGaN/GaN high electron mobility transistors (HEMTs) are promising for high-power and high-frequency applications.

Table 1-1: Comparison of material properties at room temperature (300K) (Si [10],GaAs[10], 4H-SiC [11], GaN [4][5][6],and AlN [4][5][6])

	Si	GaAs	4H-SiC	GaN	AlN
Eg(eV)	1.12	1.43	3.2	3.4	6.2
ε_r	11.7	13.1	10	9	8.5
$\mu(cm^2/(Vs))$	1500	8500	800	900	300
$V_{sat}(10^7 cm/s)$	1	1	2	2.5	1.4
E_{br}(MV/cm)	0.3	0.4	3	3.3	12
$N_i(cm^{-3})$	$1.05\text{x}10^{10}$	$1.8\text{x}10^6$	$9\text{x}10^{-7}$	$1.9\text{x}10^{-10}$	$9.4\text{x}10^{-34}$

The thermodynamically stable crystal structure for GaN-based materials is wurtzite [12]. The most common growth direction of GaN epitaxial layers is along the c-axis [12]. The lack of inver-

sion symmetry along this polar axis results in a spontaneous polarization. Depending on the different growth conditions, GaN can either have a Ga-face or N-face termination, as schematically shown in Figure 1.1 [12]. A different face termination leads to different spontaneous polarization properties due to the charge transfer from the strongly electronegative N and less electronegative Ga. Nowadays, GaN-based devices are normally fabricated with Ga-face termination [13]. The alloyed AlGaN crystal shares the same polarization properties with GaN. Additionally, the lattice mismatch between GaN and AlGaN leads to a piezoelectric polarization when an AlGaN layer is epitaxially grown on top of GaN material. The spontaneous and piezoelectric polarization-induced high density 2DEG are the fundamental mechanisms for forming AlGaN/GaN-based electronics.

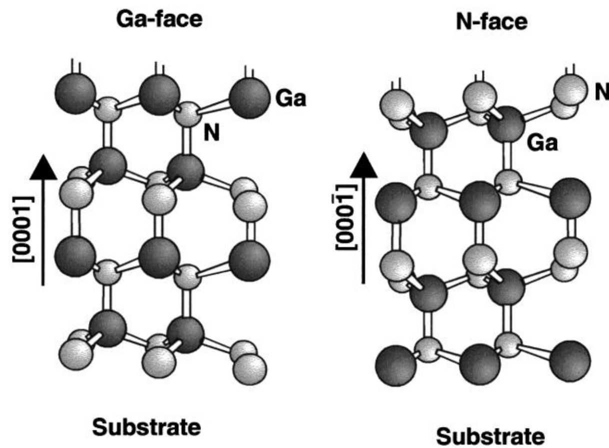

Fig. 1.1. Schematic drawing of the crystal structure of wurtzite Ga-face and N-face GaN (after [12]).

1.2 AlGaN/GaN HEMTs

1.2.1 GaN-based HEMTs architecture

An AlGaN/GaN high electron mobility transistor (HEMT) was first demonstrated in [14]. A 2DEG layer is present at the interface between the AlGaN and GaN buffer layer. Due to the high

carrier concentration and the high mobility guaranteed by the unintentional doped structure, the 2DEG works as an ideal transistor channel. An AlGaN/GaN HEMT is a three-terminal device, which has a Schottky metal gate and an Ohmic contact on the drain and source electrode. The current between the source and drain contact can flow through the two dimensional conducting channel. The channel is controlled by applying a gate voltage that can locally deplete it.

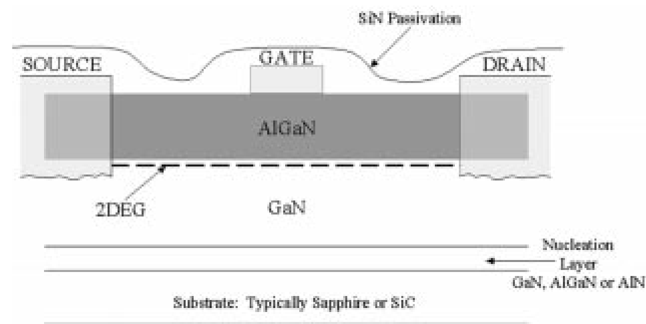

Fig. 1.2. Basic HEMT structure. (after [7])

1.2.2 Substrates

The ideal substrate for GaN epitaxy should be a GaN bulk wafer. However, due to the cost and limited size of a GaN bulk wafer, AlGaN/GaN HEMTs are typically grown on a large-size foreign substrate, such as such as sapphire, silicon carbide (SiC), diamond or silicon (Si). The GaN-based device was first demonstrated on a sapphire substrate [15], which has the advantages of low cost as well as mechanical and thermal stability. However, its low thermal conductivity severely limits the power performance of sapphire-based GaN-based power electronic devices [16][17][18]. By introducing a proper buffer layer and optimizing the growth conditions, growing high quality GaN layers on 8-inch Si substrates [19][20][21][22] has recently been demonstrated. This allows

for the implementation of the subsequent device processing in an already existing Si-based processing environment. Compared with sapphire and Si, SiC is a better a substrate to grow GaN, due to its excellent thermal conductivity and the small lattice mismatch between SiC and GaN. Diamond substrates are also investigated for their high thermal conductivity [23]. GaN-on-diamond demonstrated half of the thermal resistance of that on GaN-on-SiC, but the output power of GaN-on-diamond devices is limited by the relatively lower current density. These hetero-epitaxial growth methods pose a serious challenge on how to obtain a high quality GaN epitaxial layer due to the lattice and thermal mismatch. The typical density of threading dislocations (TDs) is on the order of 10^8 to 10^{10} cm^{-2} [13]. This high density can both reduce the electron mobility in 2 DEG [24] and increase the gate leakage current [25]. Homo-epitaxial growth of GaN on a freestanding GaN substrate can effectively reduce the density of TDs to ~$10^7 cm^{-2}$ [13][26]. Recently, AlGaN/GaN HEMT devices have often preferred to use extrinsic deep-level dopants in the GaN substrate to improve the buffer's insulating properties. The two widely used buffer dopants are iron (Fe) and carbon (C). [27][28][29]

Table 1-2. Comparison of substrate properties [30]. Note that lattice mismatch and thermal mismatch are calculated by (Substrate-GaN/GaN).

	Lattice constant (Å)	**Lattice Mismatch (%)**	**Themal Expansion Coeffecient ($10^{-6}K^{-1}$)**	**Thermal Mismatch (%)**	**Thermal Conductivity (W/(cmK))**
GaN	a=3.19	0	5.6	0	1.3
Sapphire	a=4.75	49	7.5	33.9	0.5
SiC	a=3.08	-3.5	4.2	-25	3.3
Si(111)	5.43	70	3.59	-35.8	1.5

1.2.3 Growth processing

Both metal organic chemical vapor deposition and MBE techniques are widely used in growing GaN layers. It was reported that the orientation of (Al)GaN epitaxial layers grown by metalorganic chemical vapor deposition (MOCVD) is normally (0001), whereas either the (0001) or the $(000\bar{1})$ orientation can be obtained with molecular-beam epitaxy (MBE) [31]. MOCVD growth is more widely used in industry, due to its higher growth rate. On the other hand, the MBE growth can get precise definition of interfaces, low point defect concentrations and very low carbon and hydrogen impurity concentrations. Thus, some techniques use MOCVD to grow the carbon doped GaN substrate and plasma-assisted MBE (PAMBE) for the unintentionally doped (UID) GaN layer and the AlGaN layer. On the other hand, impurities may diffuse into the UID GaN layer. To reduce this effect, an AlGaN back barrier inserted between the C doped GaN and UID GaN layer is also investigated [29]. PAMBE generally involves precisely controlled, low-temperature Ga-rich growth. The GaN buffer layer is usually grown at ~700 ^{o}C to smooth the surface and reduce TDD [32]. Another MBE technique used in GaN growth is NH_3-MBE. The NH_3-MBE technique grows at higher temperatures compared with PAMBE techniques, i.e. 800 ^{o}C to 900 ^{o}C, and can obtain high electron mobility GaN layers on sapphire and SiC substrates [13].

1.2.4 Passivation layer

It is believed that surface states at the AlGaN surface provide the source of electrons for the 2DEG channel [33]. The as-grown structure has some fixed donor-like traps on its surface [34].

This surface trap can cause a dispersion between the large signal alternating current (ac) and direct current (dc) characteristics of the HEMTs, referred to as "DC to RF dispersion" or "current collapse". Deposition of a SiN passivation layer is an effective way to eliminate this effect, though the exact mechanism is still under debate [7][8][35][36][37]. Moreover, passivation of device surfaces with Si_3N_4 can have a beneficial effect on hot carrier degradation. [38]

1.3 Reliability issues

1.3.1 Degradation mechanisms

A comprehensive understanding of degradation mechanisms and the related effects on GaN-based HEMTs is essential for the design of more effective devices and improving their robustness under operation conditions. Therefore, GaN-based devices need to be examined using various reliability tests in order to verify their capabilities for power switching applications. As schematically shown in Figure 1.3, a power device continuously switches from an OFF-state to an ON-state condition. Therefore, the stability of GaN-based devices needs to be tested in regions, such as ON-state (high current, relatively low electric field), OFF-state (very low current, very high electric field), and SEMI-ON state (medium current, relatively high electric field) [39][40][41][42].

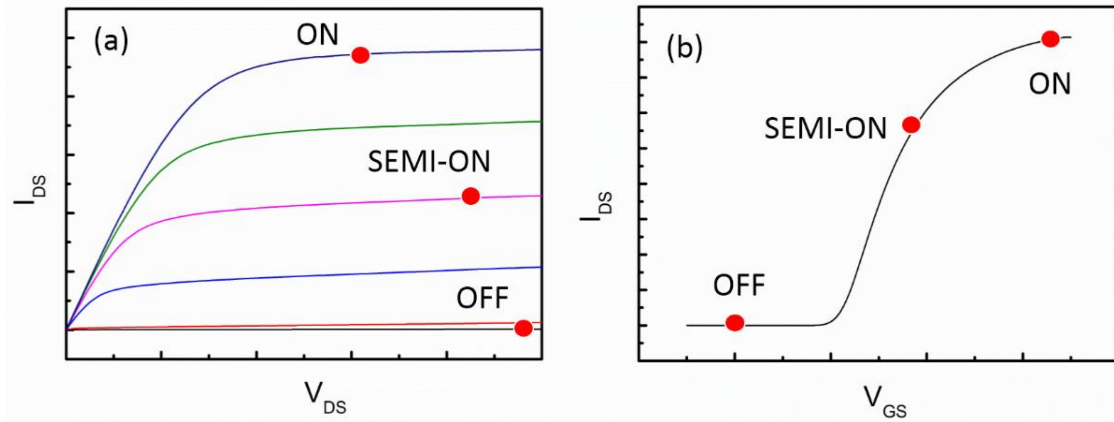

Fig. 1.3. Schematic diagrams of (a) I_D–V_D curve and (b) I_D-V_G curve. The red dot shows the typical bias point we us for reliability testing.

Ref [39]summarized the main failure mechanism in GaN-based HEMTs, as shown in Fig 1.4. At high temperature, the gate metal can diffuse into the semiconductor and form deep trap level, which is defined as "Gate sinking" [43], is one of the main reason that causes device failure in GaAs-based MOSFETs and HEMTs. But in GaN-based HEMTs, no significant degradation in gate contact is observed in either Schottky contact or Ohmic contact when the temperature is below 300 ^{o}C [44].

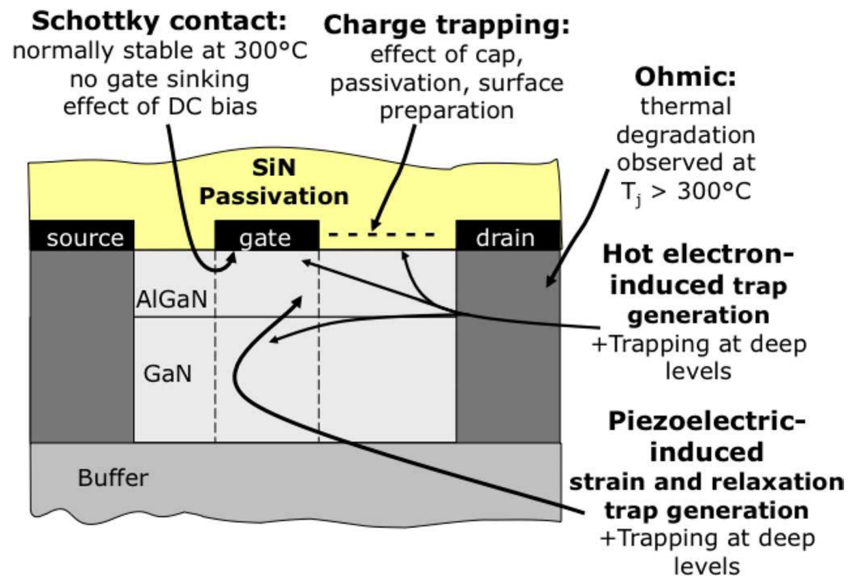

Fig.1.4 Schematic cross section of an AlGaN/GaN HEMT, identifying critical areas which can be subjected to degradation (after [39]).

Charge trapping is induced by the pre-existing defects on the AlGaN surface (for unpassivated devices) or AlGaN-SiN interface, which can be generated during or after the fabrication [45]. The charge or discharge of defects may change the surface potential and form a "virtual gate" [36]. As trapping and detrapping processes are usually very fast, charge trapping is the most important issue in device short term reliability [41]. This effect is more significant in OFF-state conditions [46] and AC testing. As mentioned in 1.2.4, charge trapping is believed to be very important to cause the "current collapse" [36][37].

Hot carrier effects can generate traps near the channel [41][47][48][49][50]. As GaN HEMTs typically work under high voltage, the high field in the channel may form "hot electrons". When devices are operating at high drain voltages with high carrier densities, energetic hot carriers produced by the high electric field can depassivate or reconfigure defects near the AlGaN/GaN interface by dehydrogenation [49] [51]. This effect will result in a degradation in transconductance and increase the ON resistence (R_{ON}), as well as cause a shift in threshold voltage. The semi-ON bias condition is typically the worst case for hot-carrier stress, because it has both high enough carrier density and electric field. This is confirmed by both electrical and electroluminescence (EL) tests [39].

Inverse piezoelectric effect is another mechanism that may generate new traps [52]–[55]. As the center of the strongly electronegative N atom and less electronegative Ga do not coincide, the electric field in the gate-drain region increases the strain in the AlGaN/GaN heterojunction ("inverse piezoelectric effect") Due to their lattice mismatch, AlGaN on GaN is typically under substantial tensile strain and therefore stores a sizable amount of elastic energy at rest. If the elastic

energy exceeds a critical value, it will eventually result in strain relaxation and crystallographic defect formation. Joh and del Alamo [54] have found that the critical gate-drain voltage occurs around $V_{GD} \approx$ 20-30 V for the tested devices. This effect results in a sudden and non-reversible increase in the gate leakage current. To solve this problem, lattice matched InAlN/GaN HEMTs are investigated [56].

1.3.2 Radiation effects with high field stress

The radiation response and reliability of AlGaN/GaN HEMTs are the subjects of intense research [1]–[3], [57]–[65] . As the gate of an AlGaN/GaN HEMT is controlled by a Schottky contact without the oxide layer, AlGaN/GaN HEMTs are believed to be super hard to total ionizing dose (TID). However, significant shifts in threshold voltage have been observed for other research- and industrial-grade devices during 10-keV X-ray irradiation [57], [58]. Besides the total ionizing dose effect, the more important radiation effect is the displacement damage caused by energetic particles such as protons. The traps generated by the displacement damage result in the reduction in device transconductance [65] and on-state current [1]. Recent work has shown that the sensitivity of AlGaN/GaN HEMTs to proton irradiation can be greatly enhanced by high-field stress during irradiation [61], with the Semi-ON bias condition demonstrated to be worst-case for both threshold-voltage shifts and trans-conductance degradation of devices fabricated by Qorvo, Inc.

1.3.3 Techniques for characterization trapping phenomena

Many electronic and electrooptical techniques are used to characterize the trapping phenomena in GaN HEMTs. Here is the list of the most widely used:

1) Deep-level transient spectroscopy (DLTS). This technique is based on the analysis of capacitor (C-DLTS) [66][67] or drain current (I-DLTS) [67] transients as a function of channel temperature. These techniques can provide very accurate information on the activation energy and cross section of the traps. But the C-DLTS is limited by the gate area of the devices. The devices should be large enough for standard capacitance measurements.

2) Low frequency $1/f$ noise. Trapping and detrapping of electrons in interface traps can result in a fluctuation in drain current, leading to noise with $1/f$ dependence [68][69][70]. Like DLTS, the temperature dependence of excess drain-voltage noise power spectral density S_v can also provide the information of defect activation energy [68][71][72]. As the measurement is taken at very small V_{ds} and V_{gs}, no damage will happen during the measurement. In this PhD defense, we use $1/f$ noise measurements for trap characterization. A more detailed introduction of this technique will be included in Chapter 3.

3) Gate (drain) lag measurements [72]. This technique measures the drain current at fixed drain voltage and the gate voltage pulsed from pinch-off to open channel condition (gate-lag) or fixing gate voltage and drain voltage pulsed from OFF-state to open channel condition (drain-lag). Results of gate and drain-lag measurement can provide information on the time constants of traps.

4) Electroluminescence [39][73][74]. With the combination of electrical and optical methods, electroluminescence is widely used in characterization of hot carrier effects. This measurement is can be taken at the nominal operating conditions and provides information about the electric field and equivalent temperature of hot-electrons. This technique is also used to identify the failed regions.

1.4 Overview

This PhD thesis focuses on the bias dependence of radiation effects and reliability of AlGaN/GaN HEMTs. For the reliability part, we tested the device under three bias conditions: ON, semi-ON and OFF. For radiation effects, both 1.8 MeV proton irradiation and 10 keV X-ray irradiation are investigated.

In Chapter I, we presented a brief introduction of GaN material and GaN-based HEMTs structures. Reliability issues and the most common experimental methods used to study the reliability of AlGaN/GaN HEMTs were discussed.

In Chapter II, we give a more detailed introduction about the background knowledge for this work. Physical mechanism and previous work in hot carrier effects, off state degradation, total ionizing dose effects and displacement damage will be included. We give a summary of the defect candidates that have been found to be responsible for the high field stress induced degradation and radiation effects in AlGaN/GaN HEMTs.

In Chapter III, the information of the devices we tested is given. We also introduce our setup for experiments, including stress setup, DC measurements and 1/*f* noise measurements.

In Chapter IV, we report the degradation and room temperature annealing effects in AlGaN/GaN HEMTs grown under NH_3-rich conditions. After stress and annealing, the peak transconductance of unpassivated devices is often higher than its original value. This "super-recovery" is not observed in passivated devices. Density functional theory (DFT) calculations suggest that

dehydrogenation of pre-existing O_N-H defects in AlGaN plays a significant role in hot carrier degradation of NH_3-rich AlGaN/GaN HEMTs. The resulting bare O_N impurity centers can naturally account for the observed super-recovery in peak transconductance.

In Chapter V, we first compare device response to 10 keV X-ray irradiation in unpassivated and passivated devices. Ammonia-rich unpassivated devices show peak transconductance degradation and negative threshold voltage shifts after X-ray irradiation. But only negative V_{th} shifts are observed in passivated devices. Oxygen and hydrogen impurities are found to contribute to the responses.

In Chapter VI, we evaluate the gate dependence of hot carrier effects under fixed drain bias (20 V) and the device performance under a series of drain biases increasing from 10 V to 30 V or 40 V at two fixed gate biases: 1 V for ON state and -6 V for OFF state. Devices with two different processes are studied for comparison. In both kinds of devices, a positive shift in V_{th} is observed in the "ON" state and a large negative V_{th} shift in the "OFF" state. The worst cases for transconductance degradation are "ON" states for both devices. For step drain-bias stress testing, devices show typical hot carrier degradation under the "ON" state, which is similar to results obtained in previous devices [72]. But under the "OFF" state stress condition, both devices show increases in peak transconductance at low drain bias. The direction of the V_{th} shift changes from negative to positive with the drain bias increasing in one kind of device. The two different directions of V_{th} shift indicate at least two different kinds of defects or mechanisms should be responsible for high field stress-induced degradation in the "OFF" state.

In Chapter VII, we report the effects of 1.8 MeV proton irradiation, 10-keV X-ray irradiation,

and high-voltage stress on AlGaN/GaN HEMTs with two different processes, for a range of typical bias conditions: "ON" state, "Semi-ON" state and "OFF" state. The devices' response to irradiation is enhanced by the high electrical field stress but different devices show different worst cases. The worst-case response for transconductance degradation is observed for the "ON" bias condition, in one kind of devices, and "Semi-ON" for another. Significant total-ionizing dose (TID) effects are observed during 10-keV X-ray irradiation in each type of device. Low-frequency noise measurements are performed to evaluate the types of defects and the resulting defect energy distributions both before and after proton irradiation, for these devices.

In the Chapter VIII, a brief summary and conclusions are presented.

CHAPTER II

BACKGROUND

This PhD thesis focuses on the bias dependence of radiation effects and reliability of Al-GaN/GaN HEMTs. The reliability tests involve three bias conditions: ON state, semi-ON state and OFF state. For radiation effects, both 1.8 MeV proton irradiation and 10 keV X-ray irradiation are investigated. Hot carrier effects, total ionizing dose effects and/or displacement damage may occur during the stress and radiation processes. In this chapter, we will give a brief introduction of the mechanisms of these effects.

2.1 Hot carrier degradation in GaN HEMTs

In high power conditions, GaN HEMTs are often subject to high voltage and non-negligible drain current. Electrons injected from the source can be accelerated by the electric field and become “hot”. Hot carrier induced degradation is one of the most significant failure mechanisms of GaN HEMTs, due to shifts in threshold voltage and increases in on-resistance. This degradation can be recoverable [75], when caused by charge trapping, or permanent, if lattice defects are generated [49][76]. The density of hot electrons is determined by the source current, while the energy of hot carriers is defined by the electric field. Hot carrier effects need both high field and large current.

To get the information about electric field effects and hot electron concentrations, electroluminescence (EL) characterization is a technique often used to study hot carrier effects [39] [73][74].

Fig 2.1 shows an example of EL micrographs for ON-state and OFF state stress [39]. In Fig. 2.1(a), the false colors indicate a high density of hot carriers evenly distributed along the channel during ON-state stress. In Fig. 2.1 (b), the density of carriers is much smaller and the distribution shows a discontinuity. When measured as a function of V_{GS}, keeping V_{DS} constant, the EL intensity has a nonmonotonic "bell-shaped" behavior similar to that of gate current in GaN HEMTs [77], as shown in Fig. 2.2 . When V_{GS} is smaller than the pinch-off value, the gate-drain voltage V_{GD} and the electric field are maximum, but there are no carriers in the channel, so no light is emitted. The intensity of the EL signal starts increasing when the gate voltage becomes higher than the pinch-off voltage. However, with a further increase in V_{GS}, a decrease in the average energy of the electrons in the channel and of the electroluminescence signal will be observed because the gate-to-drain electric field will decrease. The measurement of EL intensity as a function of V_{DS} and V_{GS} allows one to evaluate the severity of the "hot-electron-stress" in the device under test. The peak of the bell-shaped curve suggests a region with high density of carriers with high energy, which should be the most dangerous bias conditions for hot-electron-induced degradation, the so-called "semi-ON" region.

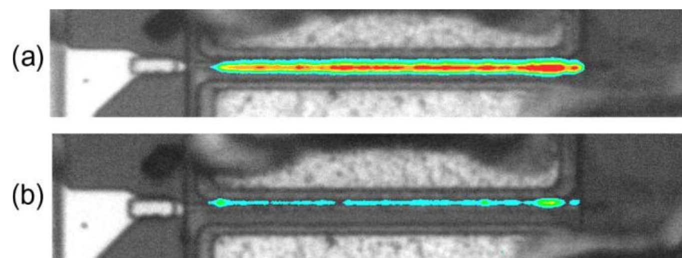

Fig. 2.1. (a) Top: EL image (intensity in false colors) of a device biased at $V_{DS} = 20$ V, $V_{GS} = 0$ V. (b) Bottom: EL image taken in the same electrical conditions after 5-h OFF-state test at $V_{DS} = 27$ V, $V_{GS} = -8$ V. (after [39])

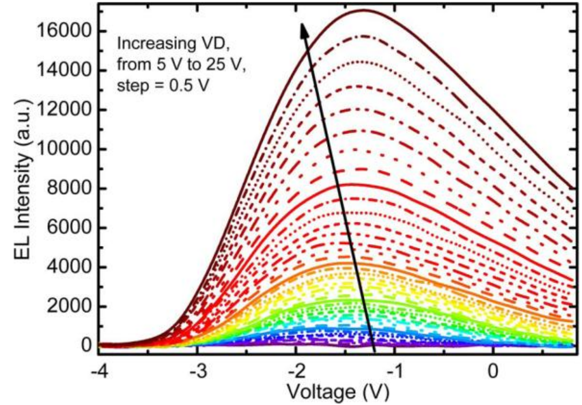

Fig. 2.2. Intensity of the EL signal emitted by one of the analyzed HEMTs, as a function of the drain and gate voltage levels. (after [74])

Monte Carlo analysis of hot-electron degradation in AlGaN/GaN HEMTs also suggests the maximum degradation occurs in the semi-ON bias condition [78][79]. Fig. 2.3 shows the number of electrons as a function of energy near the edge of the gate [78]. A spatial peak of electron density with an activation energy of 1.5 eV is observed for the Semi-ON bias condition, with a large tail extending over 3 eV. Electrons in the distribution tail have high energy, and the energy is sufficient for dehydrogenation of pre-existing defects, such as N antisites and Ga vacancies, which play an important role in hot carrier induced degradation [49][80].

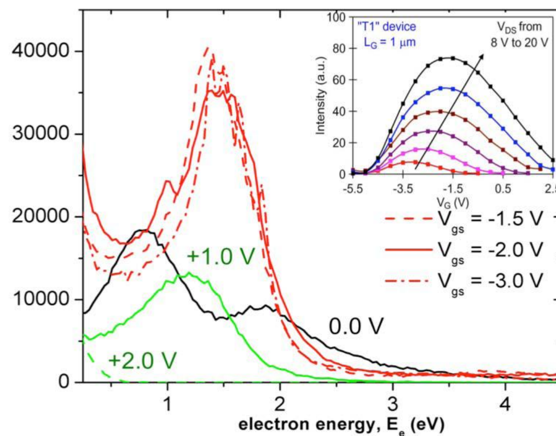

Fig. 2.3. Electron-energy distribution at x = 0.4 μm with different gate biases (after [75]). The inset is [36, Fig. 6].

2.2 OFF state dc degradation

DC degradation under OFF state bias is also described in this dissertation. Under the OFF-state condition, the device is biased at a high drain voltage with a negative gate bias under the cut-off condition, as shown in Fig. 1.3. The degradation is caused by the high electric field [40][81]. For DC characterization, the degradation mainly is observed as: 1) output current drop [53], 2) permanent leakage current increase [81][82] and 3) negative threshold voltage shift [83].

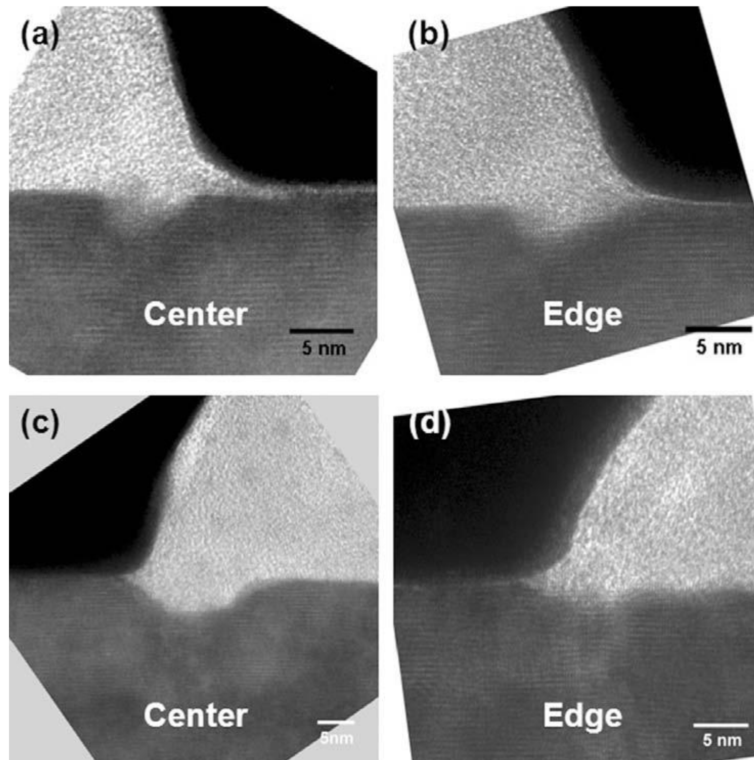

Fig. 2.4. TEM images showing the variation of defect sizes at the center and near the edge along the gate finger; (a) and (b) are images from the same finger, but in different positions. (c) and (d) are images from the same positions as (a) and (b), but on a finger from a different device (after [48]).

TEM analysis revealed that electrically degraded devices always contain a pit-like defect next to the drain [52] and/or gate [53] in the top AlGaN layer, as shown in Fig. 2.4. One of the most widely used theories to explain the formation of the pit-like defect is the inverse piezoelectric effect

[84]. As GaN and AlGaN are both polarized materials [4], large electric fields between the gate and drain can modify the strain configuration in the AlGaN layer. When a high electric field is applied, the AlGaN barrier expands due to the inverse piezoelectric effect. If the total strain exceeds a critical value, strain can relax through defect formation, such as dislocations. These traps can be charged and result in the reduction in the carrier concentration in the channel. This mostly happens right next to the gate where the fields are highest [85]. This effect can be resolved by using strainless InAlN instead of AlGaN. But this structure suffers the localization of In clusters, which can make the device performance unstable [86].

The hypothesis of inverse piezoelectric effects has several challenges. Marcon et al. found that gate degradation can occur under a lower gate voltage, which is below the critical voltage, mentioned by Joh, et al. in [54]. In Ref. [81], Marcon et al. showed that the gate leakage current increase should be due to the random formation of percolation path along the gate width, which is not related to inverse piezoelectric effect and does not lead to permanent output current drop. This degradation does not happen above or below a certain voltage. Instead, it is a time-dependent voltage accelerated phenomenon. Another explanation for the generation of the pit-like defect is vacancy migration [87]. Although the migration barrier for the vacancies are high, the barrier can be decreased significantly when a high electric field is applied by

$$\Delta E_{migr} = Eqd \cdot \tag{2.1}$$

Here E is the electric field strength along the direction of atomic migration, q is the charge state of the defect, and d is the distance from the initial site to the point of highest energy. The migration energies of Ga and Al vacancies in AlGaN under the combination of lattice mismatch, piezoelectric

effect, and electric-field-induced barrier lowering become 1.0 and 0.9 eV, respectively. Thus, this migration can happen at room temperature.

The hypothesis of inverse piezoelectric effects also cannot explain the threshold voltage shift after stress [83][88]. Meneghini et al. observed a significant negative threshold voltage shift when the devices were stressed using V_{gs} = -10V with other pins grounded at 150 ℃. The result suggests that V_{th} shifts may originate from trapping/detrapping from traps located at the SiN/AlGaN interface at the edge of the gate overhang, on the drain side [83]. This positive charge may originate from the generation of holes [88], or generation of donor defects at the AlGaN/GaN heterointerface [89]. The released electrons can tunnel into the AlGaN/GaN interface when negative gate bias is applied, and results in an increase in drain-source current and yellow band in EL spectra [46].

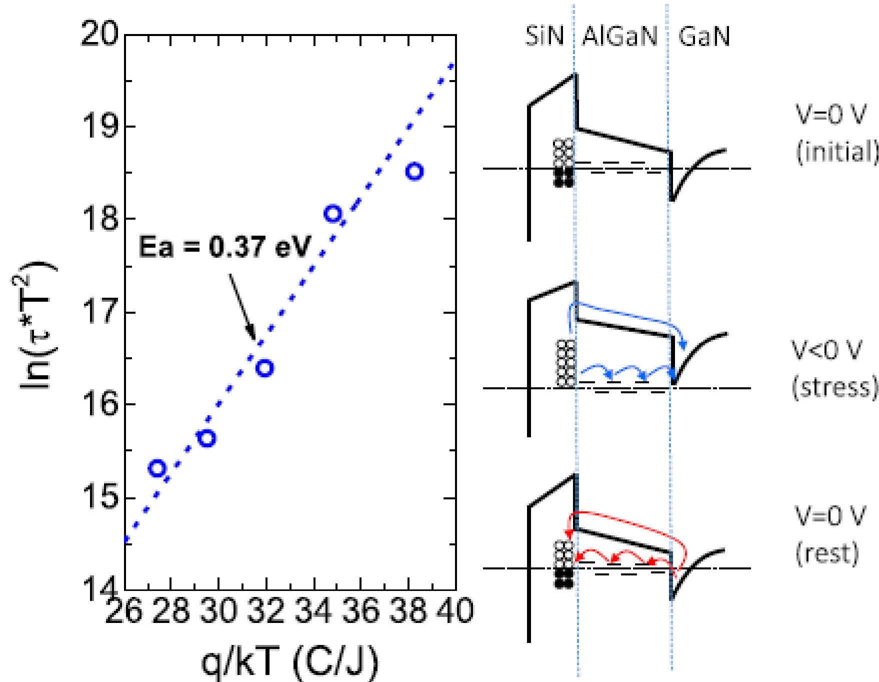

Fig. 2.5. (left) Arrhenius plot of the time constant of the process responsible for the negative V_{th} shift during stress. The activation energy of 0.37 eV is reported. (right) Schematic representation of the process responsible for the negative Vth shift. The surface donors are not indicated for simplicity. (after [83])

2.3 Radiation effects in AlGaN/GaN HEMTs

The energetic particles in space such as protons, electrons and heavy ions can cause permanent damage in electronic devices by creating electron-hole pairs or displacement damage [90]. These can lead to a variety of effects on the performance of GaN HEMTs, including pinch-off voltage shift, increased junction leakage current, transconductance degradation and noise enhancement [57]–[65]. GaN is believed to be a radiation hard semiconductor material due to its wide bandgap (3.4 eV) and the strong bond between Ga and N. Compared to its competitors like AlGaAs/GaAs devices, GaN-based HEMTs are about two orders of magnitude less sensitive to displacement damage due to proton irradiation [1]. The lack of an oxide layer makes the AlGaN/GaN HEMTs less sensitive to total ionizing dose effects [2]. This makes AlGaN/GaN HEMTs very promising in aerospace applications, and it is very useful to study the combination effects of radiation effects and high field stress.

2.3.1 Total ionizing dose effects

When sufficiently energetic particles interact with semiconductor devices, ionization can occur. Charged particles hit the target materials and create electron-hole pairs. Fig. 2.6 shows a schematic energy diagram of a MOS structure under positive bias applied to the gate and indicates the major physical processes that contribute to the total ionizing dose effects in a MOS device [91]. When a MOS devices is exposed to high energy ionizing radiation, electron-hole pairs are created in the oxide layer. Because the electrons have a much higher mobility than the holes in SiO_2 [92], most of the electrons are rapidly swept out of the oxide, and holes are trapped in the pre-existing

traps or further transport to the Si/SiO_2 interface by hopping. At the Si/SiO_2 interface, some of the holes are neutralized by electrons tunneling from the silicon and others get trapped at deep states forming positive oxide trap charges. These oxide trapped charges can cause a shift in the threshold voltage. At the same time, hydrogen ions can be released in the oxide bulk as holes transport toward the interface. Those protons can drift to the Si/SiO_2 interface under positive gate bias and react with Si-H to form H_2, leaving silicon dangling bonds at the interface. These dangling bonds can act as interface traps, leading to a change of threshold voltage and a decrease of carrier mobility.

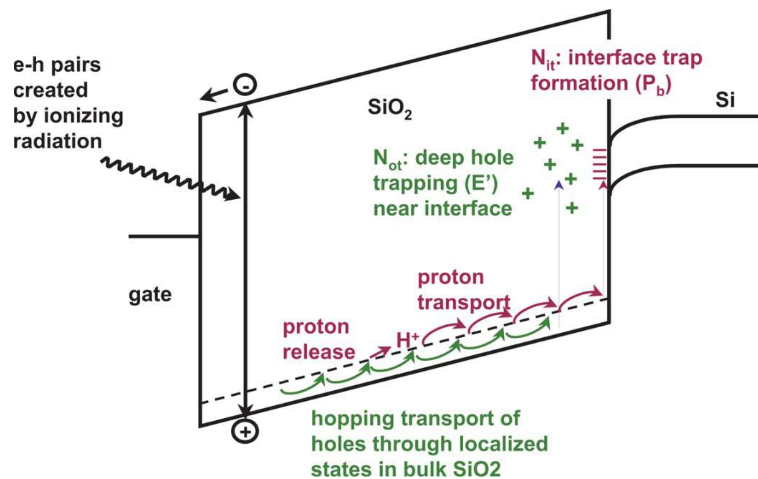

Fig. 2.6. Schematic energy band diagram for MOS structure under positive bias, indicating major physical processes underlying radiation response. After [91].

The most total-dose radiation sensitive parts are the oxide insulators because the large difference in electron and hole mobility in SiO_2 and the fixed deep hole trapping in the oxide layer. In AlGaN/GaN HEMTs, this effect is not significant because it typically lacks the oxide insulator. Earlier 10-keV X-ray experiments with the AlGaN/GaN high electron mobility transistors found no significant changes after a total ionizing dose of 30 Mrad(SiO_2) [93] and gamma irradiation of AlGaN/GaN HEMTs up to a dose of 600 Mrad(SiO_2) did not substantially change the characteristics [2]. However, in some recent works, significant shifts in threshold voltage have been observed

for both research- and industrial-grade devices during 10-keV X-ray irradiation [57], [58]. This TID sensitivity occurs most likely because the density of native defects in AlGaN/GaN HEMTs is being reduced by improvements in fabrication technology, making TID effects caused by radiation exposure more easily observed. Thus, it is increasingly important to understand the mechanisms of total ionizing dose effects in AlGaN/GaN HEMTs.

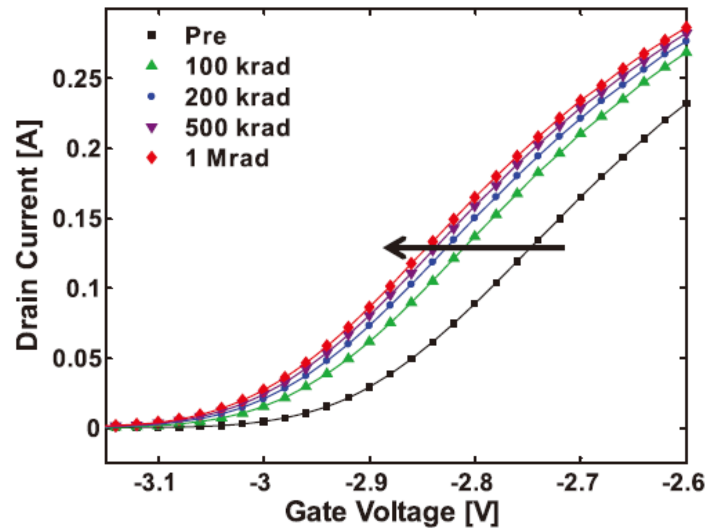

Fig. 2.7. Drain current vs. gate voltage for the CGH40006P as a function of total ionizing dose using 10 keV X-rays up to a dose of 1 Mrad(SiO_2). Note a negative shift in threshold voltage. This plot shows the worst-case threshold voltage shift of the two Cree devices tested for TID. The arrow indicates the direction in increasing radiation. (after [58])

2.3.2 Displacement damage

When energetic nuclear radiation interacts with a semiconductor material, it may displace some atoms from their original sites in the semiconductor lattice. The displaced atoms may form pairs of vacancies and interstitials. These are called Frenkel pairs [1]. Most will recombine after some time, while others can form stable defects. This radiation-induced displacement damage in the crystal lattice may lead to changes in the properties of the devices. Compared with total ionizing

dose effects, displacement damage is a more critical radiation effect in GaN-based devices [1].

In an ideal lattice, the Frenkel pair generated in GaN lattice, gallium vacancies V_{Ga} and gallium interstitials Ga_i, nitrogen vacancies V_N, and nitrogen interstitials Ni will form shallow donors and deep acceptors at E_c - 0.06 eV (V_N^+), E_c - 0.8 eV (Ga_i^{++}), E_c - 1.0 eV (N_i^-) and E_c - 2.6 eV (V_{Ga}^+) [1]. But generally this is not the case. Theoretical calculation of displacement defects in GaN shows that there exists a wide distribution of threshold energies for both Ga and N sublattices, with minimal energies of defect formation of 18 eV for Ga and 22 for nitrogen, with average displacement energy of 45 for Ga and 110 for N [94]. This difference is because of the high density of as-processed defects, both during and after fabrication [95]. These preexisting defects and the complexes formed by as-processed defects with irradiation induced defects are dominant in the radiation response of GaN-based HEMTs [61][96].

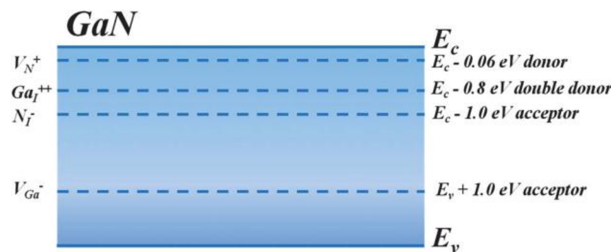

Fig.2.8. Simple model for radiation defects created in GaN by protons and other ionizing radiation. After [62].

Proton irradiation damage and its annealing effects in AlGaN/GaN HEMTs were first reported by Cai et al. [97]. After exposure to 1.8 MeV proton irradiation to a fluence of 10^{14} p/cm^2, the saturation current of HEMTs dropped from 260 mA/mm to about 100 mA/mm, and the device transconductance was also degraded from about 80 mS/mm to 26 mS/mm. The electrical performance can gradually recover with increasing RTA (rapid thermal anneal) temperature, and can re-

cover significantly after the annealing temperature reaches 600 ℃. This annealing effect is consistent with experiments that show the low annealing temperature of Ga and N interstitials and the high annealing temperature of V_{Ga} in GaN material [98].

Several groups studied the energy dependence of proton-induced degradation in AlGaN/GaN HEMTs, and found that at fixed fluence, including low fluence (10^{13} cm^{-2}) and high fluence (10^{15} cm^{-2}), the devices showed the largest changes for the lowest proton energies [63], [93], [99], [100]. These effects are explained by the decrease of the energy transferred to Al, Ga and N atoms in elastic collisions occurring within the active region of devices as the range of protons increased with increasing energy, i.e., the larger non ionizing energy loss of low energy protons. So 1.8 MeV protons are commonly used to study the displacement damage in GaN-based HEMTs.

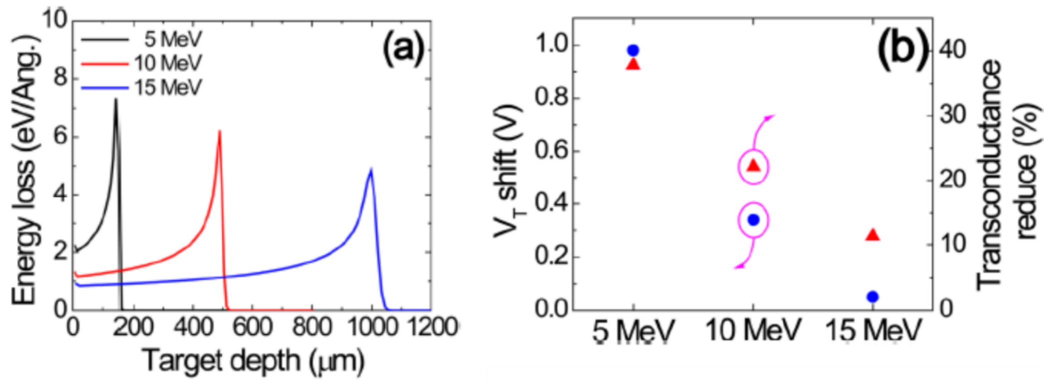

Fig.2.9 (a) SRIM simulation results of (a) energy loss and as a function of target depth, (b) Threshold voltages shift and transconductance reduction as a function of irradiation energies at a fluence of $5x10^{15}cm^{-2}$. (after [98])

As various processing technologies employ different surface and layer growth, the radiation response of AlGaN/GaN HEMTs also shows sensitive dependence on processing, similar to electrical stress. Roy et al. [64] and Chen et al. [65] studied 1.8 MeV proton induced degradation in

AlGaN/GaN HEMTs fabricated using Ga-rich, N-rich and NH_3-rich conditions using dc measurements and low frequency 1/*f* noise. Similar positive shifts in pinch-off voltage were obtained in all cases. The 1/*f* noise testing results suggest that N vacancies and divacancies generated during the irradiation are responsible for the pinch-off voltage changes. At the operating bias condition, these acceptor-like traps are negatively charged, leading to the positive shift in V_{th}. Besides N vacancies, the dehydrogenation of O_N-H results in similar effects. Chen's [61] work on the combined effects of proton irradiation with high electrical field stress shows the sensitivity of AlGaN/GaN HEMTs to 1.8 MeV proton irradiation is greatly enhanced by biasing the devices during irradiation and/or applying high field stress before irradiation. Noise test results also support that the dehydrogenation of O_N-H is responsible for the proton-induced degradation.

2.4 Defects that cause degradation

Fig. 2.8 suggests the deep levels formed by Frenkel pair defects may result from the displacement damage. But in fact the defects types and the charge states are more complex [101] [102]. In this section, a brief summary of most common defects are presented. By helping to identify the activation energy, temperature-dependent low frequency 1/*f* noise can help us to identify the defects that causes the degradation before and after high field stress with/or irradiation. The activation energies are calculated by density functional theory (DFT) [51], [60], [76], [78], [79].

2.4.1 Ga and N vacancies and interstitials

After proton irradiation, Frenkel pairs may be generated in a GaN lattice, including gallium

vacancies V_{Ga} and gallium interstitials Ga_i, nitrogen vacancies V_N, and nitrogen interstitials N_i. Ga-N divacancies can also formed. The defects that dominate the degradation are strongly dependent on the grown process of GaN and AlGaN [49], [64], [70], [71],. The charge state of the defects is controlled by the position of Fermi level. For example, in devices grown by Ga-rich and N-rich MBE, the dominant defects are suggested to be N vacancies and Ga-N vacancies [103]. Fig 2.10 shows the formation energy of (a) Ga-N divacancies and (b) N vacancies as a function of the position of the Fermi level in the band gap of $Al_{0.3}Ga_{0.7}N$ and the slope indicate charge state. For n-type AlGaN and GaN, the charge state can change from -2 to -3 for Ga-N divacancies (Fig. 2.10 (a)) and -1 to -3 for N vacancies (Fig. 2.10 (a)) when the Fermi level is changed by the bias.

Unlike displacement damage, hot electrons with several electron volts of energy are not able to create stable point defects in a perfect crystal. Dehydrogenation of preexisting defects that were passivated by hydrogen can then be the dominant degradation mechanism. Fig. 2.11 summarizes the activation energy of the most common defects: hydrogenated N vacancies, Ga vacancies, Ga-N divacancies and nitrogen antisite defects. The detailed formation energy and charge states of specific defects can be found in Ref [49].

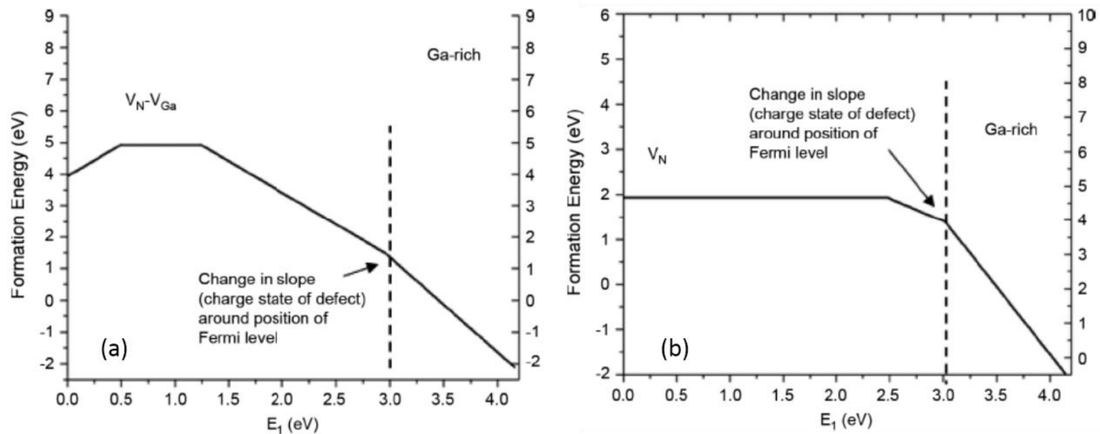

Fig. 2.10. Formation energy of (a) Ga-N divacancies and (b) N vacancies as a function of the position of the Fermi level in the band gap of $Al_{0.3}Ga_{0.7}N$. (after [64]). The slopes indicate different charge states.

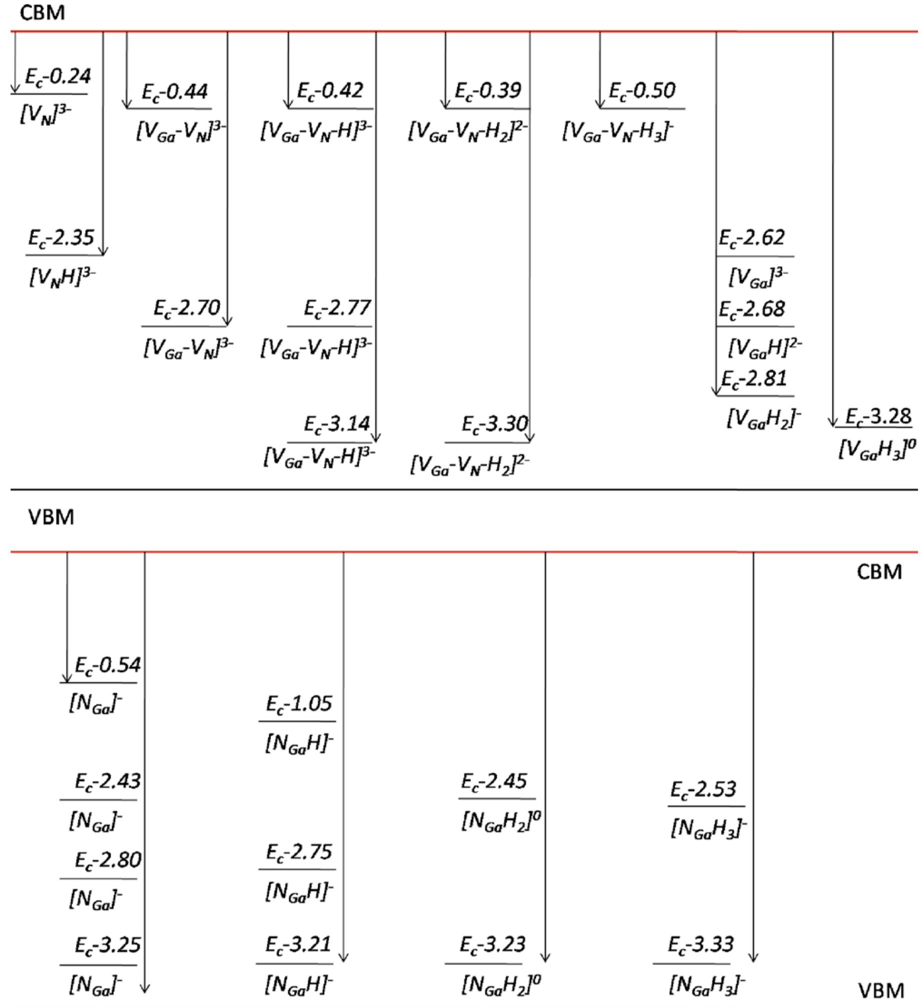

Fig. 2.11. Comparison of defect levels calculated from first-principles and trap concentration dependence on ammonia flow as in Ref. 44.

Previous research from our group has suggested several defect candidates that are mostly possible for hot carrier or radiation induced degradation. Table 2-1 summarized the defects that we have seen in previous studies. N vacancies (V_N^{3-}), with an activation energy of 0.24 eV and Ga-N divancancies (V_{Ga}-V_N-H_x) with an activation energy around 0.4 eV to 0.5 eV are responsible for displacement damage in Ga-rich and N-rich devices [60]. Dehydrogenation of triply hydrogenated

Ga-vacancies into the $[V_{Ga}H_2]^{-1}$ or $[V_{Ga}H]^{-2}$ complexes is responsible for hot carrier effects in ammonia-rich devices [70]. The nitrogen antisite defect $[N_{Ga}]$ with activation energy of 0.54 eV and $[N_{Ga}H_x]$ with activation energy of 1.05 eV are responsible for hot carrier effects in N-rich devices [80].

Table 2-1. Defects that responsible for electrical and radiation-induced degradation seen in previous work. The activation energy are calculated by DFT.

Type of defects		Process	donor or acceptor	Defect Energy (eV, below Ec),	Type of stress
Ga and N vacancies	V_N	Ga-rich [64]	acceptor ($[V_N]^{3-}$)	0.25 in GaN [49] 1.2 in AlGaN [64]	Proton irradiation [64] [65],
	V_{Ga}	N-rich [70],[103]	acceptor ($[V_{Ga}H_x]^-$) (x=0~3)	> 2 [70] (Not observed in 1/f noise)	1. Dehydrogenate at high electric field &low current (gate voltage close to V_{th}) [70],[103] 2. High electric field: [60] $[N_{Ga}]^- \rightarrow [V_{Ga}]^{3-} + N_i^-$
	V_{Ga}-V_N-H_x (x=0~3)	Ga-rich [64] [72]	acceptor ($[V_{Ga}\text{-}V_N]^{3-}$)	0.6 in GaN [49] 1.1 in AlGaN [49],[60], [64]	1. Proton irradiation [64] 2. High electric field: [60] $[V_{Ga}]^{3-} \rightarrow [V_{Ga}\text{-}V_N]^{3-} + N_i^-$ 3.Semi-ON state stress [72]
N antisite	N_{Ga}	NH_3-rich [49], [103]; N-rich [70][80]; Qorvo [61]	acceptor ($[N_{Ga}]^-$)	0.65 in GaN [49] [80] 1.7 in AlGaN [70][80]	1.As-processed [61] 2. proton irradiation and/or high field stress [61] 3. High electric field &low current

					(gate voltage close to V_{th}) [70][80]
	$N_{Ga}H_x$ (x=1~3)	NH_3-rich [49],[103] N-rich [71]	acceptor ($[N_{Ga}H_3]^-$, $[N_{Ga}H]^-$)	>1.5 [80] (Not observed in 1/f noise)	As-processed [61] [80]
O related	O_N^{-1}DX center	All processes [65][71][96][104]	acceptor	0.25 (barrier from O_N^- to O_N^0) [71]	As-processed [71]
	O_N		neutral		1.Semi-ON state stress [104] 2.TID [96] 3.Proton irradiation [65]
	O_N^+		donor	0.5 (O_N^+ to O_N^-) [71]	
	O_N-H		neutral & acceptor	1 (configuration I to II) 0.5 (configuration II to II, $[O_N\text{-}H]^-$) [65]	
	V_{Ga}-O_N-H	Qorvo [61]	acceptor	~0.7 [61] [105]	1.As-processed [61] 2.Dehydrogenate at high electric field &low current [49]
Fe complexes	Fe_{Ga}–H	Ga-rich [72], [21]	donor (Fe_{Ga}^+)	~0.55 (Fe_{Ga}^+) [106][105] ~1.5 (Fe_{Ga}–H) [106]in GaN	Hot carrier degradation [72] [106]
	Fe_{Ga}–V_N–H		donor ($[Fe_{Ga}$–$V_N]^+$)	~0.55 ($[Fe_{Ga}$–$V_N]^+$) [106] [105] ~1.5 (Fe_{Ga}–V_N–H) [106] in GaN	Hot carrier degradation [72], [106]

2.4.2 Oxygen related defects

Although oxygen is not used in any fabrication step of AlGaN/GaN HEMTs, oxygen is an impurity that almost cannot be avoided [65][71][104]. Oxygen diffusion and moisture diffusion during and after fabrication, residual gases in the chamber, and the oxide plasma surface treatment can all introduce oxygen related impurities into the AlGaN or GaN layer [104], [107], [108]. ON

related defects can exhibit different charge states which may depend on the position of the Fermi-level. The O_N^{-1} DX center is the most stable state before stress. Thermal excitation of an O_N^{-1}DX center can lead to the emission of an electron to the AlGaN conduction band, which converts the negatively charged DX center into a neutral O_N. The activation energy here is ~0.25V. Neutral O_N^0 can further emit an electron, resulting in O_N^{+1}, with essentially no energy barrier. The energy barrier for O_N^+ capturing an electron and converting into O_N^0 is 0.3 eV [68].

Hydrogenated substitutional oxygen, i.e., O_N-H defects, are also common in AlGaN/GaN HEMTs. The O_N-H defect complex shows two configurations I and II with activation energy of 1.0 eV and 0.5 eV respectively [61]. As shown in Fig. 2.12, the activation energy required is 1.0 eV for reconfiguration from I to II and 0.5 eV for reconfiguration from II to I. During proton irradiation and/or high field stress, the H atom can be removed from the O_N-H. This occurs easily via interaction of transporting holes with the O_N–H; this process is similar to H transporting in irradiated Si/SiO_2 and interaction with a hydrogen atom to release a proton, as shown in Fig. 2.6. This reaction occurs with a low energy barrier. The dehydrogenation can result in an increase in noise spectrum at low temperature, corresponding to a peak at 0.2 eV, which is often observed in AlGaN/GaN HEMTs [61][65][72][80]. Additionally, a hydrogenated oxygen impurity can be complexed with a Ga vacancy and form V_{Ga}-O_N-H; this defect has a charge transition level of ~ 0.7 eV. [61]

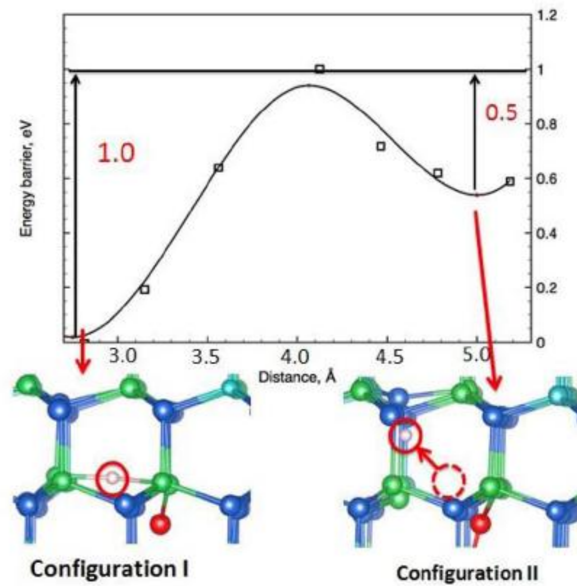

Fig. 2.12. Energy barriers as a function of O–N distance and defect configurations (I) and (II) of O –H (smaller light atom). (after [65])

2.4.3 Other defects

Carbon and iron are two elements often used in doping of GaN substrates. The related defects have very high probability to exist in an AlGaN/GaN HEMTs. A yellow band can be observed in the EL of carbon-doped GaN, which suggests that the carbon can act as a deep acceptor with an energy level around 860 meV [109], 1040 meV, or 650 meV [110]. In Ref. [106], Mukherjee et al. suggested two iron complexes can be responsible for hot carrier effects in AlGaN/GaN HEMTs: Fe_{Ga}–H with an activation energy of 0.6 eV [105], and Fe_{Ga}–V_N–H, whose activation barrier is 1.4 eV. The dehydrogenation of these two defects can result in positively charged defects: Fe_{Ga}^{+}, and Fe_{Ga}–V_N^{+}, resulting in the negatively shifted threshold voltage.

CHAPTER III

EXPERIMENTAL SETUP

3.1 Device information

In this dissertation, we studied devices with several different structures. Fig 3.1 shows the schematic cross-section of the devices. AlGaN/GaN HEMTs were fabricated in AlGaN/GaN heterostructures grown by ammonia-rich or Ga-rich plasma-assisted molecular beam epitaxy (PAMBE) on 4H-SiC substrates (group A) or on GaN-on-SiC substrates (Ga-rich, group B) or freestanding (FS) GaN substrates (Ga-rich, group C) at the University of California, Santa Barbara [13][25][27]. The top view of the device is shown in Fig. 3.2. Devices with a T-shaped layout, and 2x 75 μm gate width were tested. The gate has the shape of an inverted trapezoid, with a length (L_G) of 0.7 μm. The gate-to-drain separation (L_{GD}) is 1 μm and the gate-to-source separation (L_{GS}) is 0.5 μm. In Chapter IV and V, we study both unpassiavated and passivated devices of group A.

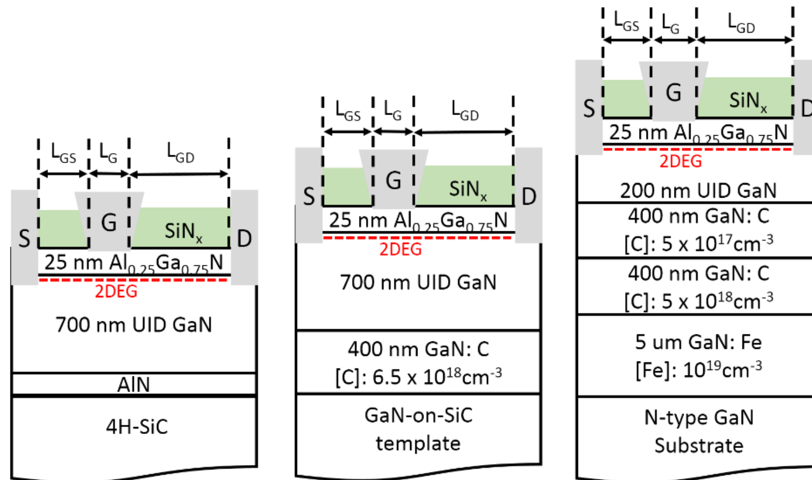

Fig. 3.1. Schematic diagrams of passivated AlGaN/GaN HEMT structures ([13][25][27]).

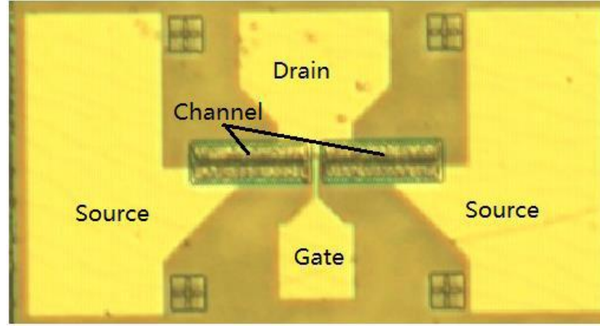

Fig. 3.2 Topview of DUT [111].

3.2 DC Measurement

Fig. 3.3 shows the typical DC characteristics of an AlGaN/GaN HEMT. In this dissertation, the DC characteristics are measured with HP 4156 B or Agilent B1505 parameter analyzers. Fig. 3.3 (a) shows the I_d-V_g curves of AlGaN/GaN HEMTs. An effective value of threshold voltage V_{th} was extracted from the I_d-V_g curves in the linear range of transistor response. For the sample in Fig. 3.3 (a), the threshold voltage is around -4.5 V. The gate leakage current is about 300 nA at V_{gs} = -7 V, corresponding to a gate leakage current density of 0.4 mA/mm. Fig. 3.3 (b) shows the I_d-V_d curves of AlGaN/GaN HEMTs, with V_{gs} - V_{th} varied from -0.5 V to 5.5 V with V_{gs} steps of 1 V. V_{ds} was swept from 0 to 10 V. The saturation current is around 90 mA at V_{gs} - V_{th} = 3.5 V, i.e., V_{gs} = 0 V in this device. The dc electrical properties may vary in devices with different structures. To reduce the thermal effects, the devices were bonded using a high speed package, which is a good heat sink [112].

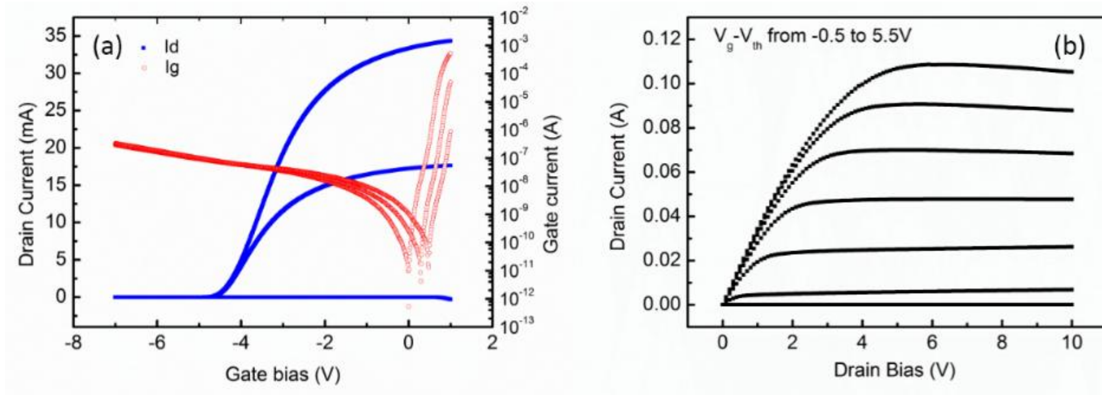

Fig. 3.3. DC characterstics (a) I_d-V_g (left) and I_g-V_g (right) curves and (b) I_d-V_d curves for AlGaN/GaN HEMTs.

Fig. 3.4. high-speed package (after [112].)

3.3 Low frequency 1/f noise

3.3.1 Introduction of 1/f noise testing

When a constant bias is applied to a semiconductor device, the current can exhibit spontaneous fluctuation. Several mechanisms contribute to the noise and result in a unique noise spectral power distribution in the frequency domain. For transistors, two mechanisms are dominate [113]: 1) thermal noise or white noise, caused by random thermal motion of charge carriers at any temperature, with the voltage noise power spectral density S_{vd} independent of frequency [114]; 2) flicker noise

[68], [69], [113], [115], exhibiting a frequency dependence of $S_{vd} \propto 1/f^{\alpha}$ (with α in the range 0.8~1.4), where

$$\alpha = -\partial(\ln S_{vd})/\partial(\ln f) \tag{3.1}$$

This 1/*f* noise dominates the noise spectrum at low frequency.

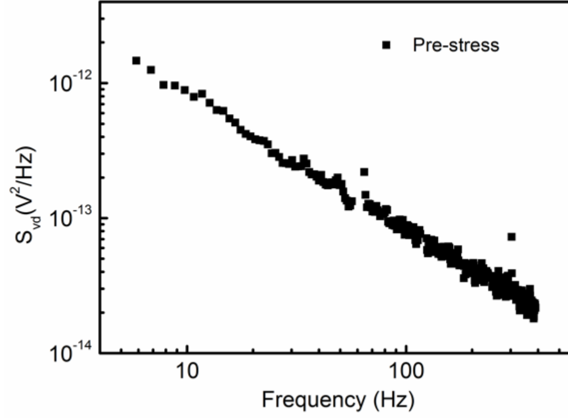

Fig. 3.5. Example: excess voltage noise power spectral density S_{vd} as a function of frequency for AlGaN/GaN HEMTs at 300 K, V_{gs} - V_{th} = 0.8 V, V_d = 0.05 V.

Flicker noise is also called 1/*f* noise. An example spectrum of 1/*f* noise in AlGaN/GaN HEMTs is plotted in Fig 3.5. There are variety of mechanisms that have been considered to be responsible for 1/*f* noise. In general, the noise results from the trapping and de-trapping of electrons in defects near the AlGaN/GaN channel [116]–[118]. Two models are most popular to explain the noise spectrum: Hooge's mobility fluctuation model [115] and McWhorter's number fluctuation model[119]. Hooge's model attributes the 1/*f* noise to fluctuation in the mobility of individual channel carriers and can be described by the following relationship [115]:

$$\frac{S_V(f)}{V^2} = \frac{S_I(f)}{I^2} = \frac{S_R(f)}{R^2} = \frac{\alpha_H}{fN} \tag{3.2}$$

where α_H is the Hooge's constant. Many experimental results strongly suggest that this model does not correctly identify the origin of the noise in these devices, and often does not describe accurately

the frequency, voltage, and/or temperature dependence of these devices [120].

The McWhorter number fluctuation (ΔN) theory states that flicker noise is generated by fluctuations in the number of carriers due to charge trapping in surface (or near-interface) states, where free carriers are randomly trapped by trap centers with different life times. The simplest version of this model assumes that trap centers are uniformly distributed near the channel, and that time constants increase with the distance from the channel. According to this model, if a MOS device is operated in its linear region at constant drain current and gate bias, the $1/f$ noise can be described approximately by[120] :

$$S_{Vd} = \frac{q^2}{C_{ox}^2} \frac{V_d^2}{\left(V_g - V_{th}\right)^2} \frac{k_B T D_t(E_f)}{LW \ln(\tau_1 / \tau_2)} \frac{1}{f} \tag{3.3}$$

where S_{Vd} is the excess drain-voltage noise power spectral density, V_{th}, V_g, and V_d are the threshold, gate, and drain voltages, f is the frequency, $-q$ is the electron charge, C_{ox} is the gate-oxide capacitance per unit area, L and W are the transistor channel length and width, k_B is the Boltzmann constant, T is the absolute temperature, $D_t\ (E_f\ )$ is the number of traps per unit energy per unit area at the Fermi level E_f, and τ_1 and τ_2 are the minimum and maximum tunneling times, respectively [121].

Dutta and Horn [68] have shown that an approximate $1/f$ spectrum is due to a broad distribution of activation energies. They demonstrated that the temperature dependence of the $1/f$ noise is often due to a thermally activated random process with a distribution of activation energies, which varies with temperature. According to the Dutta-Horn model of low-frequency noise [68][69], the frequency and temperature dependence of the noise are related via

$$\alpha(\omega, T) = 1 - \frac{1}{\ln(\omega\tau_0)} \left(\frac{\partial \ln S_V(T)}{\partial \ln T} - 1\right) \tag{3.4}$$

where $\omega=2\pi f$, T is the temperature and τ_o is the characteristic time of the process leading to the noise (here assumed for GaN to be ~ 3 x 10^{-14} s [65][68]). Fig. 3.6 shows that the α from experimental data are in good agreement with the value suggested by Dutta-Horn model. Thus, from the temperature dependence of the noise magnitude, we can estimate the shapes of the defect energy distributions $D(E_o)$ from low-frequency noise measurements [68][69], via

$$D(E_o) \propto \omega/(kT) * S_V, \tag{3.5}$$

where

$$E_o = -kT \ln(\omega\tau_o) \tag{3.6}$$

is the effective defect activation energy [122].

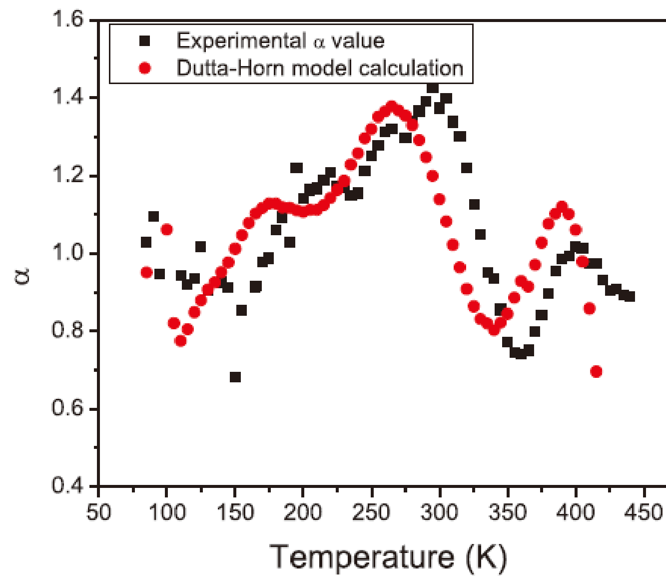

Fig. 3.6. Experimental and calculated frequency exponent of noise power spectral density as a function of temperature from 85 K to 400 K.(after [61])

3.3.2 1/f noise measurement setup

In this work, the excess noise (corrected for background noise) was measured over a frequency

span of 3 Hz to 390 Hz at constant 0.05 V supplied by a HP 4140B constant voltage supply and substrate and source grounded. The drain current was derived from a constant voltage source in series with a large resistor. The gate voltage is adjusted to make sure that the noise originates from the gated portion of the channel. Fluctuations in the drain to source voltage were measured with a low noise pre-amplifier SR 560 and SR760 FFT spectrum analyzer. The temperature dependence of 1/*f* noise is measured before and after electrical stress/irradiation.

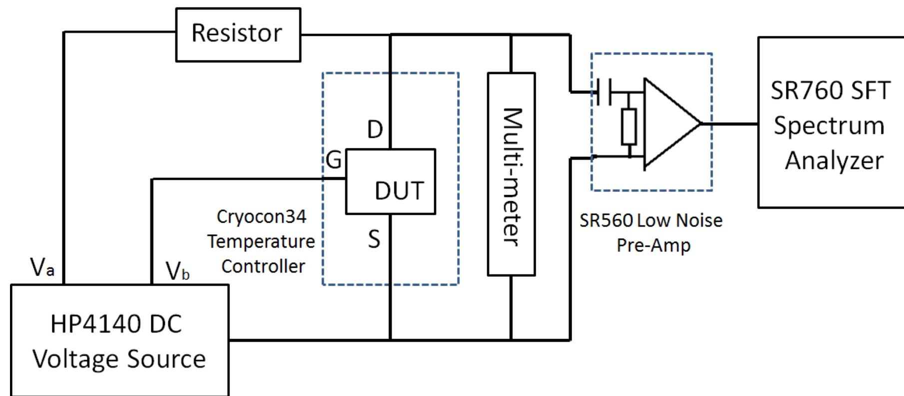

Fig. 3.7 Low frequency 1/*f* noise measurement system. (after[123])

3.4 Proton and X-ray irradiation setup

For the total ionizing dose effects study, the HEMTs were irradiated with a 10-keV ARACOR x-ray source at a dose rate of 31.5 krad(SiO_2)/min at room temperature. For the displacement damage study, the AlGaN/GaN HEMTs were irradiated with 1.8MeV protons to a maximum fluence of $1x10^{14}cm^{-2}$. The total ionizing dose effects were first investigated with all pins grounded (Chapter IV). In Chapters V and VI, the devices were irradiated at four bias conditions: GND, OFF, semi-ON and ON. The proton energy is chosen for its large non-ionizing effective loss (NIEL), and the

fluence of 10^{14} is a high particle fluence compared to realistic space environments. The irradiation is performed at room temperature. DC and $1/f$ noise measurements are taken before and after irradiation.

CHAPTER IV

DEGRADATION AND ANNEALING EFFECTS CAUSED BY OXYGEN IN ALGAN/GAN HEMTS

In this part, the effects of room-temperature electrical stress and annealing are investigated for AlGaN/GaN HEMTs grown under NH_3-rich conditions. Passivated devices and Ga-rich unpassivated devices with similar structures are also tested as controls. After hot-carrier stress, NH_3-rich devices exhibit a fast recovery during room-temperature annealing with all pins grounded. After stress and annealing, the peak transconductance of unpassivated devices is often higher than its original value. This "super-recovery" is not observed in passivated devices. We employ density functional theory (DFT) calculations to help understand this observation and the nature of the defects in these devices. Calculations suggest that dehydrogenation of pre-existing O_N-H defects in AlGaN plays a significant role in hot carrier degradation of NH_3-rich AlGaN/GaN HEMTs. The resulting bare O_N impurity centers can naturally account for the observed super-recovery in peak transconductance.

<u>4.1 Experimental details</u>

AlGaN/GaN HEMTs were fabricated on AlGaN/GaN heterostructures with a 25 nm $Al_{0.25}Ga_{0.75}N$ layer grown by NH_3-rich or Ga-rich plasma-assisted molecular beam epitaxy

(PAMBE) on 4H-SiC substrates with and without SiN passivation layers at the University of California, Santa Barbara. The width of the devices is 150 μm. The gate is trench shaped with a length (L_G) of 0.7 μm. The gate-to-drain separation (L_{GD}) is 1 μm, and the gate-to-source separation (L_{GS}) is 0.5 μm. NH_3-rich and Ga-rich unpassivated devices were electrically stressed with a drain voltage of 15 V and annealed at room temperature. Devices were packaged and not exposed to light during testing. The gate voltage during stress is V_{gs} = -2 V, corresponding to the "semi-on" state that often results in the most significant hot-carrier effects in AlGaN/GaN HEMTs [39]. Device I_d - V_g curves were measured in air using a HP 4156B Semiconductor Parameter Analyzer at source-drain voltages that ranged from 0.2 V to 5 V; the gate voltage was swept from -7 V to 1 V. An effective value of threshold voltage V_{th} was extracted from the I_d - V_g curves in the linear range of transistor operation with V_{ds} = 0.5 V. The initial values of V_{th} were approximately -4.1 V for the NH_3-rich unpassivated devices, -2.8 V for the NH_3-rich passivated devices, and -5.1 V for the Ga-rich devices. At least three devices with nominally identical pre-stress response (to within ± 10 % in starting and post-stress threshold voltage and transconductance) were tested for each process type; representative results are shown below.

4.2 Experimental results

Ammonia-rich AlGaN/GaN HEMTs were stressed for 10 h. After electrical stress, the devices were annealed at room temperature in air for 5 h with all pins grounded, stressed again for 5 h, and annealed again for 2 h under similar conditions. Figure 4.1 shows the threshold voltage shift and

peak transconductance degradation as functions of time and drain bias during measurement for this stressing and annealing sequence. Trends are similar for different drain bias during measurement, with the most negative values occurring at 0.5 V, and most positive values at 5 V bias. The degradation increases monotonically, indicating an increase in net positive charge with increasing stress time. The peak transconductance degrades about 15% after stress for V_{ds} = 0.5 V and 5% for V_{ds} = 5 V, as shown in Fig. 4.1(b), indicating that traps are generated either in the AlGaN, close enough to the channel region to degrade the carrier mobility, and/or in the GaN buffer layer, and not predominantly at the unpassivated surface of the device. After hot-carrier stress in room ambient conditions, the NH_3-rich devices exhibit a fast recovery. The threshold voltage exceeds its original value at all three drain bias values, and the peak transconductance after stress plus annealing significantly exceeds the pre-stress value for all cases.

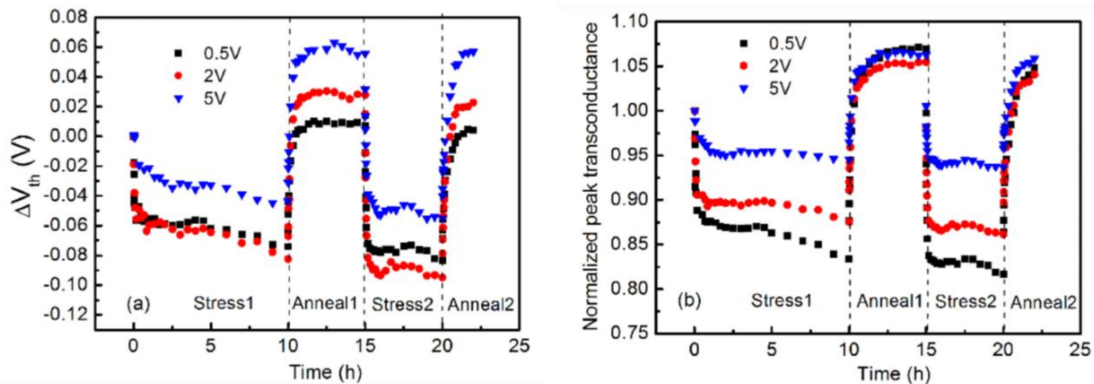

Fig.4.1 Threshold voltage shift and (b) normalized peak transconductance for V_{ds} = 0.5 V, 2 V, and 5 V as a function of stress and annealing time for NH_3-rich unpassivated devices. All measurements and stressing were performed at room temperature under room ambient conditions, with V_{ds} = 15 V and V_{gs} = -2 V. The post-stress annealing was performed with all pins grounded. Devices were not exposed to light during stressing, annealing, or measurement.

We have also investigated the responses of NH_3-rich passivated HEMTs and Ga-rich unpassivated HEMTs for comparison, as shown in Fig. 4.2. We increased the stress conditions to V_{ds} =

20 V, V_{gs} = -1 V for the NH_3-rich passivated devices in Fig. 4.2(a) so that the drain current (~ 30 mA) was similar to that of the unpassivated devices in Fig. 4.1, and Fig. 4.2 because stressing these devices at V_{ds} = 15 V did not cause significant degradation for stress times less than one day. Only partial recovery is observed during the annealing sequence in Fig. 4.2(a), in contrast with the super-recovery [124] observed in Fig. 4.1(b). Similar degradation, followed by rapid recovery, is observed for the unpassivated Ga-rich devices in Fig. 4.2(b) and NH_3 devices in Fig. 4.1(b), but again no super-recovery of peak transconductance is observed in Fig. 4.2(b). Trends in transconductance degradation and threshold voltage shifts are similar at other source-drain voltages. Hence, both the material growth and/or device processing conditions and the presence or absence of a passivation layer play critical roles in determining the degradation and recovery mechanisms in these devices.

Moisture absorption is always suspected when unpassivated devices show more significant degradation than passivated devices. Thus, we show in Fig. 4.3 the device degradation after first baking the unpassivated devices at 400 K for 1 h in an effort to drive out absorbed moisture. The peak transconductance first degrades rapidly, and then increases slowly with increasing stress. If we wait for 48 h after the devices are baked, there is no difference in the response of baked or unbaked devices. Hence, not surprisingly, moisture absorption plays at least some role in the observed degradation.

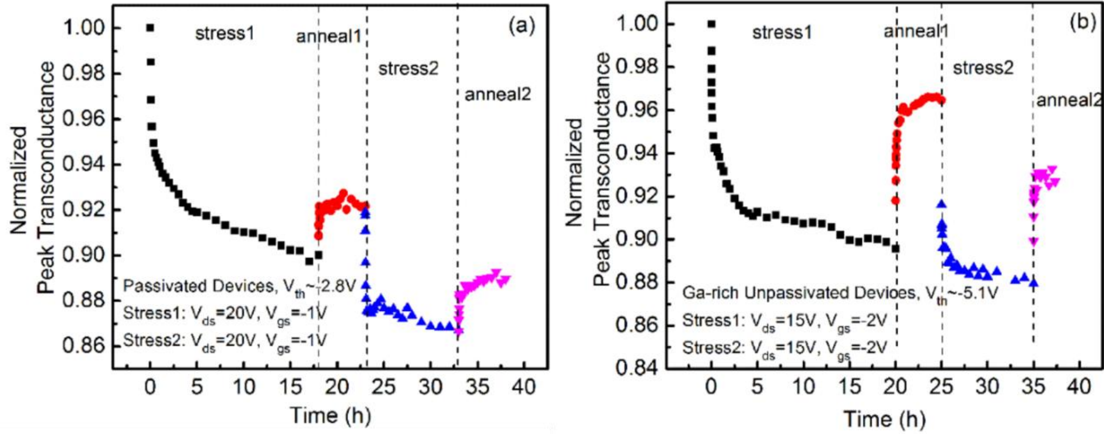

Fig. 4.2. Normalized peak transconductance at V_{ds} = 0.5 V as a function of stress and annealing time in (a) NH_3-rich passivated devices and (b) Ga-rich unpassivated devices.

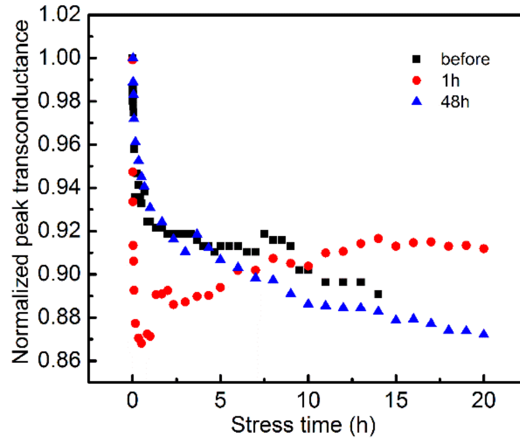

Fig. 4.3. Normalized peak transconductance at V_{ds} = 0.5V as a function of stress time in NH_3-rich unpassivated devices before and after baking in air at 400K for 1 h. The red dots and blue triangles show results for devices measured 1 hour after baking and 48 hours after baking, respectively.

4.3 Discussion

Critical factors we have identified in previous studies of the hot-carrier degradation of AlGaN/GaN HEMTs include oxygen impurity centers O_N, which can either be passivated by hydrogen (O_N-H) or remain unpassivated [49][65][72]. O_N-H defects can form during and after fabrica-

tion, with the relative densities of O_N and O_N-H subject to variation, depending on whether passivation or depassivation is favored during fabrication, stress, and/or annealing. We now consider whether this common defect may be able to account for the results shown above.

Hot carriers can remove H from hydrogenated impurities in semiconductors [51] [78]. Therefore, if the unpassivated AlGaN/GaN HEMTs contain significant amounts of O_N-H defects, electrical stress can convert some O_N-H defects into bare O_N defects. Hybrid DFT calculations show that the bare O_N defect in the AlGaN layer on the GaN substrate has a +1/0 transition level right at the CBM of GaN, as shown in Fig. 4.4. When the device is under electrical stress, the Fermi-level is 0.4 eV below the E_c of GaN [71]. Therefore, bare O_N is positively charged as O_N^+ during stress (Fig. 4.4). The resulting O_N^+ shifts the threshold voltage negatively and degrades the transconductance by scattering the carriers in the two-dimensional electron gas (2DEG) as a Coulombic monopole, consistent with the experimental data obtained during the stressing sequence in Fig. 4.1.

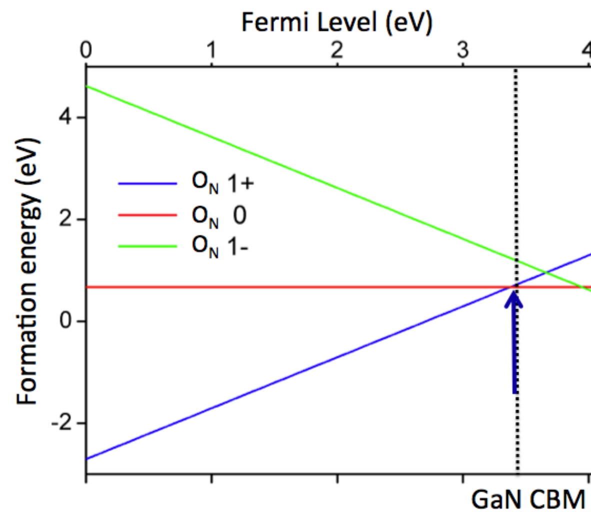

Fig. 4.4. Formation energy of O_N in AlGaN as a function of the AlGaN Fermi level. The blue arrow shows the position of the +1/0 transition level. The dotted line shows the position of the CBM of GaN. The three straight lines with different colors represent three different charge states of O_N.

Using the DFT results, we can explain the recovery of threshold voltage and transconductance. During annealing, when the negative V_{gs} stress voltage is removed, the Fermi-level at the AlGaN/GaN interface moves above the GaN CBM and O_N^+ defects capture electrons from the 2DEG to become neutral O_N. This leads to a rapid recovery in both threshold voltage and transconductance. The observed "super recovery" of the transconductance can be understood by the difference in properties between O_N-H and O_N; although both defects are charge neutral, they have slightly different strengths in scattering electrons. Neutral O_N defects have no electrical monopole or dipole moments and therefore scatter electrons negligibly in the 2DEG (only a short-range scattering potential is present), while its precursor O_N-H has an electrical dipole moment and scatters the carriers at a slightly higher rate (the scattering potential has a $1/r^2$ tail). As a result, the conversion of O_N-H to O_N after both stress and anneal can enhance the electrical mobility, relative to the pre-stress value, which may account for the super-recovery of the transconductance in Fig 4.1(b). If we apply electrical stress again, the Fermi-level moves E_c - 0.4 eV. The neutral defects O^0 emit electrons, resulting in O_N^+. Then the peak transconductance quickly drops to a value below the original level, as observed in Fig. 4.1.

The different responses of the NH_3-rich unpassivated HEMTs, NH_3-rich passivated HEMTs, and Ga-rich unpassivated HEMTs during post-stress annealing likely result from their different initial concentrations of O_N-H precursors. Although both passivated and unpassivated devices are exposed to air after fabrication, and may have similar initial amounts of O_N and O_N-H at the top surface of AlGaN before the passivation step, after storage the unpassivated samples have higher O_N and O_N-H concentrations in the interior. This is because oxygen and hydrogen diffusion can

continue at a low but finite rate for the unpassivated devices, even at room temperature, but the Si_3N_4 passivation blocks these processes effectively. To evaluate the plausibility of the idea that oxygen diffusion at room temperature after device processing may contribute to the observed degradation and recovery, we estimate the diffusion length x of oxygen in AlGaN using $x = (2Dt)^{1/2}$, where D is the diffusivity and t is the time. Assuming that an unpassivated device is exposed in air for 6 months and taking an value of oxygen diffusivity in GaN as $D = 6 \times 10^{-16} cm^{-2} s^{-1}$ [125],the calculated diffusion length is 400 nm. As the AlGaN layer in the unpassivated device is only 30 nm thick, it is likely that oxygen can diffuse through the AlGaN and arrive at the AlGaN/GaN interface, leading to an enhanced concentration of O_N, and the observed super-recovery in Fig. 4.1. Moreover, water molecules dissociate into H and OH when absorbed at the surface of GaN or AlGaN [126][127][128]. Thus, O_N-H diffusion is also likely to occur, and H diffusion and passivation of pre-existing O_N is also likely, further supporting the plausibility of these mechanisms.

For control NH_3-rich passivated HEMTs (Fig. 4.2(a)), no super-recovery [72] occurs in passivated devices. Moreover, the recovery of the transconductance is more complex in Ga-rich unpassivated devices (Fig. 4.2a) than for the NH_3 unpassivated devices (Fig. 4.1). As shown in Fig. 4.2(b), after the first stress, the device shows more recovery in peak transconductance than observed in NH_3-rich passivated devices, and no super-recovery is seen. Our DFT calculations show that a reduction in density of Ga-vacancies inhibits O diffusivity in GaN and AlGaN [104]; hence, it is likely that the devices fabricated under Ga-rich conditions may have fewer O_N and O_N-H impurities than NH_3-rich samples, leading to less super-recovery in transconductance. Finally, we note that the “super recovery” of transconductance also has not been observed in previous experiments on

different types of passivated devices [49][65][72], suggesting that the responsible defects in these NH_3 unpassivated devices are different from those in previous devices, i.e., $V_{Ga}H_x$ and $N_{Ga}H_3$. [49]

4.4 Conclusion

In summary, we have investigated hot carrier stress and annealing effects in unpassivated and passivated ammonia-rich AlGaN/GaN HEMTs. Devices exhibit fast recovery during annealing with all pins grounded, with super-recovery of the peak transconductance observed in the unpassivated devices. DFT calculations suggest that dehydrogenation of pre-existing O_N-H defects plays a significant role in hot carrier degradation of NH_3-rich AlGaN/GaN HEMTs. The super-recovery in peak transconductance can be naturally caused by a change of the Fermi-level during the annealing process and the resulting neutralization of stress-induced bare O_N defects at the AlGaN/GaN interface.

CHAPTER V

TID EFFECTS IN PASSIVATED AND UNPASSIVATED HEMTS

In this chapter, we report the effects of 10-keV X-ray irradiation and high-voltage stress on AlGaN/GaN HEMTs. Significant non-recoverable negative threshold voltage shifts are found in both passivated and unpassivated devices, but transconductance degradation is only observed in unpassivated devices. We attribute the variations in the observed response to differences in relative densities of charged oxygen and hydrogenated oxygen impurity centers among the various types of devices.

5.1 Experimental details

AlGaN/GaN HEMTs were fabricated on AlGaN/GaN heterostructures grown by ammonia-rich or Ga-rich plasma-assisted molecular beam epitaxy (PAMBE) on 4H-SiC substrates (group A) or on GaN substrates (group B) at the University of California, Santa Barbara [13][29][65]. The HEMTs were irradiated with a 10-keV ARACOR x-ray source at a dose rate of 31.5 krad(SiO_2)/min at 295 K with all pins grounded. Some devices were subjected to voltage stress under semi-on bias conditions [39][72] (15 V drain voltage and -2 V gate voltage). Device responses to annealing after irradiation were evaluated at room temperature. I_D−V_G curves were measured in air before and after irradiation with a HP 4156B Semiconductor Parameter Analyzer with 0.5 V source-drain voltage and gate voltage swept from -7 V to 1 V. An effective value of threshold voltage V_{th} was extracted

from I_D-V_G curves in the linear range of the transistor response. For group A, initial values of V_{th} were approximately -4.1 V for NH_3-rich unpassivated devices, -2.8 V for NH_3-rich passivated devices, and -5.1 V for Ga-rich unpassivated devices. For group B, the initial value is -4 V. Pre-irradiation device characteristics of similar devices vary by less than ~ 10%.

5.2 Experimental results and analysis

5.2.1 TID and annealing responses of unpassivated HEMTs

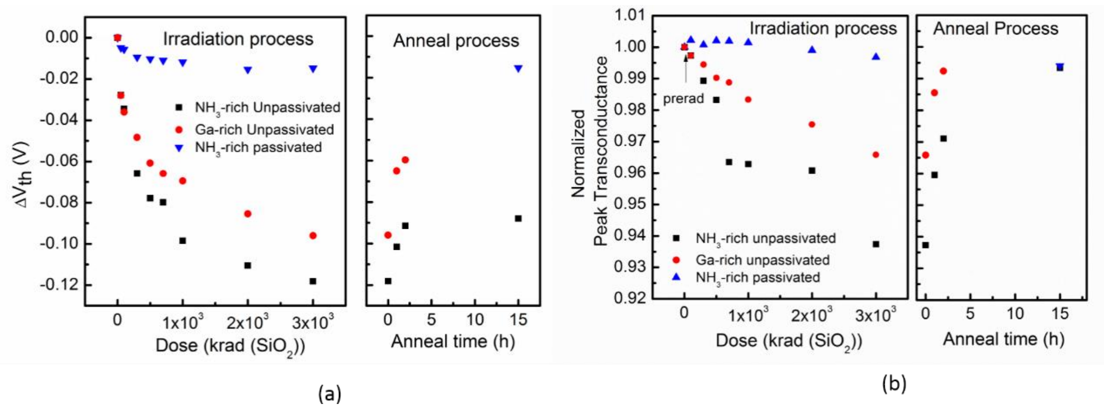

Fig. 5.1. Changes in (a) threshold voltage and (b) normalized peak transconductance as a function of total ionizing dose and annealing time for Ga/AlGaN HEMTs that vary in device processing and passivation.

For group A, devices were irradiated to 3 Mrad(SiO_2) with all pins grounded. The shifts in threshold voltage and changes in normalized peak transconductance are shown in Fig. 5.1. Three kinds of devices with the same structure were tested: NH_3-rich unpassivated devices (V_{th} shift = -0.12 V), Ga-rich unpassivated devices (V_{th} shift = -0.10 V) and NH_3-rich passivated devices (V_{th} shift less than -0.02 V). After 15 hours of annealing, there is still a -0.08 V shift in NH_3-rich unpassivated devices. The peak transconductance degrades about 7% after 3 Mrad(SiO_2) X-ray irradiation for NH_3-rich unpassivated devices and 4% in Ga-rich devices, as shown in Fig. 5.1(b). This

degradation is recoverable after 5 hours of annealing for Ga-rich devices and 15 hours of annealing for NH_3-rich ones. The passivated devices show no changes in peak transconductance. In addition to the significant negative shift in threshold voltage, the gate leakage current also shows a significant increase in unpassivated devices, as shown in Fig. 5.2. The leakage current increases almost one order of magnitude after 3 Mrad(SiO_2) X-ray irradiation for both NH_3-rich and Ga-rich unpassivated devices, as compared to pre-irradiation gate leakage.

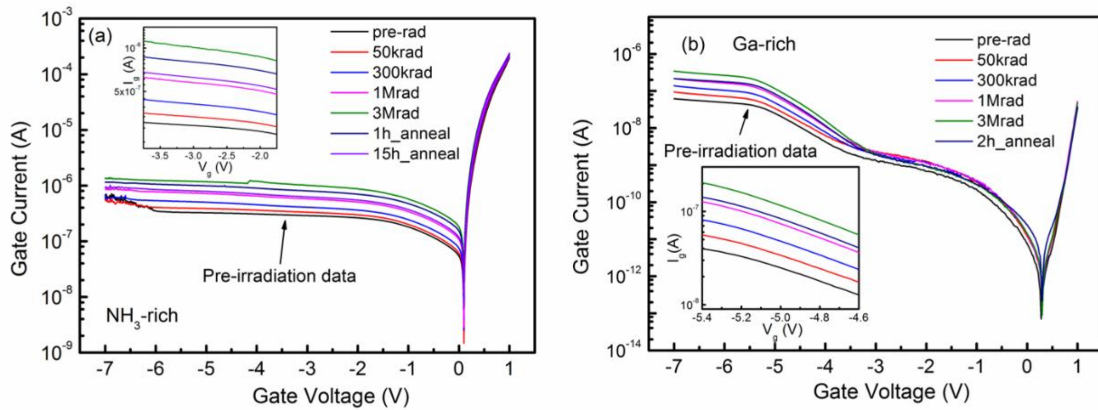

Fig.5.2. I_g-V_g curves for (a) ammonia-rich unpassivated HEMTs and (b) Ga-rich unpassivated devices at $V_d = 0.5$ V before and after X-ray irradiation.

5.2.2 TID and annealing responses of passivated HEMTs

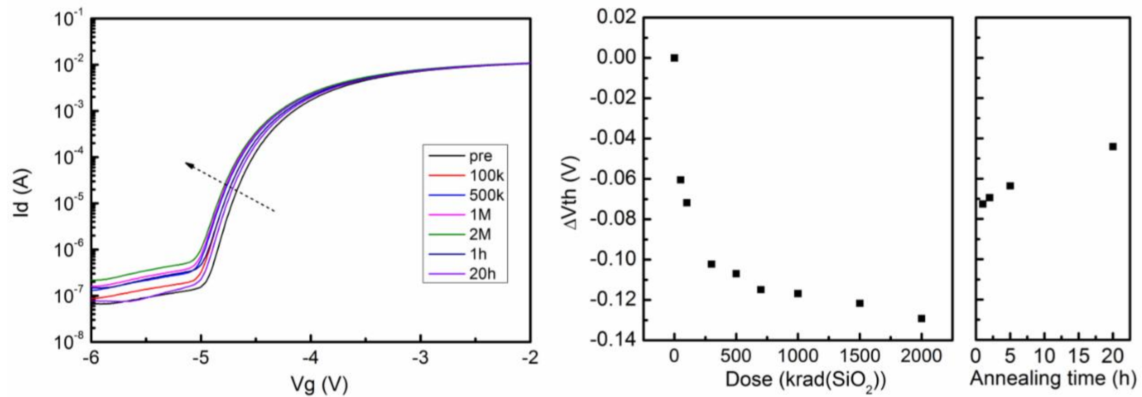

Fig. 5.3. (a) I_d-V_g curves AlGaN/GaN HEMTs at $V_d = 0.5$ V before and after X-ray irradiation with all pins grounded. (b) The threshold voltage as a function of total ionizing dose and time.

We have also evaluated the X-ray irradiation response of passivated HEMTs fabricated with several different processes. Unlike the control passivated HEMTs in group A, a significant negative shift in threshold voltage is also observed in at least two kinds of HEMTs fabricated by UCSB using different processes. Fig. 5.3(a) shows the I_d-V_g curves of AlGaN/GaN HEMTs fabricated on free-standing GaN substrates (group B) before and after irradiation with all pins grounded. The threshold voltage shift vs. dose is shown in Fig. 5.3(b). Here a negative shift in V_{th} is observed, with a maximum shift of -0.1 V at 2 Mrad(SiO_2), with recovery to -0.04 V after 2 hours of annealing. This response is similar to that observed in industrial grade devices in [58]. No peak transconductance degradation is observed in these devices, and the gate leakage current only increases by about 50% after 2 Mrad(SiO_2) irradiation.

5.2.3 Irradiation and annealing responses of unpassivated HEMTs with hot-carrier injection

The combined effects of voltage stress and X-ray irradiation in unpassivated devices were also investigated. Devices were stressed with V_{ds} = 15 V, V_{gs} = -2 V during the X-ray irradiation. The threshold voltage shifts are plotted in Fig. 5.4(a). X-ray irradiation combined with large drain bias stress results in a shift of -0.16 V, which is much larger than the -0.03 V shift caused by hot carrier effects only. We calculate the sum of the threshold voltage shift caused by hot carrier effects and the shift caused by X-ray irradiation with all pins grounded, as shown by the blue triangles in Fig. 5.4(a). The value is about the same as the shift caused by X-ray irradiation with large drain bias stress on, indicating that the radiation-induced and voltage-stress induced threshold voltage shifts are simply additive. This contrasts with the more complex interaction between proton irradiation

and high-voltage stress in [61] and [96]. In Fig. 5.4(b), the peak transconductance of irradiated devices shows a degradation of 10% which is larger than either hot carrier effects (8%) or X-ray irradiation (7%) alone.

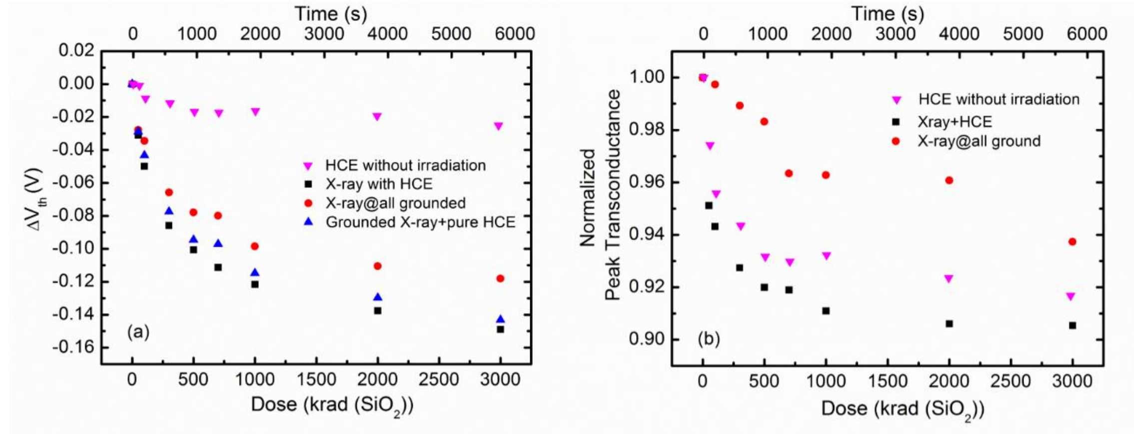

Fig. 5.4. (a) Threshold voltage shift and (b) changes in peak transconductance as a function of time under X-ray irradiation and/or voltage-stress at 15 V drain bias and -2 V gate bias.

5.3 Discussion

The above results demonstrate the sensitivity of AlGaN/GaN HEMTs to ionization effects, and show that ionization effects can be comparable to the degradation observed under typical voltage-stress conditions. Moisture absorption is always suspected when unpassivated devices show significant degradation relative to passivated devices. Other critical factors include oxygen impurity centers O_N, which can either be stand-alone impurity defects or hydrogenated as (O_N-H) [49][65][72][76]. O_N and O_N-H defects can form both during and after fabrication, with the relative densities of O_N and O_N-H subject to variations, depending on whether hydrogenation or dehydrogenation is favored during fabrication, stress, and/or annealing. Our previous work suggested that

dehydrogenation of pre-existing O_N-H defects plays a significant role in hot carrier degradation of NH_3-rich AlGaN/GaN HEMTs [104]. Similarly, the unrecoverable negative shift in threshold voltage in both passivated and unpassivated HEMTs indicate that positive charges are generated in the device by irradiation. Such an increase of positive charge is likely caused by the dehydrogenation of pre-existing O_N-H defects in AlGaN layer, which leave bare O_N defects that are positively charged when the Fermi level is below the conduction band minimum of the GaN, according to density functional theory calculations [104]. In the AlGaN barrier layer, the Fermi level is usually below that of the GaN conduction band [71], therefore most of the newly generated bare O_N defects in AlGaN barrier layer are O_N^+. The passivated devices show no degradation in peak transconductance, indicating that the newly generated bare O_N^+ defects in these devices are far away from the AlGaN/GaN interface and thus do not affect the carrier mobility in the channel. Unpassivated devices show degradation of peak transconductance by irradiation, indicating that a non-negligible amount of the newly generated O_N^+s are close to the channel and behave as Coulombic scattering centers.

The contrast between passivated and unpassivated devices in transconductance degradation is consistent with the identification that pre-existing O_N-H defects are the main source of the irradiation response. In unpassivated devices, oxygen can diffuse through the AlGaN and arrive at the AlGaN/GaN interface, leading to the formation of O_N and water molecules dissociate into H and OH when absorbed at the surface of GaN or AlGaN[104]. So the unpassivated devices have higher concentration of O_N-H defects in the AlGaN layer, both far away from and close to the AlGaN/GaN

interface. After irradiation, there are more O_N^+ defects near the interface in these devices. In contrast, the passivated devices have low concentration of O_N-H defects in the AlGaN layer and as a result few O_N^+ defects are generated near the interface, thus having a negligible impact on the channel mobility. The higher concentration of O_N-H defects in unpassivated devices also explains the greater threshold shifts in these devices compared to the passivated one, as shown in Figure 5.1. Moreover, our DFT calculations show that a reduction in density of Ga-vacancies inhibits O diffusivity in GaN and AlGaN [104]; hence, it is likely that the devices fabricated under Ga-rich conditions may have fewer O_N and O_N-H impurities than NH_3-rich samples, leading to smaller degradation in Ga-rich unpassivated samples, as shown in Fig.5.1.

5.4 Conclusion

We investigated total ionizing dose effects in unpassivated and passivated AlGaN/GaN HEMTs with 10-keV x-rays, as well as the combined effects of irradiation and hot carrier stress in unpassivated devices. Significant non-recoverable negative threshold voltage shifts are found in devices fabricated using both passivated and unpassivated devices, but transconductance degradation is only observed in unpassivated devices. DFT simulations suggest that X-ray irradiation causes degradation by generating positively charged O_N^+ centers from the pre-existing O_N-H defects on the surface of the devices. In passivated devices, the O_N^+ traps are only generated on the surface and only cause shifts in V_{th}, while in passivated devices these centers can be generated on both the surface and near the 2DEG layer, resulting in degradation in transconductance.

CHAPTER VI

BIAS DEPENDENCE OF HIGH FIELD STRESS INDUCED DEGRADATION IN HEMTS

As mentioned in Chapter 2.4, several types of defects can lead to hot-carrier induce degradation, and donor-like and acceptor-like defects result in oppositely directed shifts in threshold voltage V_{th}, although in past studies a single defect type tended to dominate device degradation [49][61][72][95][101]. As AlGaN/GaN HEMTs advance in maturity and overall defect densities are reduced, there is an increasing likelihood that multiple defects may contribute to device degradation simultaneously, at least over particular ranges of bias conditions, complicating the analysis of device response and of long-term reliability prediction.

In this work, the gate and drain bias dependence of hot electron-induced degradation of AlGaN/GaN HEMTs is evaluated for two differently processed types of devices. In each case, both donor- and acceptor-like defects play significant roles in the device degradation. Whether the observed *Vth* shift is positive or negative depends strongly on biasing conditions. The largest transconductance degradation is observed under the "ON" bias condition for types of devices. Low-frequency noise measurements are performed as a function of temperature to identify the defects responsible for the observed degradation. The observed defects in this study are compared with a broad range of defects identified in previous work involving both irradiation and high-voltage stress. Oxygen and hydrogen related impurities centers play significant roles in these devices.

6.1 Experimental details

AlGaN/GaN HEMTs were fabricated on AlGaN/GaN heterostructures grown by Ga-rich plasma-assisted molecular beam epitaxy (PAMBE) with 700 nm unintentionally doped (UID) GaN on GaN substrates grown by PAMBE (sample A) or MOCVD (sample B) on SiC, as shown in Fig. 6.1. The gate has the shape of an inverted trapezoid, with a length (L_G) of 0.7 μm. The gate-to-drain separation (L_{GD}) is 1 μm, and the gate-to-source separation (L_{GS}) is 0.5 μm[25], [29]. The tested devices have a T-shaped layout, and 2 x 75 μm gate width. The top view of the device was shown in Fig 6.1(b). I_{ds} - V_{gs} device characteristics were measured in air before and after irradiation with a HP 4156B or Agilent B1505 Semi-conductor Parameter Analyzer with 0.5 V source-drain voltage and the gate voltage swept from -7 V to 1 V.

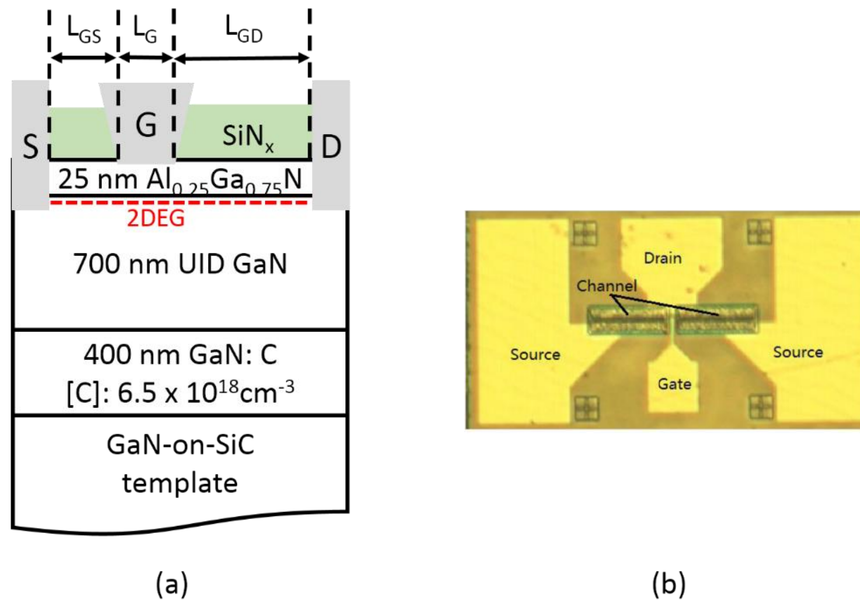

Fig. 6.1. (a) Schematic diagram of HEMT structures grown on GaN-on-SiC substrates – not to scale. (After [23].) (b) Top view of DUT. The devices have two sources. For stressing and device testing in the OFF and Semi-ON states, both sources are connected. For ON state stressing and testing, only one of the two sources is connected to limit heating effects.

To minimize heating effects during stress and testing, the devices were bonded using a high speed package [112], which provides an effective heat sink [72]. For ON state bias stress, to further reduce the possibility of significant heating, only one of the sources was connected during the stress and I_{ds} - V_{gs} test. For devices with both sources connected, the package tem-perature, as measured with a thermocouple, is stable at ~ 330 K after 1 h of ON state bias stress, 309 K for Semi-ON stress, and ~ 295 K (room temperature) for OFF state stress. In con-trast, the package temperature for an ON state device with a single source is ~ 307 K, which provides a closer temperature match to Semi-ON and OFF-state devices stressed with both sources connected.

An effective value of V_{th} was extracted from I_{ds} - V_{gs} curves in the linear range of transistor response [3][129]. For sample A, the pre-irradiation value is V_{th} = -4.3 $\pm$0.2 V, and for sample B, V_{th} = -4.0 $\pm$0.2 V. At least two devices were measured for each test condition. The responses of the devices were evaluated over a range of gate and drain biases at room temperature, with a limited number of measurements performed for comparison at 400 K (both stress and test).

6.2 Experimental Results

6.2.1 Gate bias dependence of high field stress induced degradation HEMTs at room temperature

Figs. 6. 2(a) and (b) show V_{th} shifts versus stress time for devices with PAMBE and MOCVD grown substrates, as a function of applied gate bias during stress. Devices were stressed at drain bias V_{ds} = 20 V, at biases V_{gs} -$V_{th}(0)$ from -2.0 V to 5.5 V (PAMBE devices) and -3.6 V to 5.3 V

(MOCVD devices), where $V_{th}(0)$ is the pre-stress threshold voltage. For reference, we plot the resulting V_{th} shifts in each case at 10 h in Fig. 6.4(a).

A large positive V_{th} shift (~ 0.35 V at a stress time of 12 h) is observed in devices with PAMBE substrates under ON-state bias stress (V_{gs} - $V_{th}(0)$ = 5.5 V in Fig 6. 2(a)). On the other hand, a large negative shift is observed for OFF state stresses (V_{gs} - $V_{th}(0)$ = -1.5 V and -2V in Fig 2(a)). In both the ON and OFF states, stress-induced V_{th} shifts are larger than those in otherwise similar devices from previous process runs [61][72][104]. Fig. 6.3 (c) shows that V_{th} shifts are less negative (or increasingly positive) as the value of V_{gs} -$V_{th}(0)$ is varied from -4 V to 5.5 V. For the "Semi-ON" state, with V_{gs} -$V_{th}(0)$ in the range of +1 to +2 V for these devices, often found to be the worst case for hot carrier effects in AlGaN/GaN HEMTs [37][39] [49][71][78], V_{th} shifts are smaller in magnitude than for "OFF" state stress.

The results of Fig. 6.2 and Fig. 6.4 (a) indicate that precursors for both electron (acceptor-like) and hole (donor-like) traps most likely exist in these devices. Electron traps are dominant when devices are stressed in the ON state, hole traps are dominant when devices are stressed in the OFF state, and the two types of defects evidently lead to offsetting effects when devices are stressed in the Semi-ON state. Except at the most positive stress voltage, where devices on PAMBE substrates show larger shifts, V_{th} shifts are generally similar for the two device types.

Normalized peak transconductance G_M degradation is shown as a function of stress time in Fig. 6.3 for (a) PAMBE and (b) MOCVD substrate devices. The degradation in peak G_M after 10 h stress is plotted as a function of gate bias in Fig. 6.4(b). For both device types, "ON" state stress results in the largest reduction in peak G_M. Peak G_M is reduced by up to 25% For PAMBE devices

and by up to 15% for MOCVD devices. Figs. 6.3(a) and 6.3(b) show that both types of devices show initial increases in peak G_M at very short times under off-state stress, with degradation following at later times. “Semi-ON” stress leads to little change in peak G_M, again in contrast to previous results [37][39][49][71][78], reinforcing the evidently offsetting effects of hole and electron trapping in these devices.

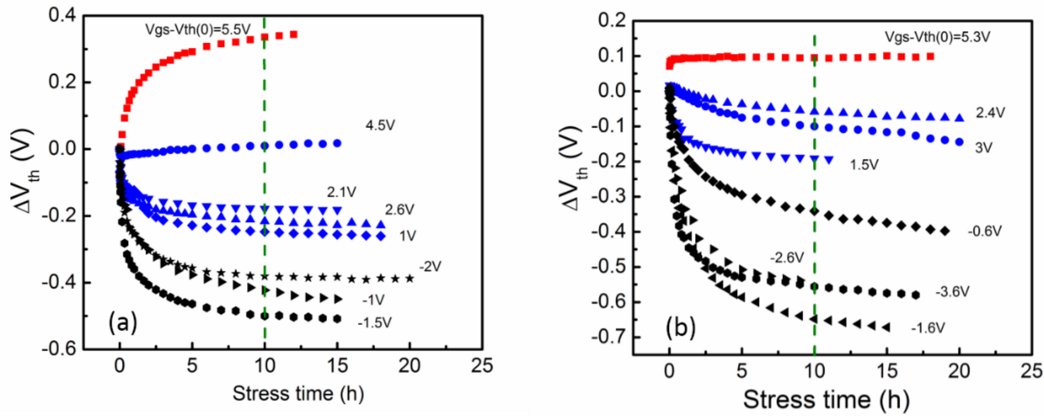

Fig. 6.2. V_{th} shifts versus stress time and gate bias in AlGaN/GaN HEMTs with (a) PAMBE GaN substrates and (b) MOCVD GaN substrates. Red data points show the ON bias condition, blue points show the Semi-ON bias condition, and black points show OFF bias conditions. The applied drain voltage is 20 V in all cases, and all stresses and measurements were performed at room temperature.

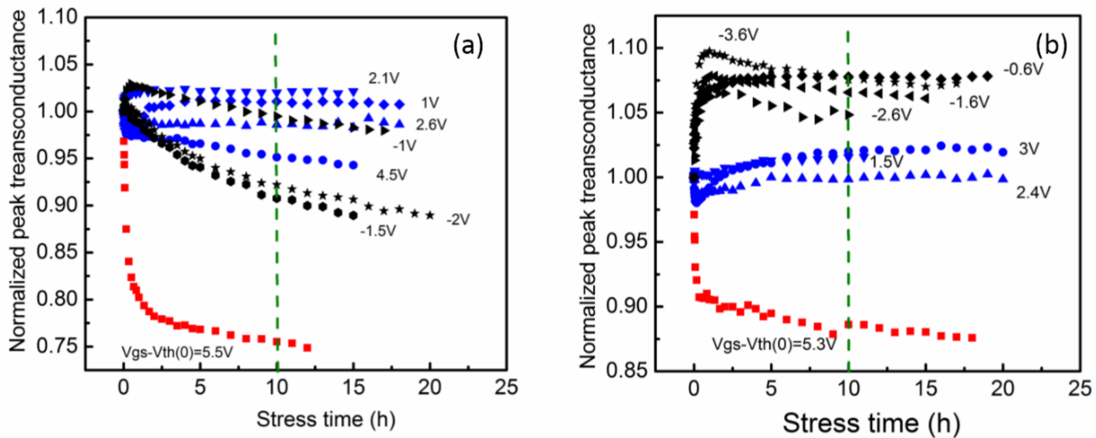

Fig. 6.3. Normalized peak transconductance degradation as a function of stress time under different gate bias in AlGaN/GaN HEMTs with (a) PAMBE GaN substrate and (b) MOCVD GaN substrate . The red data points show ON bias condition, blue points show Semi-ON bias condition and black points show OFF bias conditions

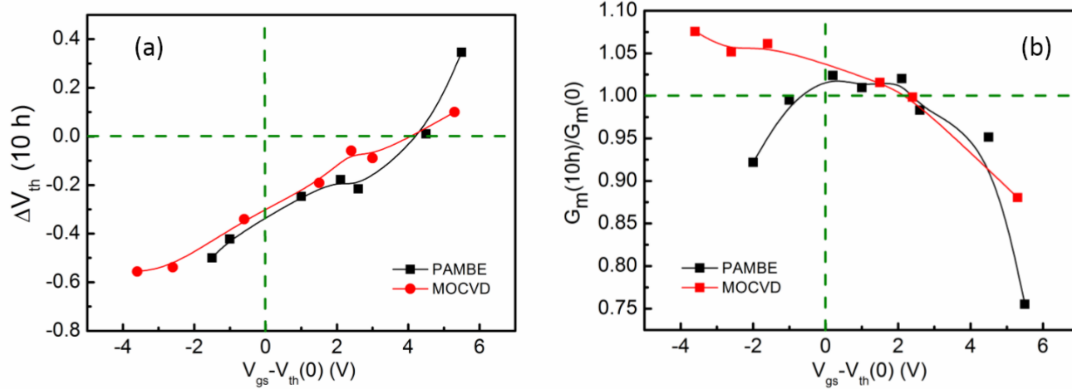

Fig 6. 4. (a) Measured V_{th} shifts and (b) peak transconductance degradation after 10 h stress as a function of gate bias.

To further demonstrate the importance of minimizing heating, Fig. 6.5 compares (a) the V_{th} shifts and (b) the G_M degradation for MOCVD substrate devices with single or double sources. Large shifts are observed for the double source connection as a result of additional heating effects. This additional heating occurs because the drain current during stress with $V_{ds} = 20$ V, $V_{gs} - V_{th} = 5.5$ V is ~40 mA for a single source device, but it can reach ~110 mA for devices with both sources connected, as a result of the effective channel resistance decrease. The calculated channel temperature will be around 400 K for single source device and 420 K for double source [130]. Note that the devices with two source connections stressed in the ON condition show a V_{th} shift greater than that of any of the devices with MOCVD substrates in Fig. 6. 2(b), and a greater G_M degradation than any of the devices with MOCVD sub-strates in Fig. 6.3(b).

We have also evaluated the device annealing response during two hours of storage at room temperature with all pins grounded, as shown in Fig. 6.6, for devices stressed under representative ON, Semi-ON, and OFF stress conditions. The V_{th} shifts in Fig. 6. 6(a) are nearly unchanged during annealing, consistent with previous work [104]. The relative stability of V_{th} during annealing with

all pins grounded reaffirms that the changes in threshold voltage are associated primarily with defects created (and/or passivated) during voltage stress, and not associated with heating effects, for example. There is a relatively significant recovery during the post-stress annealing for the peak G_M in Fig. 6.6 (b) for the MOCVD devices stressed in the ON state, but small or negligible changes in peak G_M for the other stress conditions.

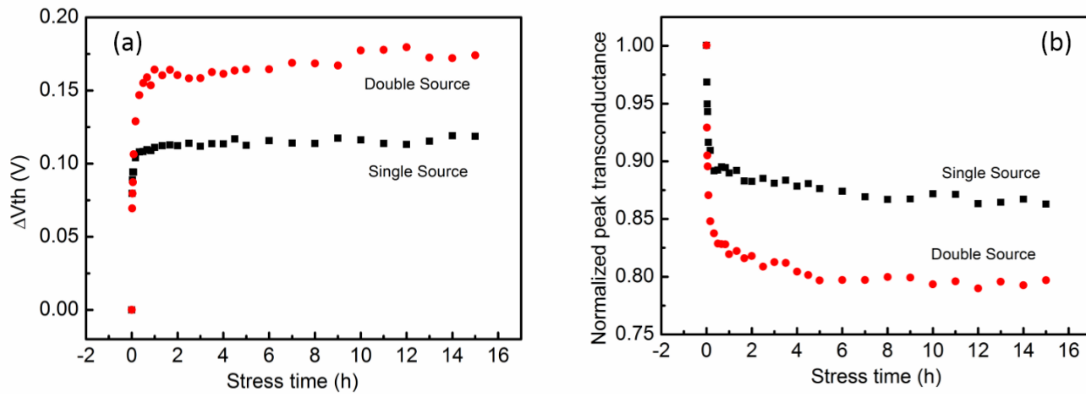

Fig. 6. 5. (a) Threshold voltage and (b) normalized peak transconductance degradation as a function of stress time under V_{ds}=20V, V_{gs}-V_{th}=5.5V in AlGaN/GaN HEMTs with MOCVD GaN substrate for half device with single source and whole device with double source.

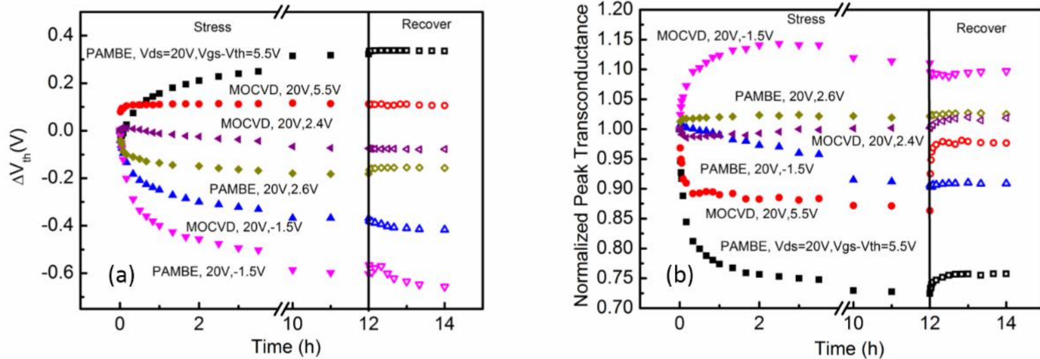

Fig 6. 6 (a) Threshold voltage shift and (b) normalized peak transconductance degradation as a function of stress time and room-temperature annealing time for AlGaN/GaN HEMTs with PAMBE and MOCVD grown substrates stressed under represenrative ON state, Semi-ON state and OFF state. Annealing was performed at room temperature with all pins grounded.

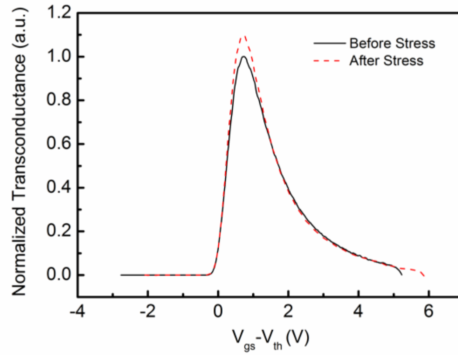

Fig. 6. 7. the normalized transconductance as function of V_{gs}-V_{th} (over drive gate bias) for MOCVD GaN substrate devices before and after 10 hours stress with V_{gs}-V_{th}=-3.6V, V_{ds} =10V

The transconductance is plotted as function of V_{gs}-V_{th} before and after stress in Fig. 6.7. The positions of the peaks and the shapes of the transconductance-voltage curves show little change with stress, indicating that the increases in peak transconductance is due to a decrease in scattering rate, and not the results of V_{th} shifts. Similar results are observed for devices on PAMBE substrates.

6.2.2. Gate bias dependence of high field stress induced degradation at high temperature

Because the results of Figs. 6.2-6.7 suggest that at least two defects are influencing the device response to voltage stress at room temperature, it is important to determine whether the defects are present in similar proportions at other temperatures [106]. Fig. 6.8 compares the responses of devices on PAMBE substrates that were stressed and measured at 300 K and 400 K. In all cases, devices stressed and measured at 400 K show more positive V_{th} shifts than devices stressed and measured at 300 K. The increase in V_{th} shift with temperature is ~ 0.5 V for OFF state and Semi-ON state stresses, and only 0.2 V for ON bias stresses. Larger decreases (up to 20 %) in normalized peak transconductance are also observed in OFF state and Semi-ON state stresses at 400 K than at 300 K. There is little change in peak transconductance degradation with stress and measurement

temperature for the "ON" state bias condition. These results show that additional electron trapping (activation of acceptor-like defects) is favored in these devices at higher stress temperatures, as compared to hole trapping (activation of donor-like defects). Moreover, Fig. 6.9 shows that the changes in V_{th} and G_M that occur as a result of changing the measuring temperature alone than the observed changes in Fig. 6.8 that are due to stressing the devices at elevated temperature.

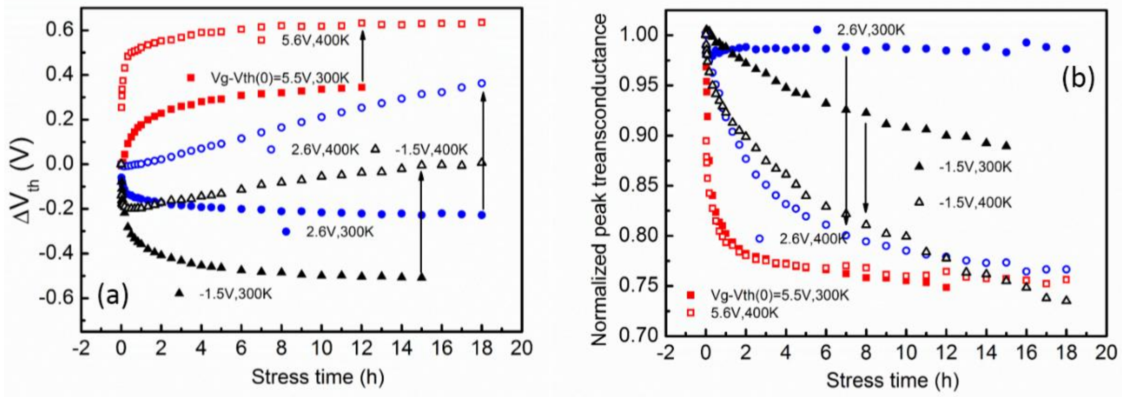

Fig. 6.8. (a) Threshold voltage and (b) normalized peak transconductance degradation for ON (squares), OFF (triangles), and Semi-ON (circles) state stressed for Ga-rich PAMBE GaN substrate devices from UCSB that were stressed and measured at 300 K (solid symbols) and 400 K (open symbols). Similar trends in response were observed for devices on MOCVD substrates.

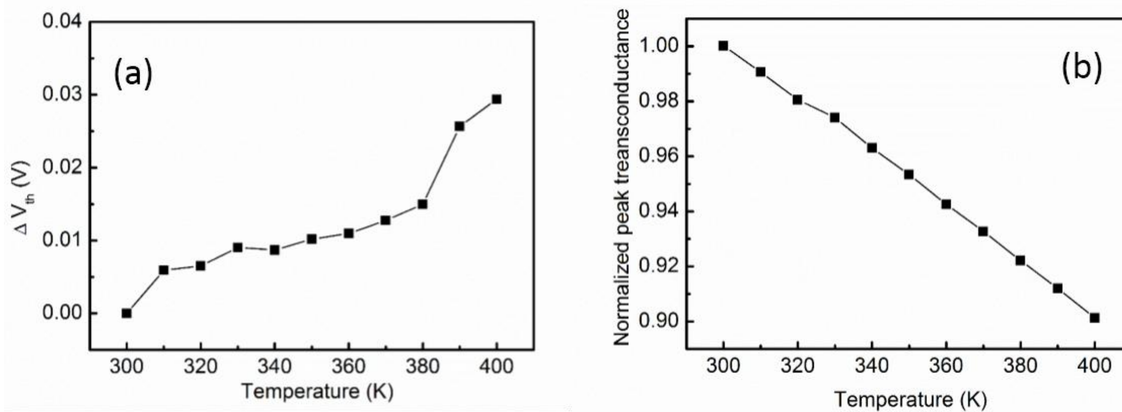

Fig. 6.9. Temperature dependence of (a) V_{th} shifts and (b) normalized peak transconductance degradation for Ga-rich PAMBE GaN substrate devices.

6.2.3. Step drain bias stress induced degradation in AlGaN/GaN HEMTs

We now consider the evolution of device response as individual devices are subjected to progressively higher stress voltages. Fig. 6.10 shows I_d-V_g curves and Fig. 6.11 shows (a) threshold voltage shifts, and (b) transconductance degradation as a function of stressing time for devices with PAMBE substrates stressed at a constant gate bias of 1 V, and drain biases increasing in stages from 10 V to 30 V, in 5 V steps. This corresponds to the ON condition for these devices. The stress period is 10 h for each drain bias. The results of Fig. 6.10 show increasingly larger degradation in ON-state current after higher drain voltage stresses. Correspondingly larger and more positive V_{th} shifts and greater peak transconductance degradation are observed in Figs. 6.11 (a) and (b). The largest rate of change in V_{th} is observed for $V_{ds} = 20$ V, and the largest rate of change in peak transconductance is observed at $V_{ds} = 15$ V, consistent with an acceleration in the rate of electron trapping and the resulting increase in carrier-defect scattering [49][51][76].

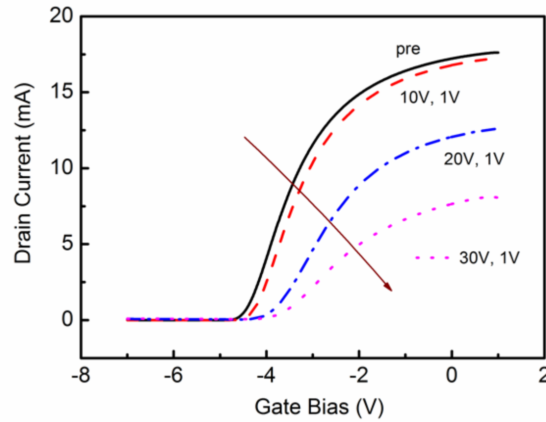

Fig. 6.10. I_d-V_g curves for AlGaN /GaN HEMTs at $V_d = 0.5$ V for Ga-rich PAMBE GaN substrate devices from UCSB before and after ON state bias stress. The gate bias is 1 V during the stressing process (ON state). The drain bias stress starts at 10 V, with a step of 5 V. For each condition, devices are stressed for ~ 10 h.

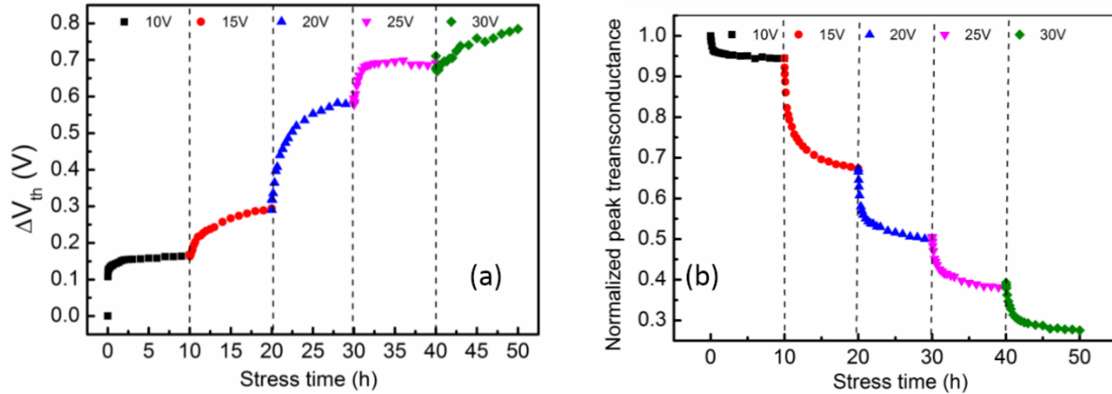

Fig. 6.11. (a) Threshold voltage and (b) normalized peak transconductance degradation under a series of drain biases for Ga-rich PAMBE GaN substrate devices from UCSB. The transconductance is normalized to the peak transconductance of a fresh device.

Fig. 6.12 and 6.13 shows results for similar stepped-drain voltage stresses for similar devices under OFF state bias conditions. These devices were stressed stressed at a constant gate bias of -6 V, and drain biases increasing in stages from 10 V to 40 V, in 5 V steps. The stress period is 8 h for each drain bias. A clear turnaround is observed in the V_{th} shifts in Fig. 6.13(a), with negative shifts observed at lower drain biases, and increasingly positive shifts observed at higher drain biases. Very little transconductance degradation occurs at low drain biases in Fig. 6.13(b), with much larger degradation in transconductance observed at larger stress biases. This result suggests that acceptor-like defects dominate the transconductance degradation in these devices under OFF state conditions, while donor-like defects are relatively more important to threshold voltage shifts at lower drain biases than at higher drain biases. These differences in effectiveness of donor- and acceptor-like defects on the V_{th} shifts and transconductance degradation suggest that these defects may be located in different regions of the devices, with the acceptor-like defects located closer to the edge of the gate that is closest to the drain, in the AlGaN layer, and not in immediate proximity to the conducting channel [72][83][131][132]. This is the region of the device where the electric

field tends to be highest [76][83][106][131][132]. In contrast, the donor-like defects that are created above a "critical" drain voltage[54] of ~ 15-20 V are evidently located in the GaN buffer layer and closer to the drain, where the current is highest, and/or in the AlGaN layer in very close proximity to the conducting channel [72][78][133][134][135][136]. The microstructure and locations of these devices are discussed further below.

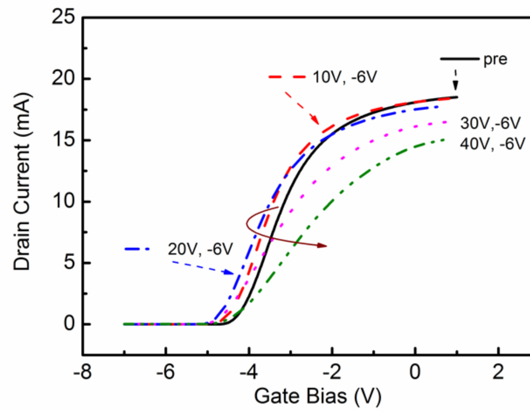

Fig. 6.12. I_d-V_g curves for AlGaN /GaN HEMTs at V_d = 0.5 V for Ga-rich PAMBE GaN substrate devices from UCSB before and after OFF state bias stress. The gate bias is -6 V during the whole process (OFF state). The drain bias starts from 10 V, with a step of 5 V. For each condition, devices are stressed for around 8 hours, which is sufficiently long for degradation to reach saturation at low biases.

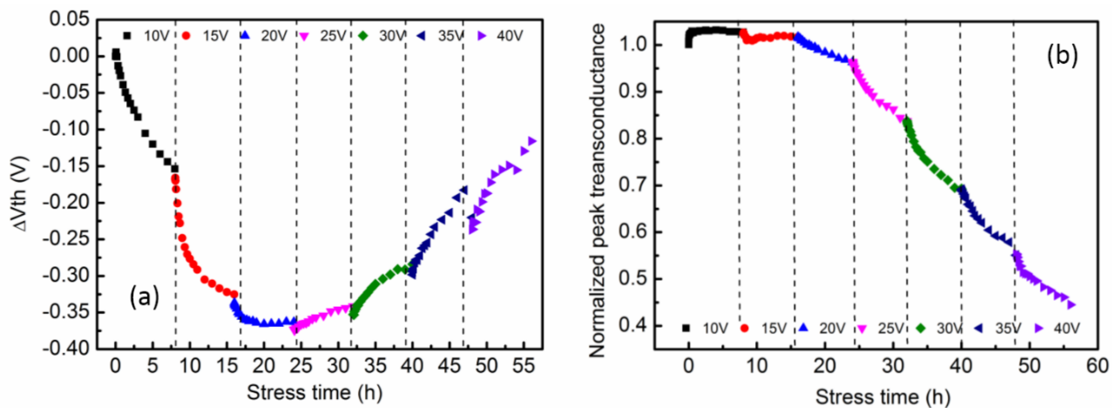

Fig. 6.13 (a) Threshold voltage shift and (b) normalized peak transconductance degradation under a series of drain biases for Ga-rich PAMBE GaN substrate devices. The transconductance is normalized to the peak transconductance of a fresh device.

6.2.4 Low frequency noise

To obtain insight into the nature and energy distribution of the defects responsible for the stress-induced degradation, we have measured the temperature dependence of the low frequency 1/*f* noise of representative devices [61] [65] [69][72]. Fig. 11 shows the excess drain voltage noise power spectral density S_V (corrected for background noise) for AlGaN/GaN HEMTs with PAMBE-grown GaN on SiC substrates (sample A) at constant $V_{gs} - V_{th}$ = 0.8 V and V_{ds} = 0.05 V at room temperature. The bias voltages chosen here and for the measurements of the temperature dependence of the noise that follow ensure that the noise originates primarily from the gated por-tion of the channel, and the channel resistance is an approximately constant [120] [129]. As shown in Fig. 6.14, noise originating in the channel follows a $1/f^{\alpha}$ dependence, where

$$\alpha = -\partial\left(\ln S_{vd}\right)/\partial\left(\ln f\right) \tag{3.1}$$

is approximately unity in magnitude. According to Dutta-Horn model of low-frequency noise [68] [69], the frequency and temperature dependence of the noise are related via,

$$\alpha(\omega, T) = 1 - \frac{1}{\ln(\omega\tau_0)}\left(\frac{\partial \ln S_V(T)}{\partial \ln T} - 1\right) \tag{3.4}$$

where ω=2π*f*, *T* is the temperature and τ_o is the characteristic time of the process leading to the noise (here assumed to be ~ 3 x 10^{-14} s [68] [71]). Fig. 6.15 shows that the α from experimental data are in good agreement with the value suggested by Dutta-Horn model. Thus, from the temperature dependence of the noise magnitude, we can estimate the shapes of the defect energy distributions *D(E0)* from low-frequency noise measurements [68] [69], via

$$D(E_0) \propto \omega/(kT)*S_{V,} \tag{3.5}$$

where

$$E_0 = -kT \ln(\omega\tau_0) \tag{3.6}$$

is the effective defect activation energy[68][122].

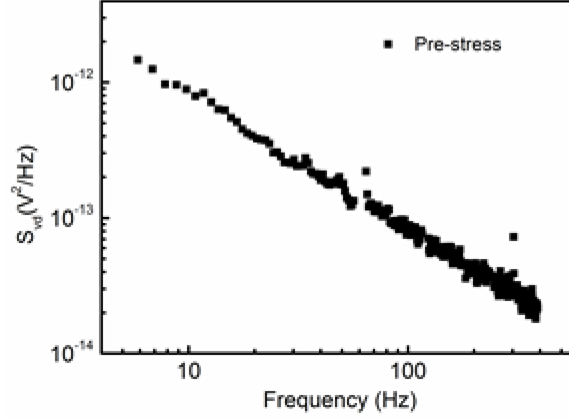

Fig. 6.14 Example: excess voltage noise power spectral density S_{vd} as a function of frequency for AlGaN/GaN HEMTs at 300K, V_{gs}-V_{th} = 0.8 V, V_d = 0.05 V.

In Fig. 6.15 we plot the excess drain-voltage noise power spectral density S_{Vd} (corrected for background noise) as a function of temperature, before and after stress. For the stressed devices, we first anneal the device for 20 minutes with all pins grounded to allow the device to stabilize before the noise measurement process is initiated. The energy scale on the upper x-axis is derived from Eq. (3.6). Fig. 6.16 shows that the measured values of α from the experimental pre-stress noise data are in general agreement with the value suggested by Dutta-Horn model. Similar results are found for the post-stress data (comparisons not shown).

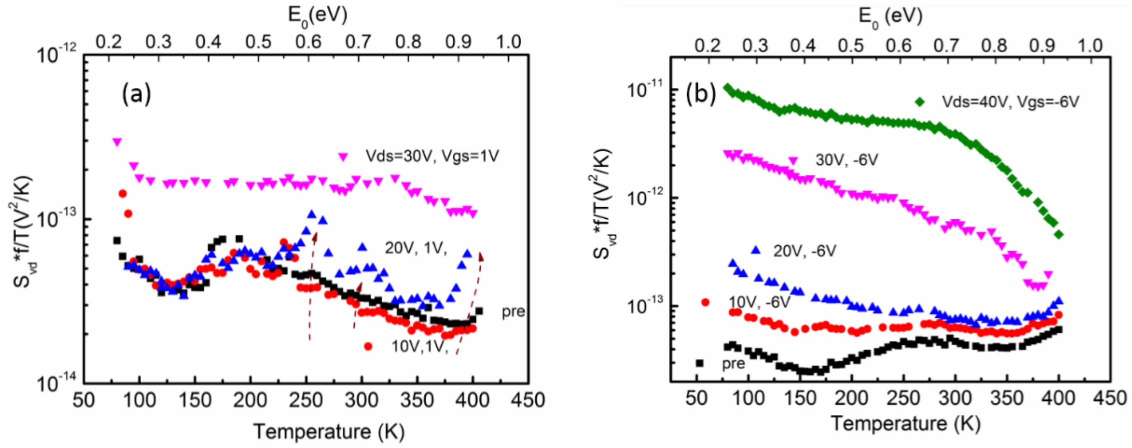

Fig. 6.15. Temperature-dependent noise measurements from 85 to 400 K, at f = 10 Hz for Ga-rich PAMBE devices fabricated at UCSB. The noise is measured under the same conditions as in Fig. 5. The temperature range corresponds to an activation energy scale ranging from 0.2 to 0.95 eV (top *x*-axis). The stress bias condition is (a) ON state and (b) OFF state.

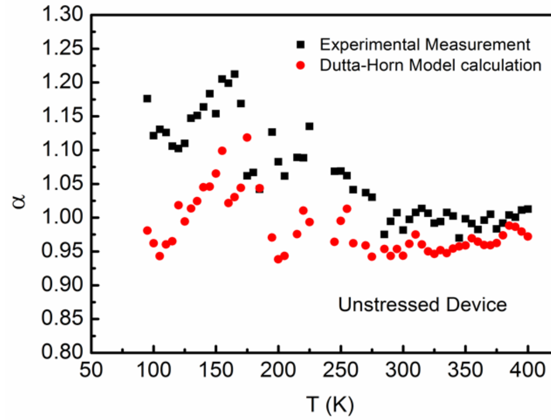

Fig. 6.16 Experimental and calculated frequency exponent of noise power spectral density as a function of temperature from 85 K to 400 K.

The energy scale on the upper x-axis of Figs. 6.15(a) and (b) is derived from Eq. (3.6). Fig. 6.15(a) shows the noise for devices stressed under ON state bias. Before stress, the normalized noise shows a broad maximum in magnitude around ~ 150 K to 200 K (~ 0.4 to 0.5 eV). Stressing the device with V_d = 10 V does not significantly change the noise magnitude. After stressing the device at V_d = 20 V, several local maxima appear in the normalized noise magnitude at ~ 250 K (0.6

eV), 300 K (0.7 eV), and 400 K (0.9 eV) or above. Similar peaks in noise magnitude were observed in other GaN-based HEMTs during studies of their radiation response [61] [65] [71] [72], suggesting that these are likely common defects in Al-GaN/GaN HEMT fabrication. The large increase in effective defect density in Fig. 6.15 (a) is consistent with the increase in peak G_M degradation between V_{ds}=15 V and 20 V in Fig. 6.11(b). After 30 V stress, the noise increases significantly over the entire range of temperatures, which indicates the generation of multiple defects with energies more evenly distributed throughout the band gap.

Fig. 6.15 (b) shows the noise data after "OFF" state stressing at drain voltages of 10 V, 20 V, 30 V and 40 V. Before stress, the normalized noise shows a broad maximum in magnitude around 250 to 300 K (0.6 to 0.7 eV). After stressing the devices at drain voltages less than 20 V, the noise increases more at low temperatures than at higher temperatures. After 20 V stress, the noise exhibits a small local maximum in the effective defect energy distribution at ~0.6 eV, with generally increasing normalized noise magnitude with decreasing temperature below ~ 240 K, and generally increasing noise magnitude above 350 K. For higher stress voltages, again we see a large increase in noise magnitude at all temperature and energies.

6.3 Discussion

The results of Fig. 6. 2-Fig. 6.16, show that positive threshold voltage shifts tend to be observed in these AlGaN/GaN HEMTs under "ON" stress conditions at all drain voltages, and for "OFF" stress conditions only at high drain voltages. A negative V_{th} shift is only observed under "OFF"

stress conditions and low drain bias. Above we have identified two general types of processes that most likely account for the V_{th} shifts and G_M degradation: (1) creation of traps in the channel when devices are stressed under large positive gate bias in the ON-state, or in the gate-drain access region when the device is stressed at high drain voltage in the OFF-state, and (2) creation or activation of hole traps in the AlGaN layer, near the drain-edge of the gate, when devices are stressed under large negative gate voltage in the OFF-state condition at low drain voltages.

For “ON” state stress, the acceptor-like defects responsible for the V_{th} shifts and peak G_M degradation are most likely generated in or near the channel region where current is high-est. High current stressing activates defect precursors by re-moving the H from a pre-existing point defect and/or impurity complex [49] [51]. On the other hand, hole traps generated during “OFF” state stress, leading to much lower G_M degradation than the electron traps, are generated at a location in the device where carriers are energetic and fields are higher, but the charged defects are evidently more distant from the device channel. These traps could be generated, for example, (1) at the SiN/AlGaN interface [83], (2) within the AlGaN layer near the drain edge of the gate, mostly above the 2DEG [131], and/or (3) distributed within the GaN buffer layer, mostly below the 2DEG [133]. As a result, the hole traps are less detrimental to the carrier mobility in the channel, although their density and effects on V_{th} may be significant.

At large OFF state drain voltages, V_{th} shifts positively and the transconductance decreases significantly, similar to what is observed for “ON” state stress at similar drain voltages, confirming that the responsible electron traps are located near the channel, thus reducing the mobility. These traps can result from vacancy migration under high-field stress [87], or by the inverse piezoelectric effect [54]. The

reversal of sign of the V_{th} shifts from negative to positive at higher drain biases shows that generation of electron traps is favored under these stress conditions over generation of hole traps. This is additional evidence that the electron traps responsible for the increasing device degradation at higher drain voltages are most likely formed near the drain end of the channel, in close proximity to the 2DEG.

The low frequency $1/f$ noise results in Fig. 6.15 provide additional physical insight into the micro-structures of the defects that are likely responsible for the degradation. To facilitate the identification of candidate defects that may account for the observed device degradation and low frequency noise, Table 2.1 summarizes a number of defect properties observed in previous studies of the responses of Al-GaN/GaN HEMTs to voltage stress and/or proton irradiation. The direction of V_{th} shift is determined by the type of the traps (donor or acceptor like), while the locations of peaks in noise magnitude as a function of temperature provides information about the energy levels of defects[60] [64] [65] [69] [70] [80] [103] [105][120] [137]. This facilitates the selection of candidate defects that may lead to the observed degradation.

Before stress, as-processed defects with small E_0, such as the nitrogen vacancy V_N ($E_0 \sim 0.25$ eV) [49], [72] and oxygen impurity O_N ($E_0 \sim 0.2$ eV [18]) may contribute to increases in noise magnitude that occur at low temperatures. The dehydrogenation of H-V_N defects and H-O_N defects with bias stressing are therefore logical candidates for increases in noise at low temperature that occur for any of the stressing conditions [60] [64] [65] [69] [70] [80] [103] [105].

Under ON state bias, V_{th} shifts positively for all drain bias stress conditions, suggesting the activation and/or creation of acceptor-like defects. The noise magnitude exhibits local maxima at energies of ~0.6 eV, ~0.7 eV, and ~0.9 eV in Fig. 12(a) after devices are stressed with V_{ds} = 20 V and V_{gs} = 1 V.

Peaks with similar energy levels have been observed in previous work using devices based on materials with a wide range of different processing [61] [71] [72] [80] [96].

The 0.9 eV peak has been identified with an acceptor-like defect that contributes to the observed degradation and low-frequency noise because of changes in the defect charge state that result from H migration within an O_N-H complex [65], as shown in Fig. 14. Above ~ 375 K (~ 0.9 eV), a neutral O_N-H can reconfigure into another structure that is negatively charged, as discussed in detail in [65].

Within Table 1, there are at least three candidate defects in GaN that are acceptor-like after dehydrogenation that may account for the ~0.6 eV and ~0.7 eV peaks in Fig. 12(a). These are the divacancy defect V_{Ga}-V_N, the nitrogen anti-site defect H-N_{Ga}, and iron complexes Fe_{Ga} and Fe_{Ga}–V_N. Hydrogen removal from either of these originally neutral, passivated defects will leave to a negatively charged center that can shift V_{th} positively and contribute to G_M degradation. In this regard, we note that Fe_{Ga} and/or Fe_{Ga}–V_N alone cannot be the only defects leading to voltage-stress induced V_{th} shifts in previous work by Mukherjee, et al. [106], because the V_{th} shifts are *negative* in that study, and cannot be solely due to an acceptor-like defect. So it is likely that multiple defects are contributing to the observed degradation in [106], such as O-related [71] and C-related donor [102].

For the OFF bias condition, after a stress of V_{ds} = 10 V and V_{ds} = 20 V, an increase in noise is observed in the low temperature region in Fig. 12(b). Because V_{th} shifts negatively for this stress condition, it cannot be explained by the activation of acceptor-like defects. But because there is no significant increase in G_M during this stressing interval, the decrease in V_{th} and the increase in noise may result from the thermal transition of an O_N^- DX center to a neutral O_N^0, as illustrated in Fig. 15 [71]. Further emission of an electron from O_N^0 to O_N^+ has essentially no energy barrier [71]. The median energy of

~0.4 eV for this transition is also close to the activation energies of ~0.5 eV for the transition between an O_N^- DX center and O_N^+, as shown in Fig. 15. This mechanism can explain the initial increase in tranconductance during OFF bias stress in two ways: 1) the neutralization of negatively charged defects in the as-processed material can reduce the initial scattering rates [71] [104] and 2) electrons can be injected into the channel by tunneling from the SiN/GaN interface into the AlGaN/GaN channel layer and become trapped [83]. This process is unlikely to happen under ON state bias because the Fermi-level is relatively high [104] and the field is not enough for electron tunneling [83].

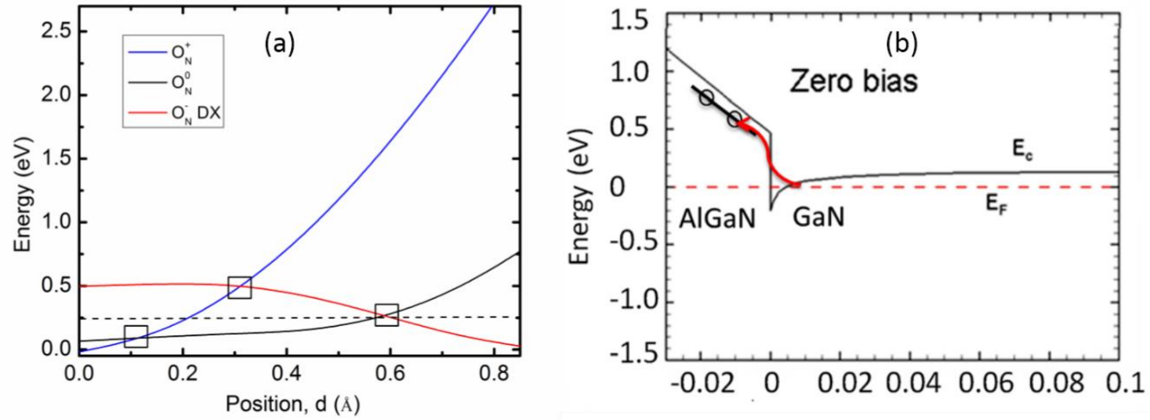

Fig. 6.17. (a) Defect energy of substitutional O in AlGaN as a function of the distance from the ideal lattice site, showing the existence of a DX configuration. Black squares represent transition points between the charge states of O_N during the electron emission. The dashed line shows that the energy barrier to emit one electron from a negatively charged O DX center is 0.25 eV. (b) This diagram schematically illustrates the capture of one electron by the neutral charged oxygen O_N^0, which involves thermally excited tunneling (red arrow) of an electron from a GaN Fermi level to the empty level of O_N^0 defect in AlGaN. The activation energy of the capture is 0.35 eV. (After [71].)

When the drain voltage is larger than 30 V, a larger overall increase of the noise is observed, which can be caused by the generation and increasing dehydrogenation of a large number of (predominantly acceptor) defects with a broad range of activitation energies, similar to what is observed by Chen et al. under similar stress conditions in [72]. These likely include the nitrogen vacancy V_N (E_0~ 0.25 eV) [49] [51], oxygen impurity O_N (E_0~ 0.2 eV [71]), and Fe-related [72] [105] [106] [135] defects discussed

above, as well as additional point defects and defect complexes that can be created as a result of the vacancy and interstitial migration that occurs at high electric fields in AlGaN/GaN HEMTs [87].

6.4 Conclusion

We studied the gate bias dependence of hot carrier effects under fixed drain bias (20 V) and the devices performance under a series of drain biases increasing from 10 V to 30 V or 40 V at two fixed gate bias: 1 V for ON state and -6 V for OFF state. Devices with two different processes were studied for comparison. Unlike previous results, the worst cases for transconductance degradation were "ON" state for both devices. For step drain bias stress testing, devices undergo typical hot carrier induced degradation under "ON" state stress. But under the "OFF" state stress condition, both devices showed a small increase in peak transconductance at low drain bias. The direction of the V_{th} shift changed from negative to positive with the drain bias increasing in one kind device. The two different directions of V_{th} shift indicate that multiple kinds of defects or mechanisms should be responsible for high field stress induced degradation at "OFF" state. However, the specific mechanisms are not identified yet. This work also demonstrates that a single worst-case bias condition cannot be defined for all varieties of AlGaN/GaN HEMTs. Each processing technology must be characterized in detail.

CHAPTER VII

WORST-CASE BIAS FOR PROTON AND 10-KEV X-RAY IRRADIATION OF AL-GAN/GAN HEMTS

In this chapter, we report the effects of 1.8 MeV proton irradiation, 10-keV X-ray irradiation, and high-voltage stress on AlGaN/GaN HEMTs fabricated at the University of California, Santa Barbara, with two different processes, for a range of typical bias conditions [39]. The worst-case response for transconductance degradation is observed for the "ON" bias condition, in one kind of devices, and "Semi-ON" for another. Significant total-ionizing dose (TID) effects are observed during 10-keV X-ray irradiation in each type of device. Low-frequency noise measurements are performed to evaluate the types of defects and the resulting defect energy distributions both before and after proton irradiation, for these devices. We compare these results with those from a previous study of commercial devices processed by Qorvo, Inc.

7.1 Experimental details

AlGaN/GaN HEMTs were fabricated on AlGaN/GaN heterostructures grown by Ga-rich plasma-assisted molecular beam epitaxy (PAMBE) with 700 nm unintentionally doped (UID) GaN on GaN substrates grown by MOCVD on (A) SiC or (B) n-type free standing (FS) GaN substrates, as shown in Fig. 7.1. A two-step carbon-doped buffer was included in the re-growths on FS GaN, reducing the d_{UID} to 200 nm [29]. The width of the devices is 150 μm. The gate has the shape of an

inverted trapezoid, with a length (L_G) of 0.7 μm. The gate-to-drain separation (L_{GD}) is 1 μm and the gate-to-source separation (L_{GS}) is 0.5 μm.

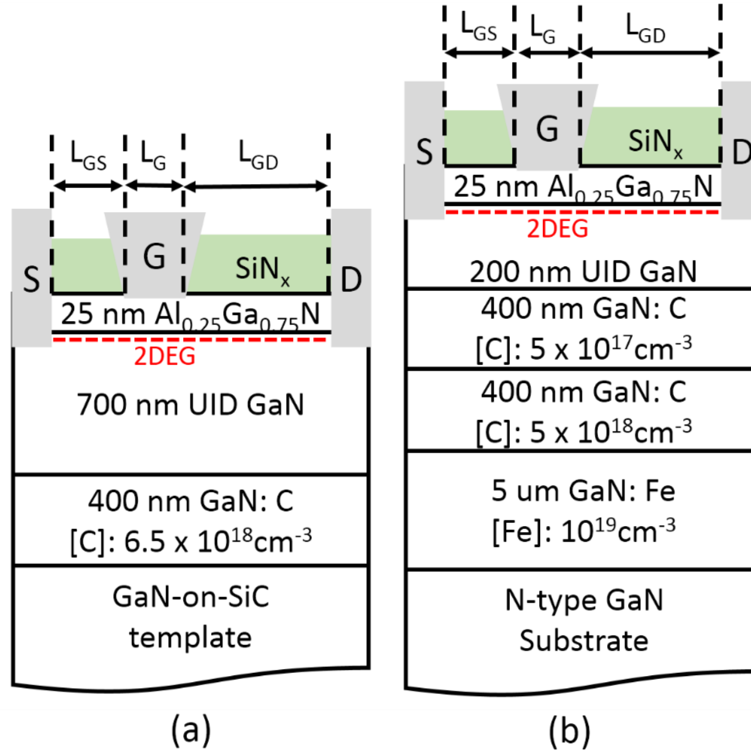

Fig. 7.1. Schematic diagrams of HEMT structures regrown on GaN-on-SiC templates and FS GaN substrates[29]: (a) HEMT structures on GaN-on-SiC and (b) HEMT structures on FS GaN.

The HEMTs were irradiated with 1.8 MeV protons to a fluence of 10^{14}/cm^2 at a flux of 2 x 10^{13} protons/h using the Vanderbilt Pelletron or with 10-keV x-rays using an ARACOR Model 4100 Irradiator to a dose of 2 Mrad(SiO_2) at a rate of 31.5 krad(SiO_2)/min at room temperature. Proton irradiations were performed under four different bias conditions: (1) GND (V_{ds} = 0 V, V_{gs} = 0 V), (2) OFF (V_{ds} = 20 V, V_{gs} = -6 V), (3) Semi-ON (V_{ds} = 20 V, V_{gs} = -2 V) and (4) ON (V_{ds} = 20 V, V_{gs} = +1 V). To compare the biased irradiation response with shifts under high-field and/or high-voltage stress, control devices were monitored under OFF (high field, zero current), Semi-ON (higher field, moderate current), and ON (lower field, high current) conditions for times similar to those of

the proton irradiations. To see whether these devices are sensitive to TID effects, 10-keV X-ray irradiations were also performed. Device I_d-V_g curves were measured in air before and after irradiation with a HP 4156B or Agilent B1505 Semiconductor Parameter Analyzer with 1 V source-drain voltage, with the gate voltage swept from -7 V to 1 V. An effective value of threshold voltage V_{th} was extracted from the I_d-V_g curves in the linear range of transistor response. For the GaN on SiC devices, the pre-irradiation value of V_{th} = -4.2 $\pm$0.2 V and for the devices on FS GaN substrates, V_{th} = -4 $\pm$0.2 V. At least two devices were measured for each of the test conditions shown below.

7.2 Experimental results

7.2.1 Proton irradiation: GND bias

Fig. 7.2 shows the I_d-V_g curves for AlGaN/GaN HEMTs before and after proton irradiation with all pins grounded. Increasingly, positive threshold voltage shifts are observed with increasing fluence in both samples, indicating an increase in net negative charge as a result of the creation of deep acceptor traps. These have been attributed to N vacancy-related defects in our previous work [61] [65].

Fig. 7.3 shows the peak transconductance G_m degradation and threshold voltage shift vs. fluence for these devices. In Fig. 7.3(a) the peak G_m degrades about 7% after a fluence of 10^{14} cm^{-2} for the GaN on SiC devices and degrades by about 12% for the FS GaN substrate devices. However, in Fig. 7.3(b) the GaN on SiC devices show larger positive V_{th} shifts (~ 0.4 V at 10^{14}/cm^2) than the FS GaN substrate devices (~ 0.27 V at 10^{14}/cm^2). At low fluence, a small increase in peak G_m is

observed in the GaN on SiC devices, while a negative V_{th} shift is observed in the FS GaN substrate devices. This change suggests that at least two different kinds of defects likely contribute to the radiation response in both samples. This should not be surprising, given the large number of defects found to be significant in previous studies of AlGaN/GaN HEMTs subjected to proton irradiation and/or high field stress, e.g., N-vacancy-related defects, O and Fe related impurities, hydrogenated point defects, etc. [64][65][104][138][139].

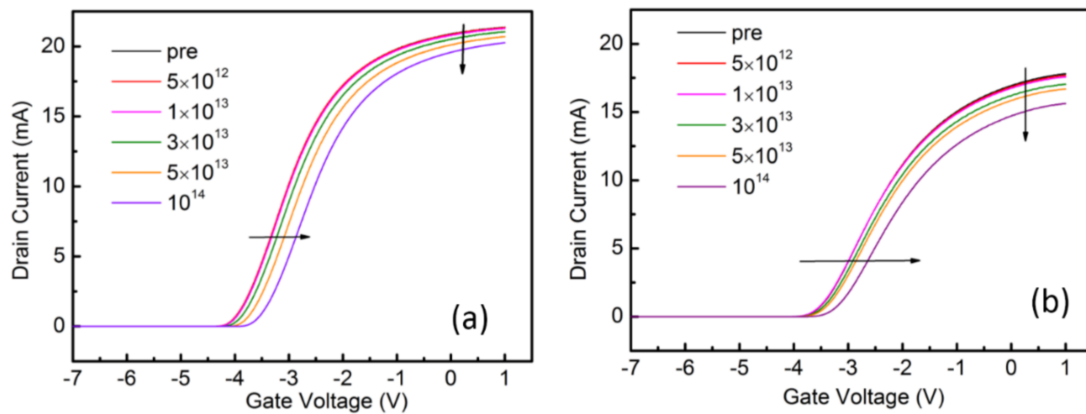

Fig. 7.2. I_d-V_g curves for AlGaN/GaN HEMTs at V_d = 1 V before and after proton irradiation with all pins grounded: (a) HEMT on GaN-on-SiC and (b) HEMT on FS GaN. DC characterization was performed with V_{ds} = 0.5 V.

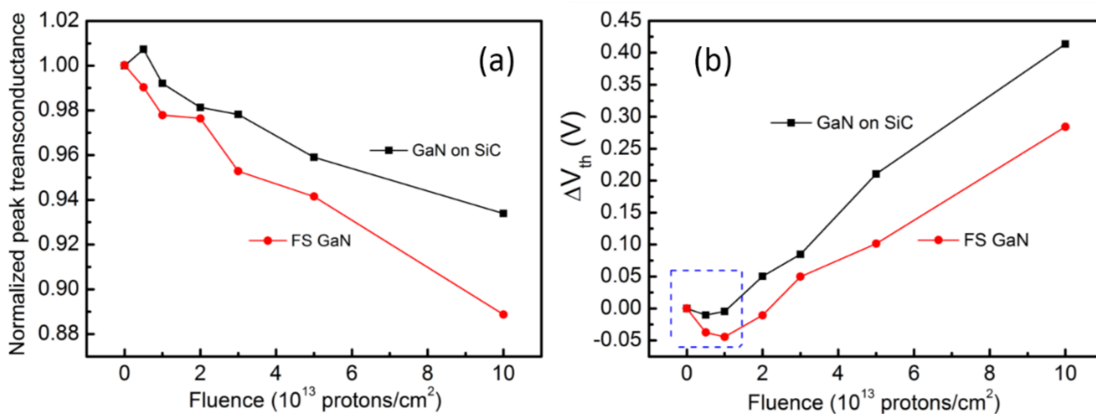

Fig. 7. 3 (a) Peak transconductance and (b) threshold voltage as a function of proton fluence for the devices of Fig. 7.2.

7.2.2 Proton irradiation and stress: OFF bias

Fig. 7.4 compares peak G_m degradation and V_{th} shifts for OFF (V_{ds} = 20 V, V_{gs} = -6 V) and GND state irradiations of the two types of AlGaN/GaN HEMTs. Stress-only results are also shown under OFF-state bias for comparison; the applied gate voltage during OFF-state irradiation or stress is 2 V more negative than V_{th}. For OFF state irradiations of GaN on SiC devices in Fig. 7.4(a), the peak G_m first increases by 6% at low fluence and then drops to 95% of the original value by 10^{14}/cm^2. Only a positive shift in G_m is observed for OFF-state bias stress (no irradiation) for the same amount of time. As shown in the inset, the shape of the G_m vs. V_g-V_{th} curve and position of the G_m peak do not change significantly during OFF-bias stress with no proton irradiation. In Fig. 7.4(b), the value of G_m for the FS GaN substrate devices increases slightly at low fluence, and drops to 88% of its initial value by 10^{14}/cm^2. In each case, at 10^{14}/cm^2 fluence, the OFF state bias degradation caused by proton irradiation is similar to the degradation under GND bias. The significant increase in peak G_m in Fig. 7.4(a) is most likely caused by bias-induced passivation of pre-existing, charged defects. The results of Fig. 7.4 suggest there is a larger density of pre-existing charged defects in these GaN on SiC devices than for the FS GaN substrate devices.

The V_{th} shifts for these devices are shown in Fig. 7.5. For proton irradiation under OFF-state bias stress, in each case a negative shift in V_{th} is observed at low fluence that is similar to the pure bias stress results. Increasingly positive V_{th} shifts are observed with increasing fluence for each type of device. The V_{th} shifts in each case for OFF-state bias irradiation are less positive than those observed for irradiation under positive bias. The initial decrease in threshold voltage for the OFF

state devices is evidently caused by voltage-induced passivation of acceptor defects. The threshold voltage subsequently increases at a rate similar to that of the OFF state devices. The relatively small shift in V_{th} at a fluence of 10^{14}/cm^2 evidently results from the fortuitous compensation of radiation-induced acceptor and stress-induced donors under these irradiation and stress conditions. The positive shift due to proton irradiation is once again most likely due to the creation of N-vacancy-related acceptor defects at a rate that does not strongly depend on the applied bias [64][65]. The negative shift due to bias-stress most likely results at short times and low fluences from the passivation of pre-existing charged defects, as discussed above. At longer times and higher fluences, bias-stress induced dehydrogenation of previously passivated point defects and/or impurities most likely leads to the creation of new donor traps, as often observed in AlGaN/GaN HEMTs [64][65] [138][139].

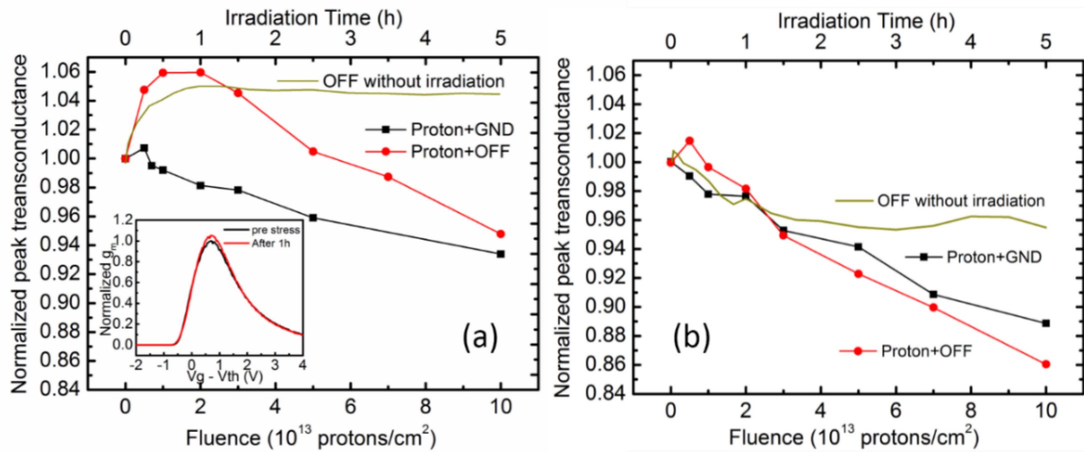

Fig. 7. 4. Normalized peak transconductance of AlGaN/GaN HEMTs with (a) GaN on SiC substrate and (b) FS GaN substrate as function of proton fluence for OFF state (V_{ds} = 20 V, V_{gs} = -6 V) and GND irradiation and/or voltage stress. The solid line shows device response to pure high field stress. DC characterization was performed with V_{ds} = 0.5 V. The inset in (a) shows the changes in normalized transconductance as a function of V_g-V_{th} before and after 1h stress.

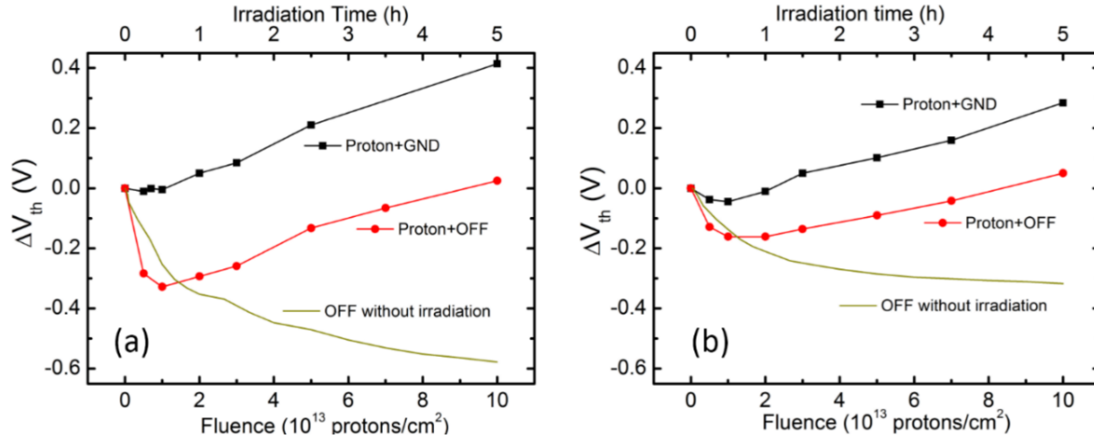

Fig. 7. 5. V_{th} shifts for the AlGaN/GaN HEMTs of Fig. 4.4 with (a) GaN on SiC substrates and (b) FS GaN substrates as function of proton fluence and/or stress time for OFF state bias (V_{ds} = 20 V, V_{gs} = -6 V) and GND bias. The solid line shows the device response to pure high field stress.

7.2.3 Proton irradiation and on/semi-on state stress

Fig. 7.6 shows peak G_m degradation for ON and Semi-ON bias conditions. Results for control parts subjected to similar biases for the same amounts of time are also shown. In the ON state, V_{gs}-V_{th} = 5 V and the drain current I_d is ~ 90 mA in both types of devices, and in the Semi-ON state, V_{gs}-V_{th} = 2 V and I_d ~ 40 mA. Under these bias conditions, the peak G_m decreases monotonically in all cases. Clearly, the peak G_m degradation is much larger when devices are irradiated under bias than when they are just subjected to pure voltage stress. The worst case bias condition is different for the two device types. For GaN on SiC devices, the peak G_m degrades by 31% at a fluence of 10^{14} cm^{-2} when irradiated under ON bias, but only degrades by 17% under the semi-ON bias condition. In FS GaN substrate devices, the peak G_m for devices irradiated with ON bias degrades by 16% at 10^{14} cm^{-2}, but degrades by 20% for semi-ON bias conditions. Comparing results in Figs. 7.4 and 7.6, it is clear that worst-case peak G_m degradation occurs for ON-bias proton irradiation of the GaN on SiC devices, but under Semi-ON bias conditions for the FS GaN substrate devices.

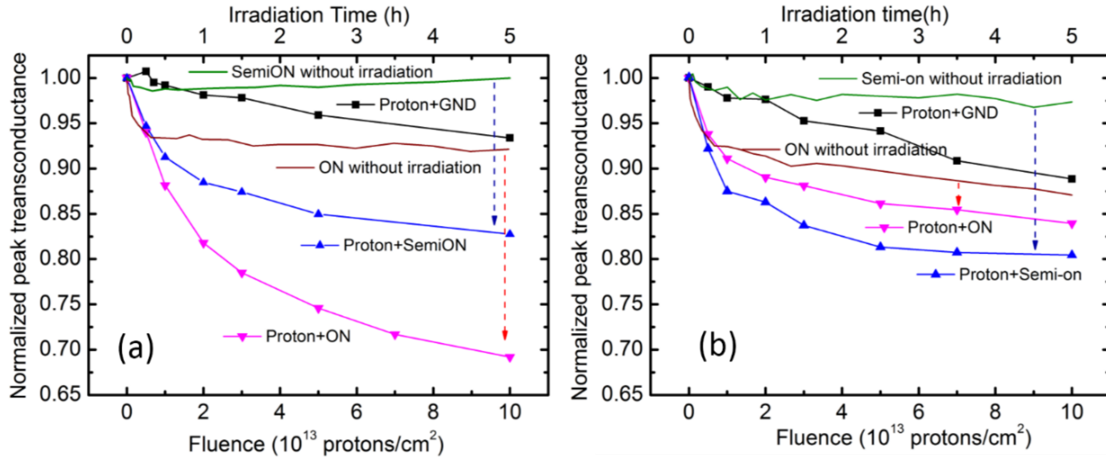

Fig. 7. 6. Normalized peak transconductance of AlGaN/GaN HEMTs with (a) GaN on SiC substrates and (b) FS GaN substrates as functions of proton fluence for ON state (V_{ds} = 20 V, V_{gs} = 1 V), Semi-ON state (V_{ds} = 20 V, V_{gs} = -2 V) and GND irradiation and/or voltage stress. The dark red and green lines (no symbols) show device response to pure high voltage stress. DC characterization was performed with V_{ds} = 0.5 V.

V_{th} shifts for the ON and semi-ON bias conditions are shown for these devices in Fig. 7.7; irradiation results for GND bias conditions and pure stress results are again shown for comparison. In contrast to GND-bias irradiation, V_{th} shifts are negative for the devices biased in the Semi-ON condition for the GaN on SiC devices in Fig. 7.7(a). In the ON condition, the V_{th} shift is initially negative, and then becomes slightly positive at higher fluence. For the devices on FS GaN substrates in Fig. 7.7(b), when devices are irradiated with Semi-ON bias, V_{th} initially shifts negatively at lower fluence and then positively at higher fluence. On the other hand, devices irradiated in the ON state bias condition show monotonically positive shifts that are smaller than the shifts in devices irradiated with all pins grounded (0.28 V at 10^{14} cm^{-2}) or devices exposed to pure ON-state bias stress (0.18 V at 5 h). These results again are consistent with a combination of donor and acceptor trap formation during proton irradiation [64][65][104][138][139]. For ON-bias irradiation, the creation of acceptor and donor defects evidently occurs at similar rates under these irradiation and bias

conditions, leading to nearly offsetting effects on V_{th}, but large G_m degradation, because each type of defect contributes strongly to carrier scattering.

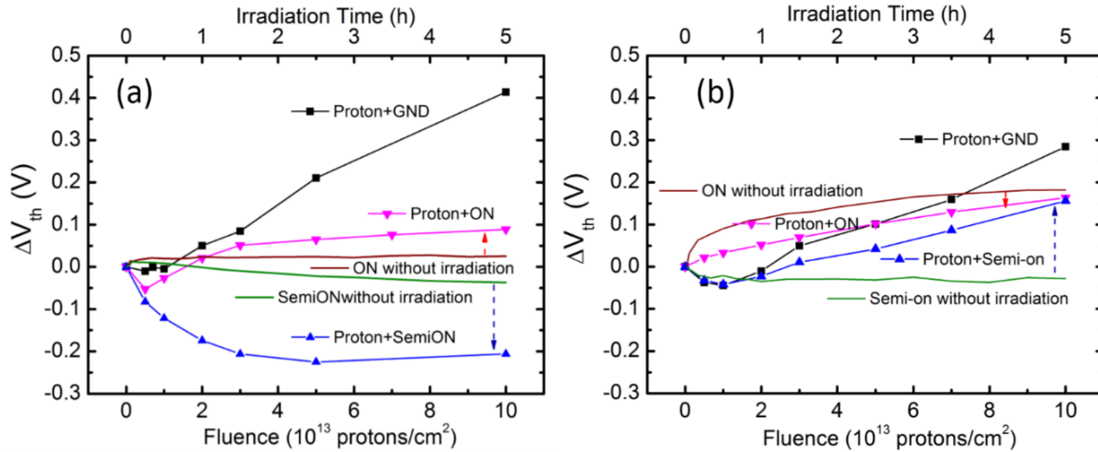

Fig. 7.7. V_{th} shift of the AlGaN/GaN HEMTs of Fig. 7.6 with (a) GaN on SiC substrates and (b) FS GaN substrates as function of proton fluence for ON state (V_{ds} = 20 V, V_{gs} = 1 V), Semi-ON state (V_{ds} = 20 V, V_{gs} = -2 V) and GND irradiation and/or voltage stress. The red and green lines (no symbols) show device response to pure high voltage stress.

7.2.4 Biased X-ray irradiation

The individual and combined effects of voltage stress and 10-keV X-ray irradiation are shown in Fig. 7.8 and Fig. 7.9. For devices irradiated with all pins grounded, no G_m degradation is observed for either type of device. But X-ray irradiation leads to significant G_m degradation when devices are biased during irradiation. In GaN on SiC devices, a 15% decrease in G_m is observed when devices are irradiated under ON-state bias in Fig. 7.8(a). This shift is larger than either the shift observed in devices exposed to pure ON-state stress for a similar time (8% at ~ 1 h Fig. 4.8a), or for similar devices irradiated under semi-ON bias to 2 Mrad(SiO_2), for which a similar 8% decrease is observed (results similar to pure bias stress in Fig. 7.8a). Moreover, about twice as much increase in G_m is observed in the OFF case for the GaN on SiC devices in Fig. 7.8(a). In contrast, X-ray

irradiation under ON-state bias leads to *less* degradation (4% at 2 Mrad(SiO_2) in Fig.7.8b) than pure ON-state biased stress (8% at 2 Mrad(SiO_2) in Fig. 7.8b). Fig. 7.9 shows that, for both types of devices, X-ray irradiation results in negative V_{th} shifts, indicating in an increase in positive charge and/or a decrease in pre-existing negative charge. The largest V_{th} shifts for each device type are now observed for the OFF-state bias condition, and for each device type, the amount of negative V_{th} shift is about 0.05 V to 0.1 V greater than that observed with pure OFF-state stress at the highest doses and longest times.

10-keV X-rays are too low in energy to result in displacement damage in either the GaN or AlGaN layers of these devices [60]. Hence, the additional degradation in G_m and shifts in V_{th} observed in these devices, relative to bias-stress alone for similar times, are the results of X-ray-induced electron-hole pair creation. The resulting charge transport can lead to (a) passivation of pre-existing charged defects (acceptors in these devices) by the capture of radiation-induced electrons, and (b) the dehydrogenation of previously passivated defects [60]. These results reinforce the interpretation of the proton irradiation results discussed above, and add to the growing number of cases in which significant ionization-induced shifts in AlGaN/GaN device parameters are observed, even in devices with no gate insulator [57][58].

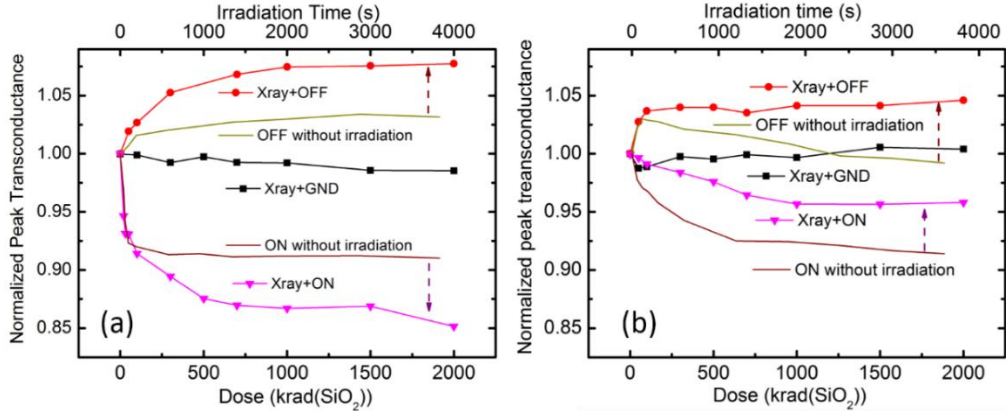

Fig. 7.8. Normalized peak transconductance of AlGaN/GaN HEMTs with (a) GaN on SiC substrates and (b) FS GaN substrates as function of total ionizing dose and/or stress time for ON state (V_{ds} = 20 V, V_{gs} = 1 V) and OFF state (V_{ds} = 20 V, V_{gs} = -6 V) irradiation and/or stress.

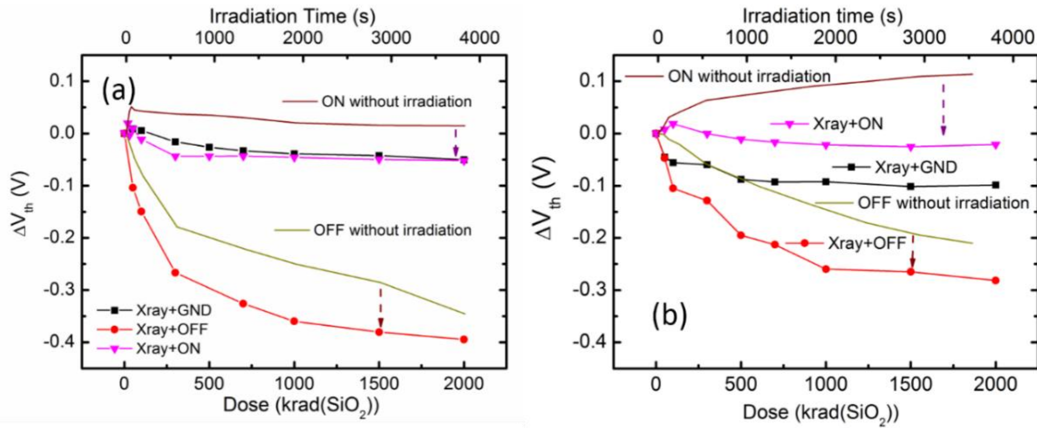

Fig. 7.9. Vth shift of the AlGaN/GaN HEMTs of Fig. 4.8 with (a) GaN on SiC substrates and (b) FS GaN substrates as function of total ionizing dose and time for ON state (V_{ds} = 20 V, V_{gs} = 1 V) and OFF state (V_{ds} = 20 V, V_{gs} = -6 V) irradiation and/or stress.

7.3 Discussion

The results of Figs. 7.2-7.9 all strongly suggest that the types of process- and radiation-induced defects and impurities in the two types of devices evaluated in this study are significantly different from ones evaluated in [61] and[65]. Moreover, the results also suggest that the rates of donor

and acceptor trap neutralization and/or buildup during bias-temperature stress also differ significantly with device processing and irradiation and/or bias-stress conditions [61][64][65] [138][139]. The difference in observed worst-case bias conditions for peak G_m degradation for the GaN on SiC devices in this work and the Qorvo devices of [61] therefore also suggest there likely are significant differences in as-processed and radiation-induced defects in these two different sets of devices.

To obtain additional insight into the defect energy distributions for the GaN on SiC devices of Figs. 7.2-7.9 and the Qorvo devices of [61], we compare the low frequency 1/*f* noise of the two types of devices in Fig. 7.10. Here we plot the excess drain-voltage noise power spectral density S_V (corrected for background noise) as a function of frequency and temperature. The bias voltages are chosen to ensure that the noise originates from the gated portion of the channel, with an approximately constant channel resistance [61][64][65]. The energy scale on the upper x-axis is derived from the Dutta-Horn model of low-frequency noise [68][69], which has been demonstrated to be applicable to each type of device [61]. Noise measurements were reproducible from run to run and from day to day on these devices. The statistical uncertainty in the noise measurements is approximately equal to the symbol size. From the temperature dependence of the noise magnitude, we can estimate the shapes of the defect energy distributions $D(E_0)$ from low-frequency noise measurements [68][69], via

$$D(E_0) \propto \omega/(kT)*S_{V,} \quad (1)$$

where $E_0 = -kT \ln(\omega\tau_0)$ is the effective defect energy [122].

At low temperatures and energies, the noise magnitude is higher for the as-processed GaN on SiC UCSB devices than the Qorvo devices, which suggests a greater density of defects with low E_0, such as nitrogen vacancy-related defects and oxygen impurities O_N ([65] [104]). A large peak in noise magnitude at 0.7 eV (due to a N_{Ga} defect [61]) is observed in the Qorvo devices [61] but not in the GaN on SiC UCSB devices. Because these devices have different types of defects and impurities before irradiation, it is not surprising that irradiated devices might not only have different defects, but also show different bias sensitivities for defect buildup and/or neutralization.

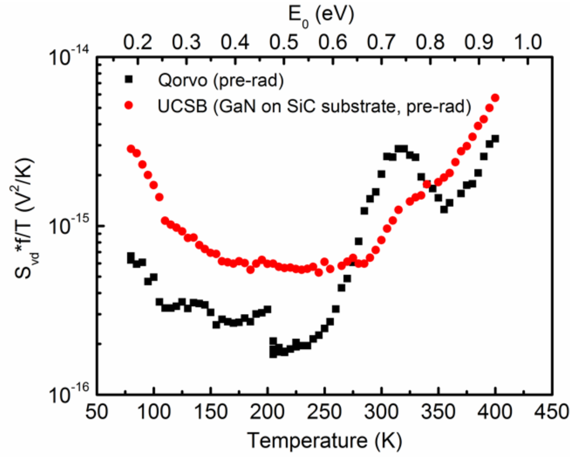

Fig. 7.10. Temperature-dependent noise measurements from 85 K to 400 K, for unirradiated GaN on SiC devices from this work, and for unirradiated Qorvo devices from [61]. Here $V_g - V_{th} = 0.4$ V, $V_d = 0.03$ V, and $f = 10$ Hz for the Qorvo devices, and $V_g - V_{th} = 0.5$ V, $V_d = 0.03$ V and $f = 10$ Hz for the GaN on SiC devices fabricated by UCSB.

As a further test, we also compare the noise of GaN on SiC UCSB devices before and after proton irradiation with the noise of Qorvo devices in Fig. 7.11. Each is irradiated under worst-case bias conditions for that process: ON for the GaN on SiC devices, and semi-ON for the Qorvo devices. For the GaN on SiC UCSB devices in Fig. 7.11(a), an increase in defect density is observed at energies from ~ 0.25 eV to ~ 0.8 eV. This result suggests the generation of several different kinds of defects with a range of energy levels. Very little increase is observed at low defect energies. For

the Qorvo devices in Fig. 7.11(b), in contrast, a significant increase in defect density with irradiation exposure is observed only at low temperature, indicating primarily an increase of low energy nitrogen vacancy-related defects and/or oxygen impurities O_N. A *decrease* in the noise at high temperature is also observed for the Qorvo devices, reflecting a decrease in density of O_N-H defects ($E_0 \sim 0.9$ eV) as a result of defect dehydrogenation [65]. Hence, both the as-processed and proton-irradiation-induced defect types and energy distributions differ significantly for these devices. These kinds of differences in dominant defect type and density evidently are responsible for the observed differences in worst-case bias conditions for radiation response of AlGaN/GaN HEMTs.

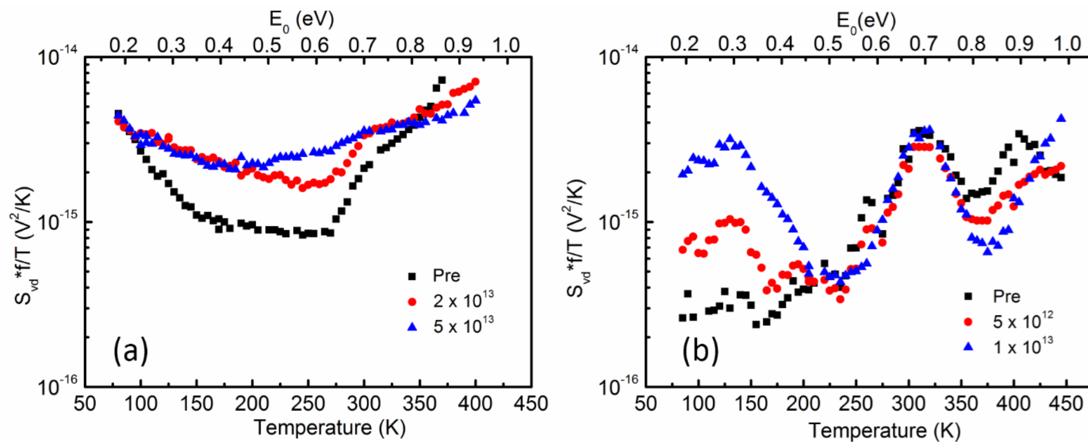

Fig. 7.11. Temperature-dependent noise measurements from 85 K to 400 K in (a) unirradiated devices and devices irradiated with worst-case ON bias for GaN on SiC devices fabricated by UCSB, and (b) Qorvo devices from [61] irradiated with worst-case semi-ON bias. Fluences are quoted in protons/cm^2.

7.4 Conclusion

We have investigated the effects of proton irradiation, X-ray irradiation, and/or hot carrier stress on AlGaN/GaN HEMTs fabricated in two different processes. Both TID and displacement damage effects are observed in these AlGaN/GaN HEMTs. The magnitude of these effects can vary

significantly with applied bias during proton or 10-keV X-ray exposure. The worst-case bias condition for transconductance degradation differ for these devices, as well as those evaluated in a previous study [61]. These results demonstrate that (1) a single worst-case bias condition cannot be defined for all varieties of AlGaN/GaN HEMTs; each technology must be characterized in detail. These differences result from differences in as-processed and radiation-induced defect types and energies in these devices. (2) In contrast to older generation AlGaN/GaN HEMTs, TID effects can contribute significantly to radiation response in these devices, complicating the interpretation of proton irradiation of newer technologies. This TID sensitivity occurs most likely because the density of native defects in AlGaN/GaN HEMTs is being reduced by improvements in fabrication technology, making TID and displacement damage effects caused by radiation exposure more easily observed.

CHAPTER VIII

SUMMARY AND CONCLUSIONS

In summary, this PhD thesis provides a systematically study of the bias dependence of radiation effects and high field stress of AlGaN/GaN HEMTs. We test devices with different processes and substrates, both unpassivated and passivated under three bias conditions: ON, semi-ON and OFF. 1.8 MeV proton irradiation and 10keV X-ray irradiation are both investigated. Both gate bias dependence and step drain bias dependence are discussed. Comparing with previous devices reported by our group, we find some new effects in high field stress induced degradation and radiation effects in AlGaN/GaN HEMTs.

First we compare the results in AlGaN/GaN HEMTs with or without passivation layers. Unpassivated devices growing using ammonia-rich condition exhibit fast recovery during annealing with all pins grounded, with super-recovery of the peak transconductance observed in the unpassivated devices. This result is consistent with the transconductance degradation in unpassivated devices after 10 keV X-ray irradiation, which is not observed for passivated ones. DFT calculations suggest that dehydrogenation of pre-existing O_N-H defects plays a significant role in hot carrier degradation of NH_3-rich AlGaN/GaN HEMTs. The super-recovery in peak transconductance can be naturally caused by a change of the Fermi-level during the annealing process and the resulting neutralization of stress-induced bare O_N defects at the AlGaN/GaN interface. X-ray irradiation

causes degradation by generating positively charged O_N^+ centers from the pre-existing O_N-H defects which can reach the region near the 2DEG layer. A significant non-recoverable negative threshold voltage shift are found in devices fabricated using both passivated and unpassivated devices. In passivated devices, the O_N^+ traps are only generated on the surface and only cause shifts in V_{th}, while in passivated devices these centers can be generated on both the surface and near the 2DEG layer, resulting in degradation in transconductance.

For passivated devices, we studied the gate bias dependence of hot carrier effects under fixed drain bias (20 V) and the device performance under a series of drain biases. Unlike previous results, the worst cases for transconductance degradation were the “ON” state for both devices. For step drain bias stress testing, devices undergo typical hot carrier induced degradation under “ON” state stress. But under the “OFF” state stress condition, both devices showed a small increase in peak transconductance at low drain bias. The direction of the V_{th} shift changed from negative to positive with the drain bias increasing in one kind of device. The two different directions of the V_{th} shift indicate that multiple kinds of defects or mechanisms should be responsible for high field stress-induced degradation in the “OFF” state. However, the specific mechanisms are not identified yet. This work also demonstrates that a single worst-case bias condition cannot be defined for all varieties of AlGaN/GaN HEMTs. Each processing technology must be characterized in detail.

Then we have investigated the combination effects of proton irradiation, X-ray irradiation, with hot carrier stress on AlGaN/GaN HEMTs fabricated in two different processes. Both TID and displacement damage effects are observed in these AlGaN/GaN HEMTs. The magnitude of these

effects can vary significantly with applied bias during proton or 10-keV X-ray exposure. These results demonstrate that (1) a single worst-case bias condition cannot be defined for all varieties of AlGaN/GaN HEMTs; each technology must be characterized in detail. These differences result from differences in as-processed and radiation-induced defect types and energies in these devices. (2) In contrast to older generation AlGaN/GaN HEMTs, TID effects can contribute significantly to radiation response in these devices, complicating the interpretation of proton irradiation of newer technologies.

To summarize, we study the combination effects of radiation effects and hot carrier effects in AlGaN/GaN HEMTs. As with the development in AlGaN/GaN HEMTs, the GaN material shows less lattice defects density and makes the role of defects depassivation during the stress or radiation become more and more important in device reliability. Effects not seen in previous devices appear such as total ionizing dose effects and negative bias-induced threshold voltage instability. Some effects show different bias dependence than previous result such as hot carrier effects. These results emphasize the need to test devices under a wide range of conditions during characterization and qualification testing.

REFERENCES

[1] A. Y. Polyakov, S. J. Pearton, P. Frenzer, F. Ren, L. Liu, and J. Kim, “Radiation effects in GaN materials and devices,” *J. Mater. Chem. C*, vol. 1, no. 5, pp. 877–887, Jan. 2013.

[2] B. Luo, J. W. Johnson, F. Ren, K. K. Allums, C. R. Abernathy, S. J. Pearton, A. M. Dabiran, A. M. Wowchack, C. J. Polley, P. P. Chow, D. Schoenfeld, and A. G. Baca, “Influence of ^{60}Co γ-rays on dc performance of AlGaN/GaN high electron mobility transistors,” *Appl. Phys. Lett.*, vol. 80, no. 4, pp. 604–606, Jan. 2002.

[3] A. Kalavagunta, A. Touboul, L. Shen, R. D. Schrimpf, R. A. Reed, D. M. Fleetwood, R. K. Jain, and U. K. Mishra, “Electrostatic mechanisms responsible for device degradation in proton irradiated AlGaN/AlN/GaN HEMTs,” *IEEE Trans. Nucl. Sci.*, vol. 55, no. 4, pp. 2106–2112, Aug. 2008.

[4] J. Piprek and Wiley InterScience (Online service), *Nitride semiconductor devices : principles and simulation*. Wiley-VCH, 2007.

[5] M. S. Shur, R. Gaska, and A. Bykhovski, “GaN-based electronic devices,” *Solid. State. Electron.*, vol. 43, no. 8, pp. 1451–1458, Aug. 1999.

[6] S. Hashimoto, K. Akita, T. Tanabe, H. Nakahata, K. Takeda, and H. Amano, “Epitaxial layers of AlGaN channel HEMTs on AlN substrates,” *SEI Tech. Rev.*, vol. 71, p. 83, 2010.

[7] U. K. Mishra, P. Parikh, and Yi-Feng Wu, “AlGaN/GaN HEMTs-an overview of device operation and applications,” *Proc. IEEE*, vol. 90, no. 6, pp. 1022–1031, Jun. 2002.

[8] U. K. Mishra, Shen Likun, T. E. Kazior, and Yi-Feng Wu, “GaN-based RF power devices and amplifiers,” *Proc. IEEE*, vol. 96, no. 2, pp. 287–305, Feb. 2008.

[9] Y. Cordier, M. Hugues, P. Lorenzini, F. Semond, F. Natali, and J. Massies, “Electron mobility and transfer characteristics in AlGaN/GaN HEMTs,” *Phys. Status Solidi*, vol. 2, no. 7, pp. 2720–2723, May 2005.

[10] R. S. Muller, T. I. Kamins, M. Chan, and P. K. Ko, Device electronics for integrated circuits, vol. 986. Wiley New York, 2003.

[11] J. Fan and P. K. Chu, Silicon carbide nanostructures: fabrication, structure, and properties. Springer, 2014.

[12] O. Ambacher, J. Smart, J. R. Shealy, N. G. Weimann, K. Chu, M. Murphy, W. J. Schaff, L. F. Eastman, R. Dimitrov, L. Wittmer, M. Stutzmann, W. Rieger, and J. Hilsenbeck, "Two-dimensional electron gases induced by spontaneous and piezoelectric polarization charges in N- and Ga-face AlGaN/GaN heterostructures," *J. Appl. Phys.*, vol. 85, no. 6, pp. 3222–3333, Mar. 1999.

[13] S. W. Kaun, M. H. Wong, U. K. Mishra, and J. S. Speck, "Molecular beam epitaxy for high-performance Ga-face GaN electron devices," *Semicond. Sci. Technol.*, vol. 28, no. 7, p. 074001, Jul. 2013.

[14] M. Asif Khan, A. Bhattarai, J. N. Kuznia, and D. T. Olson, "High electron mobility transistor based on a GaN-Al_x $Ga_{1-x}N$ heterojunction," *Appl. Phys. Lett.*, vol. 63, no. 9, pp. 1214–1215, Aug. 1993.

[15] S. Yoshida, S. Misawa, and S. Gonda, "Improvements on the electrical and luminescent properties of reactive molecular beam epitaxially grown GaN films by using AlN‐coated sapphire substrates," *Appl. Phys. Lett.*, vol. 42, no. 5, pp. 427–429, Mar. 1983.

[16] S. Rajan, " Polarization engineering for GaN-based transistors." University of California, Santa Barbara, 2006.

[17] J. Zou, D. Kotchetkov, A. A. Balandin, D. I. Florescu, and F. H. Pollak, "Thermal conductivity of GaN films: Effects of impurities and dislocations," *J. Appl. Phys.*, vol. 92, no. 5, pp. 2534–2539, Sep. 2002.

[18] D. Kotchetkov, J. Zou, A. A. Balandin, D. I. Florescu, and F. H. Pollak, "Effect of dislocations on thermal conductivity of GaN layers," *Appl. Phys. Lett.*, vol. 79, no. 26, pp. 4316–4318, Dec. 2001.

[19] A. R. Boyd, S. Degroote, M. Leys, F. Schulte, O. Rockenfeller, M. Luenenbuerger, M. Germain, J. Kaeppeler, and M. Heuken, "Growth of GaN/AlGaN on 200 mm diameter silicon (111) wafers by MOCVD," *Phys. status solidi*, vol. 6, no. S2, pp. S1045–S1048, Jun. 2009.

[20] S. Arulkumaran, G. I. Ng, S. Vicknesh, H. Wang, K. S. Ang, J. P. Y. Tan, V. K. Lin, S. Todd, G.-Q. Lo, and S. Tripathy, "Direct current and microwave characteristics of sub-micron AlGaN/GaN high-electron-mobility transistors on 8-Inch Si(111) Substrate," *Jpn. J. Appl. Phys.*, vol. 51, no. 11R, p. 111001, Oct. 2012.

[21] B. De Jaeger, M. Van Hove, D. Wellekens, X. Kang, H. Liang, G. Mannaert, K. Geens, and S. Decoutere, "Au-free CMOS-compatible AlGaN/GaN HEMT processing on 200 mm Si

substrates," in *2012 24th International Symposium on Power Semiconductor Devices and ICs*, 2012, pp. 49–52.

[22] D. Marcon, Y. N. Saripalli, and S. Decoutere, "200mm GaN-on-Si epitaxy and e-mode device technology," in *2015 IEEE International Electron Devices Meeting (IEDM)*, 2015, p. 16.2.1-16.2.4.

[23] M. A. Angadi, T. Watanabe, A. Bodapati, X. Xiao, O. Auciello, J. A. Carlisle, J. A. Eastman, P. Keblinski, P. K. Schelling, and S. R. Phillpot, "Thermal transport and grain boundary conductance in ultrananocrystalline diamond thin films," *J. Appl. Phys.*, vol. 99, no. 11, p. 114301, Jun. 2006.

[24] D. Jena, A. C. Gossard, and U. K. Mishra, "Dislocation scattering in a two-dimensional electron gas," *J. Appl. Phys.*, vol. 76, no. 13, pp. 1707–1709, Mar. 2000.

[25] S. W. Kaun, M. H. Wong, S. Dasgupta, S. Choi, R. Chung, U. K. Mishra, and J. S. Speck, "Effects of threading dislocation density on the gate leakage of AlGaN/GaN heterostructures for high electron mobility transistors," *Appl. Phys. Express*, vol. 4, no. 2, p. 024101, Jan. 2011.

[26] D. F. Storm, D. S. Katzer, J. A. Mittereder, S. C. Binari, B. V Shanabrook, X. Xu, D. S. Mcvey, R. P. Vaudo, and G. R. Brandes, "Homoepitaxial growth of GaN and AlGaN/GaN heterostructures by molecular beam epitaxy on freestanding HVPE gallium nitride for electronic device applications," *J. Cryst. Growth*, vol. 281, pp. 32–37, 2005.

[27] C. Poblenz, P. Waltereit, S. Rajan, S. Heikman, U. K. Mishra, and J. S. Speck, "Effect of carbon doping on buffer leakage in AlGaN/GaN high electron mobility transistors," *J. Vac. Sci. Technol. B Microelectron. Nanom. Struct.*, vol. 22, no. 3, p. 1145, 2004.

[28] Y. C. Choi, M. Pophristic, H.-Y. Cha, B. Peres, M. G. Spencer, and L. F. Eastman, "The effect of an Fe-doped GaN buffer on off-state breakdown characteristics in AlGaN/GaN HEMTs on Si substrate," *IEEE Trans. Electron Devices*, vol. 53, no. 12, pp. 2926–2931, Dec. 2006.

[29] S. W. Kaun, M. H. Wong, J. Lu, U. K. Mishra, and J. S. Speck, "Reduction of carbon proximity effects by including AlGaN back barriers in HEMTs on free-standing GaN," *Electron. Lett.*, vol. 49, no. 14, pp. 893–895, Jul. 2013.

[30] M. Razeghi and A. Rogalski, "Semiconductor ultraviolet detectors," *J. Appl. Phys.*, vol. 79, no. 10, pp. 7433–7473, May 1996.

[31] S. Singhal, A. W. Hanson, A. Chaudhari, P. Rajagopal, T. Li, J. W. Johnson, W. Nagy, R. Therrien, C. Park, A. P. Edwards, E. L. Piner, K. J. Linthicum, and I. C. Kizilyalli, "Qualification and reliability of a GaN process platform," in *Int. Conf. Compound Semiconductor MANTECH Tech. Dig.*, 2007, pp. 83–86.

[32] B. Heying, R. Averbeck, L. F. Chen, E. Haus, H. Riechert, and J. S. Speck, "Control of GaN surface morphologies using plasma-assisted molecular beam epitaxy," *J. Appl. Phys.*, vol. 88, no. 4, pp. 1855–1860, Jul. 2000.

[33] J. P. Ibbetson, P. T. Fini, K. D. Ness, S. P. DenBaars, J. S. Speck, and U. K. Mishra, "Polarization effects, surface states, and the source of electrons in AlGaN/GaN heterostructure field effect transistors," *Appl. Phys. Lett.*, vol. 77, no. 2, pp. 250–252, Jun. 2000.

[34] J. R. Shealy, T. R. Prunty, E. M. Chumbes, and B. K. Ridley, "Growth and passivation of AlGaN/GaN heterostructures," *J. Cryst. Growth*, vol. 250, no. 1–2, pp. 7–13, Mar. 2003.

[35] G. Simin, A. Koudymov, A. Tarakji, X. Hu, J. Yang, M. A. Khan, M. S. Shur, and R. Gaska, "Induced strain mechanism of current collapse in AlGaN/GaN heterostructure field-effect transistors," *Appl. Phys. Lett.*, vol. 79, no. 16, pp. 2651–2653, Oct. 2001.

[36] R. Vetury, N. Q. Zhang, S. Keller, and U. K. Mishra, "The impact of surface states on the DC and RF characteristics of AlGaN/GaN HFETs," *IEEE Trans. Electron Devices*, vol. 48, no. 3, pp. 560–566, Mar. 2001.

[37] G. Meneghesso, F. Rampazzo, P. Kordos, G. Verzellesi, and E. Zanoni, "Current collapse and high-electric-field reliability of unpassivated GaN/AlGaN/GaN HEMTs," *IEEE Trans. Electron Devices*, vol. 53, no. 12, pp. 2932–2941, Dec. 2006.

[38] Hyungtak Kim, R. M. Thompson, V. Tilak, T. R. Prunty, J. R. Shealy, and L. F. Eastman, "Effects of SiN passivation and high-electric field on AlGaN-GaN HFET degradation," *IEEE Electron Device Lett.*, vol. 24, no. 7, pp. 421–423, Jul. 2003.

[39] G. Meneghesso, G. Verzellesi, F. Danesin, F. Rampazzo, F. Zanon, A. Tazzoli, M. Meneghini, and E. Zanoni, "Reliability of GaN high-electron-mobility transistors: state of the art and perspectives," *IEEE Trans. Device Mater. Reliab.*, vol. 8, no. 2, pp. 332–343, Jun. 2008.

[40] M. Meneghini, I. Rossetto, C. De Santi, F. Rampazzo, A. Tajalli, A. Barbato, M. Ruzzarin, M. Borga, E. Canato, E. Zanoni, and G. Meneghesso, "Reliability and failure analysis in power GaN-HEMTs: An overview," in *2017 IEEE International Reliability Physics*

Symposium (IRPS), 2017, p. 3B–2.1–3B–2.8.

[41] M. Meneghini, D. Bisi, D. Marcon, S. Stoffels, M. Van Hove, T.-L. Wu, S. Decoutere, G. Meneghesso, and E. Zanoni, "Trapping in GaN-based metal-insulator-semiconductor transistors: Role of high drain bias and hot electrons," *Appl. Phys. Lett.*, vol. 104, no. 14, p. 143505, Apr. 2014.

[42] M. Kuball, M. Apajna, R. J. T. Simms, M. Faqir, and U. K. Mishra, "AlGaN/GaN HEMT device reliability and degradation evolution: Importance of diffusion processes," *Microelectron. Reliab.*, vol. 51, no. 2, pp. 195–200, Feb. 2011.

[43] C. Canali, F. Castaldo, F. Fantini, D. Ogliari, L. Umena, and E. Zanoni, "Gate metallization "Sinking" into the active channel in Ti/W/Au metallized power MESFET's," *IEEE Electron Device Lett.*, vol. 7, no. 3, pp. 185–187, Mar. 1986.

[44] Y. C. Chou, D. Leung, I. Smorchkova, M. Wojtowicz, R. Grundbacher, L. Callejo, Q. Kan, R. Lai, P. H. Liu, D. Eng, and A. Oki, "Degradation of AlGaN/GaN HEMTs under elevated temperature lifetesting," *Microelectron. Reliab.*, vol. 44, no. 7, pp. 1033–1038, Jul. 2004.

[45] G. Meneghesso, M. Meneghini, D. Bisi, I. Rossetto, A. Cester, U. K. Mishra, and E. Zanoni, "Trapping phenomena in AlGaN/GaN HEMTs: a study based on pulsed and transient measurements," *Semicond. Sci. Technol.*, vol. 28, no. 7, p. 074021, Jul. 2013.

[46] M. Meneghini, A. Stocco, M. Bertin, D. Marcon, A. Chini, G. Meneghesso, and E. Zanoni, "Time-dependent degradation of AlGaN/GaN high electron mobility transistors under reverse bias," *Appl. Phys. Lett.*, vol. 100, no. 3, p. 033505, Jan. 2012.

[47] M. Ruzzarin, M. Meneghini, I. Rossetto, M. Van Hove, S. Stoffels, T.-L. Wu, S. Decoutere, G. Meneghesso, and E. Zanoni, "Evidence of hot-electron degradation in GaN-based MIS-HEMTs submitted to high temperature constant source current stress," *IEEE Electron Device Lett.*, vol. 37, no. 11, pp. 1415–1417, Nov. 2016.

[48] D. Bisi, M. Meneghini, M. Van Hove, D. Marcon, S. Stoffels, T.-L. Wu, S. Decoutere, G. Meneghesso, and E. Zanoni, "Trapping mechanisms in GaN-based MIS-HEMTs grown on silicon substrate," *Phys. Status Solidi*, vol. 212, no. 5, pp. 1122–1129, May 2015.

[49] Y. S. Puzyrev, T. Roy, M. Beck, B. R. Tuttle, R. D. Schrimpf, D. M. Fleetwood, and S. T. Pantelides, "Dehydrogenation of defects and hot-electron degradation in GaN high-electron-mobility transistors," *J. Appl. Phys.*, vol. 109, no. 3, p. 034501, Feb. 2011.

[50] M. Tapajna, R. J. T. Simms, Y. Pei, U. K. Mishra, and M. Kuball, "Integrated optical and

electrical analysis: Identifying location and properties of traps in AlGaN/GaN HEMTs during electrical stress," *IEEE Electron Device Lett.*, vol. 31, no. 7, pp. 662–664, Jul. 2010.

[51] S. T. Pantelides, Y. Puzyrev, X. Shen, T. Roy, S. Dasgupta, B. R. Tuttle, D. M. Fleetwood, and R. D. Schrimpf, "Reliability of III–V devices – The defects that cause the trouble," *Microelectron. Eng.*, vol. 90, pp. 3–8, Feb. 2012.

[52] J. Joh, J. A. Del Alamo, K. Langworthy, S. Xie, and T. Zheleva, "Role of stress voltage on structural degradation of GaN high-electron-mobility transistors," *Microelectron. Reliab.*, vol. 51, no. 2, pp. 201–206, Feb. 2011.

[53] S. Y. Park, C. Floresca, U. Chowdhury, J. L. Jimenez, C. Lee, E. Beam, P. Saunier, T. Balistreri, and M. J. Kim, "Physical degradation of GaN HEMT devices under high drain bias reliability testing," *Microelectron. Reliab.*, vol. 49, no. 5, pp. 478–483, May 2009.

[54] J. Joh and J. A. del Alamo, "Critical voltage for electrical degradation of GaN high-electron mobility transistors," *IEEE Electron Device Lett.*, vol. 29, no. 4, pp. 287–289, Apr. 2008.

[55] L. Liu, T. S. Kang, D. A. Cullen, L. Zhou, J. Kim, C.-Y. Chang, E. A. Douglas, S. Jang, D. J. Smith, S. J. Pearton, W. J. Johnson, and F. Ren, "Effect of source field plate on the characteristics of off-state, step-stressed AlGaN/GaN high electron mobility transistors," *J. Vac. Sci. Technol. B*, vol. 29, no. 3, p. 032204, May 2011.

[56] F. Medjdoub, J.-F. Carlin, M. Gonschorek, E. Feltin, M. A. Py, D. Ducatteau, C. Gaquiere, N. Grandjean, and E. Kohn, "Can InAlN/GaN be an alternative to high power / high temperature AlGaN/GaN devices?," in *2006 International Electron Devices Meeting(IEDM)*, 2006, pp. 927–930.

[57] X. Sun, O. I. Saadat, J. Chen, E. X. Zhang, S. Cui, T. Palacios, D. M. Fleetwood, and T. P. Ma, "Total-ionizing-dose radiation effects in AlGaN/GaN HEMTs and MOS-HEMTs," *IEEE Trans. Nucl. Sci.*, vol. 60, no. 6, pp. 4074–4079, Dec. 2013.

[58] N. E. Ives, J. Chen, A. F. Witulski, R. D. Schrimpf, D. M. Fleetwood, R. W. Bruce, M. W. McCurdy, E. X. Zhang, and L. W. Massengill, "Effects of proton-induced displacement damage on gallium nitride HEMTs in RF power amplifier applications," *IEEE Trans. Nucl. Sci.*, vol. 62, no. 6, pp. 2417–2422, Dec. 2015.

[59] J. Chen, E. X. Zhang, C. X. Zhang, M. W. McCurdy, D. M. Fleetwood, R. D. Schrimpf, S. W. Kaun, E. C. H. Kyle, and J. S. Speck, "RF performance of proton-irradiated AlGaN/GaN HEMTs," *IEEE Trans. Nucl. Sci.*, vol. 61, no. 6, pp. 2959–2964, Dec. 2014.

[60] Y. S. Puzyrev, T. Roy, E. X. Zhang, D. M. Fleetwood, R. D. Schrimpf, and S. T. Pantelides, "Radiation-induced defect evolution and electrical degradation of AlGaN/GaN high-electron-mobility transistors," *IEEE Trans. Nucl. Sci.*, vol. 58, no. 6, pp. 2918–2924, Dec. 2011.

[61] J. Chen, Y. S. Puzyrev, R. Jiang, E. X. Zhang, M. W. McCurdy, D. M. Fleetwood, R. D. Schrimpf, S. T. Pantelides, A. R. Arehart, S. A. Ringel, P. Saunier, and C. Lee, "Effects of applied bias and high field stress on the radiation response of GaN/AlGaN HEMTs," *IEEE Trans. Nucl. Sci.*, vol. 62, no. 6, pp. 2423–2430, Dec. 2015.

[62] B. D. White, M. Bataiev, S. H. Goss, X. Hu, A. Karmarkar, D. M. Fleetwood, R. D. Schrimpf, W. J. Schaff, and L. J. Brillson, "Electrical, spectral, and chemical properties of 1.8 MeV proton irradiated AlGaN/GaN HEMT structures as a function of proton fluence," *IEEE Trans. Nucl. Sci.*, vol. 50, no. 6, pp. 1934–1941, Dec. 2003.

[63] L. Liu, C.-F. Lo, Y. Xi, Y. Wang, F. Ren, S. J. Pearton, H.-Y. Kim, J. Kim, R. C. Fitch, D. E. Walker, K. D. Chabak, J. K. Gillespie, S. E. Tetlak, G. D. Via, A. Crespo, and I. I. Kravchenko, "Dependence on proton energy of degradation of AlGaN/GaN high electron mobility transistors," *J. Vac. Sci. Technol. B,* vol. 31, no. 2, p. 022201, Mar. 2013.

[64] T. Roy, E. X. Zhang, Y. S. Puzyrev, D. M. Fleetwood, R. D. Schrimpf, B. K. Choi, A. B. Hmelo, and S. T. Pantelides, "Process dependence of proton-induced degradation in GaN HEMTs," *IEEE Trans. Nucl. Sci.*, vol. 57, no. 6, pp. 3060–3065, Dec. 2010.

[65] J. Chen, Y. S. Puzyrev, C. X. Zhang, E. X. Zhang, M. W. McCurdy, D. M. Fleetwood, R. D. Schrimpf, S. T. Pantelides, S. W. Kaun, E. C. H. Kyle, and J. S. Speck, "Proton-induced dehydrogenation of defects in AlGaN/GaN HEMTs," *IEEE Trans. Nucl. Sci.*, vol. 60, no. 6, pp. 4080–4086, Dec. 2013.

[66] Z.-Q. Fang, B. Claflin, D. C. Look, D. S. Green, and R. Vetury, "Deep traps in AlGaN/GaN heterostructures studied by deep level transient spectroscopy: Effect of carbon concentration in GaN buffer layers," *J. Appl. Phys.*, vol. 108, no. 6, p. 063706, Sep. 2010.

[67] P. Hacke, T. Detchprohm, K. Hiramatsu, N. Sawaki, K. Tadatomo, and K. Miyake, "Analysis of deep levels in *n*−type GaN by transient capacitance methods," *J. Appl. Phys.*, vol. 76, no. 1, pp. 304–309, Jul. 1994.

[68] P. Dutta and P. M. Horn, "Low-frequency fluctuations in solids: 1/*f* noise," *Rev. Mod. Phys.*, vol. 53, no. 3, pp. 497–516, Jul. 1981.

[69] D. M. Fleetwood, "1/*f* noise and defects in microelectronic materials and devices," *IEEE*

Trans. Nucl. Sci., vol. 62, no. 4, pp. 1462–1486, Aug. 2015.

[70] T. Roy, Y. S. Puzyrev, E. X. Zhang, S. Dasgupta, S. A. Francis, D. M. Fleetwood, R. D. Schrimpf, U. K. Mishra, J. S. Speck, and S. T. Pantelides, "1/*f* noise in GaN HEMTs grown under Ga-rich, N-rich, and NH_3-rich conditions," *Microelectron. Reliab.*, vol. 51, no. 2, pp. 212–216, Feb. 2011.

[71] T. Roy, E. X. Zhang, Y. S. Puzyrev, X. Shen, D. M. Fleetwood, R. D. Schrimpf, G. Koblmueller, R. Chu, C. Poblenz, N. Fichtenbaum, C. S. Suh, U. K. Mishra, J. S. Speck, and S. T. Pantelides, "Temperature-dependence and microscopic origin of low frequency 1/*f* noise in GaN/AlGaN high electron mobility transistors," *Appl. Phys. Lett.*, vol. 99, no. 20, p. 203501, Nov. 2011.

[72] J. Chen, Y. S. Puzyrev, E. X. Zhang, D. M. Fleetwood, R. D. Schrimpf, A. R. Arehart, S. A. Ringel, S. W. Kaun, E. C. H. Kyle, J. S. Speck, P. Saunier, C. Lee, and S. T. Pantelides, "High-field stress, low-frequency noise, and long-term reliability of AlGaN/GaN HEMTs," *IEEE Trans. Device Mater. Reliab.*, vol. 16, no. 3, pp. 282–289, Sep. 2016.

[73] M. Meneghini, N. Ronchi, A. Stocco, G. Meneghesso, U. K. Mishra, Y. Pei, and E. Zanoni, "Investigation of trapping and hot-electron effects in GaN HEMTs by means of a combined electrooptical method," *IEEE Trans. Electron Devices*, vol. 58, no. 9, pp. 2996–3003, Sep. 2011.

[74] N. Shigekawa, K. Shiojima, and T. Suemitsu, "Electroluminescence characterization of AlGaN/GaN high-electron-mobility transistors," *Appl. Phys. Lett.*, vol. 79, no. 8, pp. 1196–1198, Aug. 2001.

[75] M. Ruzzarin, M. Meneghini, I. Rossetto, M. Van Hove, S. Stoffels, T.-L. Wu, S. Decoutere, G. Meneghesso, and E. Zanoni, "Evidence of hot-electron degradation in GaN-based MIS-HEMTs submitted to high temperature constant source current stress," *IEEE Electron Device Lett.*, vol. 37, no. 11, pp. 1415–1417, Nov. 2016.

[76] Y. S. Puzyrev, B. R. Tuttle, R. D. Schrimpf, D. M. Fleetwood, and S. T. Pantelides, "Theory of hot-carrier-induced phenomena in GaN high-electron-mobility transistors," *Appl. Phys. Lett.*, vol. 96, no. 5, p. 053505, Feb. 2010.

[77] M. Meneghini, G. Meneghesso, and E. Zanoni, "Analysis of the reliability of AlGaN/GaN HEMTs submitted to on-state stress based on electroluminescence investigation," *IEEE Trans. Device Mater. Reliab.*, vol. 13, no. 2, pp. 357–361, Jun. 2013.

[78] Y. Puzyrev, S. Mukherjee, Jin Chen, T. Roy, M. Silvestri, R. D. Schrimpf, D. M. Fleetwood,

J. Singh, J. M. Hinckley, A. Paccagnella, and S. T. Pantelides, “Gate bias dependence of defect-mediated hot-carrier degradation in GaN HEMTs,” *IEEE Trans. Electron Devices*, vol. 61, no. 5, pp. 1316–1320, May 2014.

[79] S. Mukherjee, Y. Puzyrev, J. Hinckley, R. D. Schrimpf, D. M. Fleetwood, J. Singh, and S. T. Pantelides, “Role of bias conditions in the hot carrier degradation of AlGaN/GaN high electron mobility transistors,” *Phys. status solidi*, vol. 10, no. 5, pp. 794–798, May 2013.

[80] T. Roy, E. X. Zhang, D. M. Fleetwood, R. D. Schrimpf, Y. S. Puzyrev, and S. T. Pantelides, “Reliability-limiting defects in AlGaN/GaN HEMTs,” in *2011 International Reliability Physics Symposium*, 2011, p. 4E.4.1-4E.4.4.

[81] D. Marcon, G. Meneghesso, T.-L. Wu, S. Stoffels, M. Meneghini, E. Zanoni, and S. Decoutere, “Reliability analysis of permanent degradations on AlGaN/GaN HEMTs,” *IEEE Trans. Electron Devices*, vol. 60, no. 10, pp. 3132–3141, Oct. 2013.

[82] E. Zanoni, F. Danesin, M. Meneghini, A. Cetronio, C. Lanzieri, M. Peroni, and G. Meneghesso, “Localized damage in AlGaN/GaN HEMTs induced by reverse-bias testing,” *IEEE Electron Device Lett.*, vol. 30, no. 5, pp. 427–429, May 2009.

[83] M. Meneghini, I. Rossetto, D. Bisi, M. Ruzzarin, M. Van Hove, S. Stoffels, T.-L. Wu, D. Marcon, S. Decoutere, G. Meneghesso, and E. Zanoni, “Negative bias-induced threshold voltage instability in GaN-on-Si power HEMTs,” *IEEE Electron Device Lett.*, vol. 37, no. 4, pp. 474–477, Apr. 2016.

[84] J. Joh and J. A. del Alamo, “Mechanisms for electrical degradation of GaN high-electron mobility transistors,” in *2006 International Electron Devices Meeting(IEDM)*, 2006, pp. 148–151.

[85] J. Joh, F. Gao, T. Palacios, and J. A. Del Alamo, “A model for the critical voltage for electrical degradation of GaN high electron mobility transistors,” *Microelectron. Reliab.*, vol. 50, no. 6, pp. 767–773, Jun. 2010.

[86] J. Kuzmik, A. Kostopoulos, G. Konstantinidis, J.-F. Carlin, A. Georgakilas, and D. Pogany, “InAlN/GaN HEMTs: a first insight into technological optimization,” *IEEE Trans. Electron Devices*, vol. 53, no. 3, pp. 422–426, Mar. 2006.

[87] K. H. Warnick, Y. Puzyrev, T. Roy, D. M. Fleetwood, R. D. Schrimpf, and S. T. Pantelides, “Room-temperature diffusive phenomena in semiconductors: The case of AlGaN,” *Phys. Rev. B*, vol. 84, no. 21, p. 214109, Dec. 2011.

[88] M. Meneghini, G. Cibin, M. Bertin, G. A. M. Hurkx, P. Ivo, J. Sonsky, J. A. Croon, G. Meneghesso, and E. Zanoni, "OFF-State degradation of AlGaN/GaN power HEMTs: experimental demonstration of time-dependent drain-source breakdown," *IEEE Trans. Electron Devices*, vol. 61, no. 6, pp. 1987–1992, Jun. 2014.

[89] M. Meneghini, M. Bertin, A. Stocco, G. dal Santo, D. Marcon, P. E. Malinowski, A. Chini, G. Meneghesso, and E. Zanoni, "Degradation of AlGaN/GaN Schottky diodes on silicon: Role of defects at the AlGaN/GaN interface," *Appl. Phys. Lett.*, vol. 102, no. 16, p. 163501, Apr. 2013.

[90] J. L. Barth, C. S. Dyer, and E. G. Stassinopoulos, "Space, atmospheric, and terrestrial radiation environments," *IEEE Trans. Nucl. Sci.*, vol. 50, no. 3, pp. 466–482, Jun. 2003.

[91] J. R. Schwank, M. R. Shaneyfelt, D. M. Fleetwood, J. A. Felix, P. E. Dodd, P. Paillet, and V é Ferlet-Cavrois, "Radiation effects in MOS Oxides," *IEEE Trans. Nucl. Sci.*, vol. 55, no. 4, pp. 1833–1853, Aug. 2008.

[92] R. C. Hughes, "Charge-carrier transport phenomena in amorphous SiO_2: Direct measurement of the drift mobility and lifetime," *Phys. Rev. Lett.*, vol. 30, no. 26, pp. 1333–1336, Jun. 1973.

[93] X. Hu, B. K. Choi, H. J. Barnaby, D. M. Fleetwood, R. D. Schrimpf, S. Lee, S. Shojah-Ardalan, R. Wilkins, U. K. Mishra, and R. W. Dettmer, "The energy dependence of proton-induced degradation in AlGaN/GaN high electron mobility transistors," *IEEE Trans. Nucl. Sci.*, vol. 51, no. 2, pp. 293–297, Apr. 2004.

[94] J. Nord, K. Nordlund, and J. Keinonen, "Molecular dynamics study of damage accumulation in GaN during ion beam irradiation," *Phys. Rev. B*, vol. 68, no. 18, p. 184104, Nov. 2003.

[95] A. Ionascut-Nedelcescu, C. Carlone, A. Houdayer, H. J. von Bardeleben, J.-L. Cantin, and S. Raymond, "Radiation hardness of gallium nitride," *IEEE Trans. Nucl. Sci.*, vol. 49, no. 6, pp. 2733–2738, Dec. 2002.

[96] R. Jiang, E. X. Zhang, M. W. McCurdy, J. Chen, X. Shen, P. Wang, D. M. Fleetwood, R. D. Schrimpf, S. W. Kaun, E. C. H. Kyle, J. S. Speck, and S. T. Pantelides, "Worst-case bias for proton and 10-keV x-ray irradiation of AlGaN/GaN HEMTs," *IEEE Trans. Nucl. Sci.*, vol. 64, no. 1, pp. 218–225, Jan. 2017.

[97] S. J. Cai, Y. S. Tang, R. Li, Y. Y. Wei, L. Wong, Y. L. Chen, K. L. Wang, Mary Chen, R. D. Schrimpf, J. C. Keay, and K. F. Galloway, "Annealing behavior of a proton irradiated $Al_xGa_{1-x}N$/GaN high electron mobility transistor grown by MBE," *IEEE Trans. Electron*

Devices, vol. 47, no. 2, pp. 304–307, 2000.

[98] A. Y. Polyakov, N. B. Smirnov, A. V. Govorkov, N. G. Kolin, D. I. Merkurisov, V. M. Boiko, A. V. Korulin, and S. J. Pearton, "Neutron transmutation doping effects in GaN," *J. Vac. Sci. Technol. B,* vol. 28, no. 3, pp. 608–612, May 2010.

[99] H.-Y. Kim, J. Kim, L. Liu, C.-F. Lo, F. Ren, and S. J. Pearton, "Effects of proton irradiation energies on degradation of AlGaN/GaN high electron mobility transistors," *J. Vac. Sci. Technol. B,* vol. 30, no. 1, p. 012202, Jan. 2012.

[100] B. Luo, J. W. Johnson, F. Ren, K. K. Allums, C. R. Abernathy, S. J. Pearton, R. Dwivedi, T. N. Fogarty, R. Wilkins, A. M. Dabiran, A. M. Wowchack, C. J. Polley, P. P. Chow, and A. G. Baca, "DC and RF performance of proton-irradiated AlGaN/GaN high electron mobility transistors," *Appl. Phys. Lett.*, vol. 79, no. 14, pp. 2196–2198, Oct. 2001.

[101] S. J. Pearton, F. Ren, E. Patrick, M. E. Law, and A. Y. Polyakov, "Review-ionizing radiation damage effects on GaN devices," *ECS J. Solid State Sci. Technol.*, vol. 5, no. 2, pp. Q35–Q60, Nov. 2016.

[102] A. Y. Polyakov and I.-H. Lee, "Deep traps in GaN-based structures as affecting the performance of GaN devices," *Mater. Sci. Eng. R Reports*, vol. 94, pp. 1–56, Aug. 2015.

[103] T. Roy, Y. S. Puzyrev, B. R. Tuttle, D. M. Fleetwood, R. D. Schrimpf, D. F. Brown, U. K. Mishra, and S. T. Pantelides, "Electrical-stress-induced degradation in AlGaN/GaN high electron mobility transistors grown under gallium-rich, nitrogen-rich, and ammonia-rich conditions," *Appl. Phys. Lett.*, vol. 96, no. 13, p. 133503, Mar. 2010.

[104] R. Jiang, X. Shen, J. Chen, G. X. Duan, E. X. Zhang, D. M. Fleetwood, R. D. Schrimpf, S. W. Kaun, E. C. H. Kyle, J. S. Speck, and S. T. Pantelides, "Degradation and annealing effects caused by oxygen in AlGaN/GaN high electron mobility transistors," *Appl. Phys. Lett.*, vol. 109, no. 2, p. 023511, Jul. 2016.

[105] Y. S. Puzyrev, R. D. Schrimpf, D. M. Fleetwood, and S. T. Pantelides, "Role of Fe impurity complexes in the degradation of GaN/AlGaN high-electron-mobility transistors," *Appl. Phys. Lett.*, vol. 106, no. 5, p. 053505, Feb. 2015.

[106] S. Mukherjee, Y. Puzyrev, J. Chen, D. M. Fleetwood, R. D. Schrimpf, and S. T. Pantelides, "Hot-carrier degradation in GaN HEMTs due to substitutional iron and its complexes," *IEEE Trans. Electron Devices*, vol. 63, no. 4, pp. 1486–1494, Apr. 2016.

[107] J. W. Chung, Tae-Woo Kim, and T. Palacios, "Advanced gate technologies for state-of-the-

art f_T in AlGaN/GaN HEMTs," in *2010 International Electron Devices Meeting*, 2010, p. 30.2.1-30.2.4.

[108] J. W. Chung, J. C. Roberts, E. L. Piner, and T. Palacios, "Effect of gate leakage in the subthreshold characteristics of AlGaN/GaN HEMTs," *IEEE Electron Device Lett.*, vol. 29, no. 11, pp. 1196–1198, Nov. 2008.

[109] R. Zhang and T. F. Kuech, "Photoluminescence of carbon in situ doped GaN grown by halide vapor phase epitaxy," *Appl. Phys. Lett.*, vol. 72, no. 13, pp. 1611–1613, Jul. 1998.

[110] R. Armitage, W. Hong, Q. Yang, H. Feick, J. Gebauer, E. R. Weber, S. Hautakangas, and K. Saarinen, "Contributions from gallium vacancies and carbon-related defects to the 'yellow luminescence' in GaN," *Appl. Phys. Lett.*, vol. 82, no. 20, pp.3457–3459, May 2003.

[111] J. Chen, "Radiation response and reliability of high speed AlGaN/GaN HEMTs," Ph.D. dissertation, Vanderbilt University., Nashville, TN, USA, 2016

[112] E. X. Zhang, D. M. Fleetwood, N. D. Pate, R. A. Reed, A. F. Witulski, and R. D. Schrimpf, "Time-domain reflectometry measurements of total-ionizing-dose degradation of n-MOSFETs," *IEEE Trans. Nucl. Sci.*, vol. 60, no. 6, pp. 4470–4475, Dec. 2013.

[113] H. D. Xiong, "Low frequency noise and charge trapping in MOSFETS," Ph.D. dissertation, Vanderbilt University., Nashville, TN, USA, 2004.

[114] J. B. Johnson, "Thermal agitation of electricity in conductors," *Nature*, vol. 119, no. 2984, pp. 50–51, Jan. 1927.

[115] F. N. Hooge, "1/*f* noise sources," *IEEE Trans. Electron Devices*, vol. 41, no. 11, pp. 1926–1935, 1994.

[116] J. H. Scofield, T. P. Doerr, and D. M. Fleetwood, "Correlation between preirradiation 1/*f* noise and postirradiation oxide-trapped charge in MOS transistors," *IEEE Trans. Nucl. Sci.*, vol. 36, no. 6, pp. 1946–1953, 1989.

[117] T. L. Meisenheimer and D. M. Fleetwood, "Effect of radiation-induced charge on 1/*f* noise in MOS devices," *IEEE Trans. Nucl. Sci.*, vol. 37, no. 6, pp. 1696–1702, 1990.

[118] D. M. Fleetwood, T. L. Meisenheimer, and J. H. Scofield, "1/*f* noise and radiation effects in MOS devices," *IEEE Trans. Electron Devices*, vol. 41, no. 11, pp. 1953–1964, 1994.

[119] A. L. McWorther, "1/*f* noise and germanium surface properties," in *Semiconductor Surface*

Physics. Philadelphia, PA: Univ. of Pennsylvania Press, 1957, pp. 207-228.

[120] P. Wang, R. Jiang, J. Chen, E. X. Zhang, M. W. McCurdy, R. D. Schrimpf, and D. M. Fleetwood, "1/*f* Noise in as-processed and proton-irradiated AlGaN/GaN HEMTs due to carrier number fluctuations," *IEEE Trans. Nucl. Sci.*, vol. 64, no. 1, pp. 181–189, Jan. 2017.

[121] J. H. Scofield and D. M. Fleetwood, "Physical basis for nondestructive tests of MOS radiation hardness," *IEEE Trans. Nucl. Sci.*, vol. 38, no. 6, pp. 1567–1577, Dec. 1991.

[122] P. Dutta, P. Dimon, and P. M. Horn, "Energy scales for noise processes in metals," *Phys. Rev. Lett.*, vol. 43, no. 9, pp. 646–649, Aug. 1979.

[123] H. D. Xiong, D. M. Fleetwood, B. K. Choi, and A. L. Sternberg, "Temperature dependence and irradiation response of 1/*f*-noise in MOSFETs," *IEEE Trans. Nucl. Sci.*, vol. 49, no. 6, pp. 2718–2723, Dec. 2002.

[124] A. H. Johnston, "Super recovery of total dose damage in MOS devices," *IEEE Trans. Nucl. Sci.*, vol. 31, no. 6, pp. 1427–1433, Dec. 1984.

[125] S. J. Pearton, H. Cho, J. R. LaRoche, F. Ren, R. G. Wilson, and J. W. Lee, "Oxygen diffusion into SiO_2-capped GaN during annealing," *Appl. Phys. Lett.*, vol. 75, no. 19, pp. 2939–2941, Nov. 1999.

[126] X. Shen, P. B. Allen, M. S. Hybertsen, and J. T. Muckerman, "Water adsorption on the GaN $(10\bar{1}0)$ nonpolar surface," *J. Phys. Chem. C*, vol. 113, no. 9, pp. 3365–3368, Mar. 2009.

[127] P.-T. Chen, C.-L. Sun, and M. Hayashi, "First-principles calculations of hydrogen generation due to water splitting on polar gan surfaces," *J. Phys. Chem. C*, vol. 114, no. 42, pp. 18228–18232, Oct. 2010.

[128] Y.-W. Chen and J.-L. Kuo, "Density functional study of the first wetting layer on the GaN (0001) surface," *J. Phys. Chem. C*, vol. 117, no. 17, pp. 8774–8783, May 2013.

[129] A. Ortiz-Conde, F. J. Garc, I. S A Anchez, J. J. Liou, A. Cerdeira, M. Estrada, and Y. Yue, "A review of recent MOSFET threshold voltage extraction methods," *Microelectron. Reliab.*, vol. 42, no. 4–5, pp. 583–596, Apr. 2002.

[130] J. Joh, J. A. del Alamo, U. Chowdhury, T.-M. Chou, H.-Q. Tserng, and J. L. Jimenez, "Measurement of channel temperature in GaN high-electron mobility transistors," *IEEE Trans. Electron Devices*, vol. 56, no. 12, pp. 2895–2901, Dec. 2009.

[131] M. Meneghini, I. Rossetto, F. Hurkx, J. Sonsky, J. A. Croon, G. Meneghesso, and E. Zanoni, "Extensive investigation of time-dependent breakdown of GaN-HEMTs submitted to OFF-state stress," *IEEE Trans. Electron Devices*, vol. 62, no. 8, pp. 2549–2554, Aug. 2015.

[132] M. Meneghini, A. Stocco, M. Bertin, N. Ronchi, A. Chini, D. Marcon, G. Meneghesso, and E. Zanoni, "Electroluminescence analysis of time-dependent reverse-bias degradation of HEMTs: A complete model," in *2011 International Electron Devices Meeting*, 2011, p. 19.5.1-19.5.4.

[133] Z. Zhang, D. Cardwell, A. Sasikumar, E. C. H. Kyle, J. Chen, E. X. Zhang, D. M. Fleetwood, R. D. Schrimpf, J. S. Speck, A. R. Arehart, and S. A. Ringel, "Correlation of proton irradiation induced threshold voltage shifts to deep level traps in AlGaN/GaN heterostructures," *J. Appl. Phys.*, vol. 119, no. 16, p. 165704, Apr. 2016.

[134] N. Braga, R. Mickevicius, R. Gaska, X. Hu, M. S. Shur, M. A. Khan, G. Simin, and J. Yang, "Simulation of hot electron and quantum effects in AlGaN/GaN heterostructure field effect transistors," *J. Appl. Phys.*, vol. 95, no. 11, pp. 6409–6413, Jun. 2004.

[135] D. W. Cardwell, A. Sasikumar, A. R. Arehart, S. W. Kaun, J. Lu, S. Keller, J. S. Speck, U. K. Mishra, S. A. Ringel, and J. P. Pelz, "Spatially-resolved spectroscopic measurements of $E_c - 0.57$ eV traps in AlGaN/GaN high electron mobility transistors," *Appl. Phys. Lett.*, vol. 102, no. 19, p. 193509, May 2013.

[136] I. Hwang, J. Kim, S. Chong, H.-S. Choi, S.-K. Hwang, J. Oh, J. K. Shin, and U.-I. Chung, "Impact of channel hot electrons on current collapse in AlGaN/GaN HEMTs," *IEEE Electron Device Lett.*, vol. 34, no. 12, pp. 1494–1496, Dec. 2013.

[137] C. G. Van de Walle and J. Neugebauer, "First-principles calculations for defects and impurities: Applications to III-nitrides," *J. Appl. Phys.*, vol. 95, no. 8, pp. 3851–3879, Apr. 2004.

[138] S. J. Pearton, J. C. Zolper, R. J. Shul, and F. Ren, "GaN: Processing, defects, and devices," *J. Appl. Phys.*, vol. 86, no. 1–78, Jun. 1999.

[139] Z. Zhang, A. R. Arehart, E. C. H. Kyle, J. Chen, E. X. Zhang, D. M. Fleetwood, R. D. Schrimpf, J. S. Speck, and S. A. Ringel, "Proton irradiation effects on deep level states in Mg-doped p-type GaN grown by ammonia-based molecular beam epitaxy," *Appl. Phys. Lett.*, vol. 106, no. 2, p. 022104, Jan. 2015.